DELFT UNIVERSITY OF TECHNOLOGY
FACULTY OF CIVIL ENGINEERING
DEPARTMENT OF HYDRAULIC ENGINEERING

Coastal response during the 1953 and 1976 storm surges in the Netherlands

Field data validation of the XBeach model

MSc Thesis

Evangelos Voukouvalas

Supervisors

Prof. Dr. Ir. M.J.F. Stive
Dr. Ir. A.R. Van Dongeren
Ir. D.J.R. Walstra
Dr. Ir. R.J. Labeur

March 2010

Acknowledgements

I am grateful to my supervisors Professor Stive, Dr. Van Dongeren, Ir. Walstra and Dr. Labeur for their continuous support, motivation, suggestions and advice. Thank you for giving me the opportunity to work with you and learn from you.

I would like to thank the developers and the open source community of the XBeach model, for building, testing and releasing a tool which pointed to me a different view on the aspects of the coastal zone related hydrodynamic and morphodynamic processes.

I would also like to thank Ir. Van der Kaaij and Ir. Van Ormondt from Deltares for explaining and providing to me the two versions of the operational model that they have developed.

On the data acquisition, I would like to thank Ir. Van Geer, Dr. Caires, Dr. Verlaan and Ir. Gerritsen from Deltares, Ir. Smit from Delft University of Technology, Mr. Uppala from ECMWF and Ir. Bakker from TNO.

On the data processing which is a rather time-demanding process, I would like to thank Ir. Baart, Ir. Heijer and the members of the OpenEarth Tools team, whose libraries significantly reduced, the notorious 80% of the working time required to finish the 20% of the total job.

Without the help from my friends I would not be able to finish this thesis. Many thanks go to Sepehr, Chris, Reinoud, Burak, Marion, Maurits, Costas, Giorgos, Dimitris, Lampis, Antonis, Ariadni, Grigoris, Psilos, Vaso and all my friends who may not know how or how much they have contributed, but they have.

I would like to thank my parents and my brother for their endless encouragement and Maria for her inspiration and support.

This research has received funding from the European Community's Seventh Framework Programme under grant agreement n° 202798 (MICORE Project).

Evangelos

SUMMARY

The extreme flood events and the resulting impact on the coastal areas point at the need for an integrated coastal hazards mitigation system. This system includes the civil preparation and awareness in combination with an early-warning system. The storm surge early-warning system that is going to be established in the Netherlands, combines the accurate weather forecast with the hydrodynamic and morphodynamic models in an operational mode, in order to estimate the potential impact on the coasts. This study focuses on the morphodynamic validity of the operational model system, by studying two historical storm surge events on prototype scale.

Chapter 2 presents the mechanism for the generation of the storm surges and how the tidal areas may be influenced by these coastal threats. Furthermore, this chapter presents an overview of the empirical approximations, as well as the physical and numerical models for the long and short term coastal profile changes.

At the last half of the previous century, two major storm events hit the coastlines of the country. Due to the lack of warning, the 1953 storm surge left behind thousands of casualties and extensive wreckage of the coastline. Higher impact was recorded in the southern part of the country because of the storm track and the geometry of the area. In order to reduce the probability of experiencing again such a devastating storm surge, the coastal defense policy in the Netherlands had been reorganized on national level and more effective countermeasures had been received. When the 1976 storm surge attacked the country, the civil awareness and the reinforced coastal defense abate the impact and the fatalities. The degradation of the coastline has been recorded as part of the Jarkus coastline monitoring programme. The volumetric analysis of the most recent to the storm event coastal profiles records gave evidence of the non-uniform impact along the North Holland province. As part of the data analysis concerning the impact of the 1976 storm surge on the shoreline, this chapter ends with the overview of the natural volume variability of the North Holland province from 1974 to 1981.

The numerical implementation of the Delft3D and the XBeach models is discussed in Chapter 4 and Chapter 5 describes how these two models are coupled in an operational model schematization; the deformation and the propagation of the storm surge are simulated with the Delft3D model and the nearshore hydrodynamic and morphodynamic processes by the XBeach model. Whether the observed deflections between the measured and the computed surge level are significant for the operational model performance, are going to be examined with respect to the resulted coastal profile changes.

Chapter 6 presents the validation of the operational model schematization, by examining the profile development as indicated by the most recent records after the 1976 storm surge and the numerical results as computed by the XBeach model. Three sites are selected along the North Holland province, as indicated by the volumetric analysis presented in Chapter 3; these are Bergen, Castricum and Julianadorp. The sensitivity analysis of the XBeach model is performed in the area of Bergen and the reason is to investigate if the model reacts at changes of the numerical parameters and whether the consequent physical reflection of the extreme storm events is satisfied. These parameters are related with the waves' asymmetry, the avalanching of the wet area and the long waves' sediment stirring. The model is found to react as expected at the changes of the first two parameters, and especially their combination improves the model's performance. In contrast, the model is insensitive to the long waves' sediment stirring. By imposing the measured storm surge timeseries the model performance is improved, which may indicate a possible underestimation of this forecasted quantity. In contrast, an additional imposed wind setup does not influence the final profile significantly.

The conclusions and the recommendations of this study are presented in Chapter 7. Concerning the model performance in the area of Castricum, the model skill is excellent and very good convergence is obtained on estimating the volume change and the estimated dune retreat. In Julianadorp, while the influence of the groins is not accounted, due to the significant scouring that is observed in the backshore zone, the model performance is bad. The geological features and the bed profile of the studied areas indicate a different pattern of the energy distribution, while further research is needed to investigate their influence on the dune erosion during storm surge events.

CONTENTS

Abbreviations

DCSM = Dutch Continental Shelf Model

ECMWF = European Centre for Medium-Range Weather Forecasts

HIRLAM = High Resolution Limited Area Model, weather prediction forecast programme

HHL = Highest High water tidal level

HW = High Water tidal level

JARKUS = (jaarlijkse kustmetingen) annual coastal monitoring programme in the Netherlands since 1963

KNMI = (Koninklijk Nederlands Meteorologisch Instituut) Royal Netherlands Meteorological Institute

KST model = (Kuststrook) model schematization describing the offshore zone of the Netherlands

MKL = (momentane Kustlijn) Dutch momentary coastline

LW = Low Water tidal level

N.A.P. = (Normaal Amsterdams Peils) Amsterdam Ordnance Datum

RD = (Rijksdriehoeksmeting) A commonly used coordinate system in the Netherlands

RSP = (RijksStrandPalen) A coordinate system for the Jarkus project

RIKZ = (Rijkswaterstaat) Ministry of Transport, Public Works and Water Management

SSL = Storm Surge Level

SVSD = (stormvloedwaarschuwingsdienst) Dutch Storm Surge Warning Service

1. INTRODUCTION

1.1 Background

Over the last years the coastal communities witnessed the impact of the extreme natural events. In 2004, the Boxing Day tsunami was broadcasted while spreading the disaster over the entire Indian Ocean. One year later and despite of its accurate forecasted path, Hurricane Katrina resulted to extensive fatalities and devastation at many areas along the Eastern North America. In contrast, due to the 2010 Chilean tsunami the local authorities ordered to evacuate many coastal areas around the Pacific Ocean, even though the early warning system forecasted low impact except for Chile. According to Wisner et al. [2004], 'disasters occur when hazards meet vulnerability'.

In the Netherlands, before the application of the coastal maintenance policy in 1990, two significant storm surges attacked the coastline of the country. The fatalities and the loss due to the 1953 storm surge led to the realization of the Delta Plan. The dykes were reinforced and monitored, the coastal structures were designed to withstand extreme conditions and the flood defense system is organized on a national level. In addition, the flood early warning system was initiated, which at the early stages was consisted of a simple box model to estimate the wind set-up [Gerritsen et al. 1995]. Twenty three years after the 1953 storm another storm event threatened the country. Despite its severity, the aftermath of the 1976 storm surge was limited, as the flood protection countermeasures were enabled [Lamb 1988].

Nowadays, a real-time storm warning system will be established, which will include the morphological impact of the coastal areas. The continuous monitoring of the coastline is combined with weather prediction models coupled with hydrodynamic and morphodynamic models. The last link of this chain is the XBeach model, which is applied to calculate the coastal response due to extreme events.

The low probability of occurrence, the severity and the low predictability of the extreme events point the need for an integrated and validated hazard mitigation system. A comprehensive study of the nature of past events may assess to understand and estimate future hazards.

1.2 Problem statement

The nearshore processes related with the storm and hurricane driven forces are simulated with the XBeach model. The performance of the model has been examined through a number of cases both on laboratory [Roelvink et al. 2009 , Van Thiel de Vries 2009] and on prototype scale [McCall 2008, Pool 2009, Roelvink et al. 2009]. The model is continuously developed following the course of knowledge of the nearshore processes during extreme conditions. Therefore the validity of the model should be examined as well. As part of this validation

process, the present study investigates quantitatively the performance of the operational real-time forecast model on prototype scale, on the basis of the historical records of the 1953 and the 1976 storm surges in the Netherlands.

1.3 Objectives

The first objective is to validate the operational model-chain and the derived boundary hydrodynamic conditions during the 1953 and the 1976 storm surges. In particular, the morphodynamic impact will be examined on a prototype scale with the XBeach model, after obtaining the most recent to the storm events coastline records.

The second objective of this study is to investigate the coastal response during these storm surges. In terms of the coastal safety assessment of the Netherlands, it is necessary to investigate the reason that the recorded impact of the 1976 storm surge at the central part of the Dutch coast demonstrated an alongshore variable effect of the dune erosion, even in neighboring areas.

1.4 Reader's guide

Chapter 2 presents the mechanism for the formation of the storms and a review of the empirical, physical and numerical models for the coastline evolution during storm surges. Chapter 3 presents the recorded impact of the 1953 and the 1976 storm surges in the Netherlands, together with the records of the storm induced hydrodynamic conditions. The volumetric analysis, as recorded in the most recent measurements prior and after the 1976 storm event, shows a longshore variation along the North Holland province. In Chapter 4 the Delft3D and the XBeach models are presented and in Chapter 5 how these two models are linked to each other on operational mode, in order to simulate the propagation and the inundation of the storm events. The differences at the hydraulic boundary conditions either measured or simulated, are going to determine the aspects of the sensitivity analysis presented in the next chapter. In Chapter 6 we present the coastal response due to the 1976 storm surge. After performing the sensitive analysis on the physical parameters (related with the waves' asymmetry, the avalanching process, the sediment stirring, the wind setup and the response to different water level), the longshore variation of the coastline with respect to the local bathymetric features and characteristics, is studied at three different locations; starting from the North they are: Julianadorp, Bergen and Castricum. The conclusions and recommendations of this study are presented in Chapter 7.

2. LITERATURE REVIEW

2.1 Coastal profile

The coastal area is a dynamically changing environment due to short term (daily e.g. semidiurnal or diurnal tidal fluctuations, or fortnightly as neap and spring tides), episodic (e.g. tsunamis), seasonal (e.g. storms) and long time scale (wave climate alterations, sea-level rise) changes of the hydrodynamic conditions. Additionally, the anthropogenic actions (beach nourishments, sand mining, hydraulic constructions etc.) contribute explicitly or implicitly altering the coastal pattern. At the end of the monitoring period, a seaward or landward shift may be observed with or without alongshore migration. In general, the coastal zone is divided into four major subzones (Fig. 2.1); the offshore, the inshore, the foreshore and the backshore zone[1].

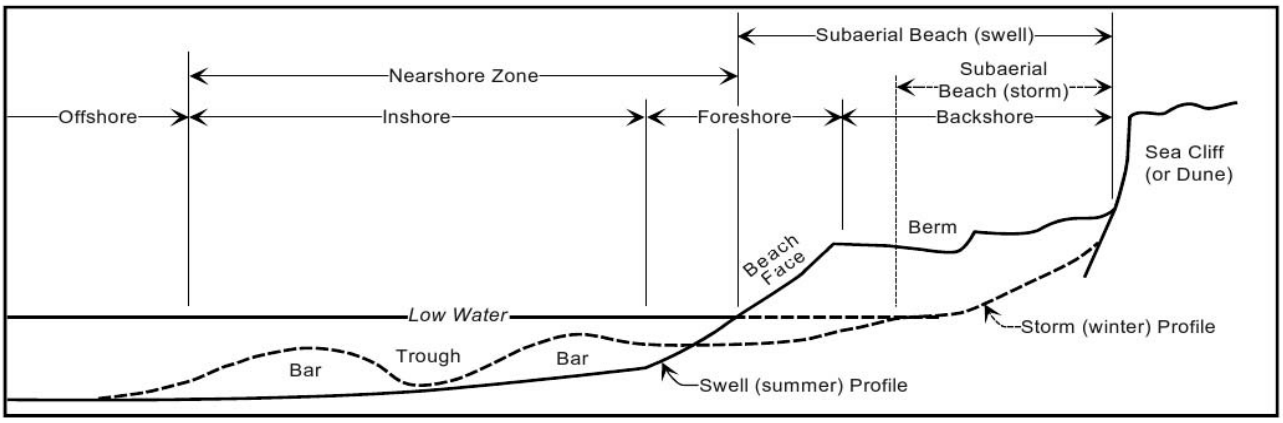

Figure 2.1: Typical natural beach profile with the major geological features (Schwartz 2005, p.162).

The first two zones are located lower than the LW line. The offshore zone is a relatively flat area extending from the tip of the continental shelf until the beginning of the breaker zone. The inshore zone includes the breaker zone and the surf zone. At this area, the gentle summer profile transforms into a system of bars and troughs during winter and vice versa, as the upper beach is eroded and migrates offshore. The foreshore zone is a slopping area, extending from the LW line up to the beach face. It is the area where the unconsolidated material is swept by the uprush and the backwash together with the tidal influence. During low tide, a system of low mounds and troughs is exposed at this area. The former ones are called ridges which run along the shore and the lateral ones are named runnels which are attached to the landward side of the shoremost ridge. Under storm conditions the beach face becomes smoother, as the sediment is transported seaward, while under calm wave conditions this part of the beach is accreted and becomes steeper. The upper part of the beach from the HW line

[1] In this study, the coastal terms and the geological components will be referred as presented at this chapter following Schwartz, 2005, p. 145, 162.

until the dune is the backshore zone. Usually, this zone is not affected by ordinary waves and tides but it becomes wet during storm surges. A common geological feature separating the foreshore from the backshore is the spring tide berms. Correspondingly, storm induced berms are formed at the end of the backshore zone. Above this zone, the natural result of the aeolian process is the system of dunes. This part of the coastal zone is a viable environment for the fauna and flora and provides a natural protection against severe storm surges.

2.2 Storm surges

A storm is characterized by a system of violent atmospheric disturbances accompanied by high wind speeds of unusual direction, lightning, and heavy atmospheric precipitation (hail, snow, ice, rain). The terms hurricane, typhoon and cyclone are used to describe the system with high wind velocities (above 120km/h) in the Atlantic, the northeastern Pacific and in the Indian Oceans respectively. As the sea-surface temperature increases, these phenomena may become stronger [Trenberth 2007].

A threat for the coastal environments is the storm surge. As storm surge are defined the long gravity ocean surface elevation generated by the low atmospheric pressure and the high wind speeds during a storm. The wave length and duration depends on the intensity of the source cyclones, roughly, a couple of kilometers and several hours to one or two days respectively. After leaving their area of generation the storm surges may hit the coastlines causing intensive damage and flooding, especially when they coincide with high astronomical tidal level. In this study the term storm surge will be referred to the total water level fluctuation, thus including the tidal range (in the literature the terms storm surge and storm tide are used interchangeably with the lateral sometimes referring at the combined effect of surge and tide).

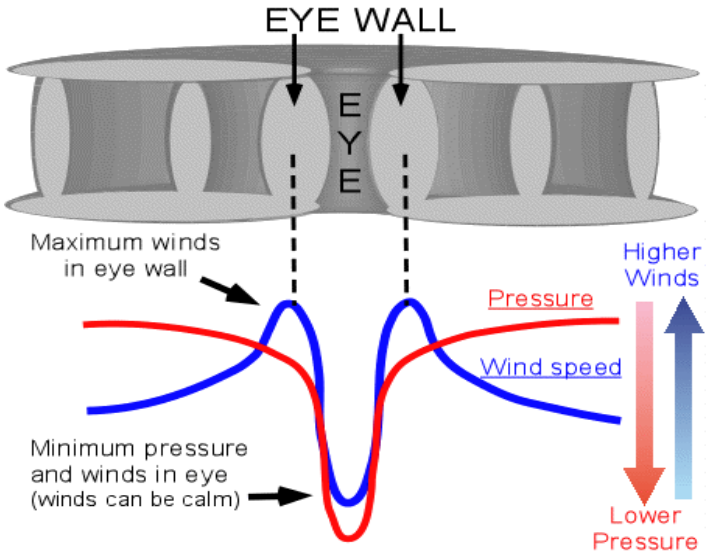

Figure 2.2: Cross-section of a hurricane system with the wind (blue lines) and the pressure (red lines) profiles. Figure obtained from the University of Illinois WW2010 Project, [1],

The storms are well organized systems with circular wind patterns around a low wind and pressure area, the eye of the storm (Fig. 2.2). In contrast, outside of the eye wall the atmospheric pressure and the winds are much more increased. As proceeding to the eye wall, the atmospheric pressure rapidly decreases while the gales increase. It is this abrupt change of the pressure that causes the uplift of water at places of low pressure and the corresponding drop at places with high pressure, deforming and then propagating the initial water surface elevation from deep to shallow water. Additionally, the induced wind stress increases the water level at the direction of the wind, the wind setup. Within the eye wall, the winds reach the maximum and suddenly at the eye drop even at the category of calm winds. While leaving the eye, both the pressure and the wind start increasing rapidly, with the winds obtaining a maximum outside of the eye wall and then start decreasing to the level of tropical storm [1].

According to Harris [1963] the processes that may alter the water level at tide water regions can be summarized to; **a.** the pressure effect (theoretically 1cm for each mbar of atmospheric pressure drop), **b.** the direct wind effect (the length of the long gravity wave is approximately four times the radius of the maximum winds), **c.** the effect of earth's rotation (the Coriolis force tends to bend the currents, increasing or lessening their amplitude), **d.** the effect of waves and **e.** the rainfall effect (amplification of the water level at rivers and estuaries). The propagation of the surge wave to shallow water is determined by the residence time at the continental shelf and the local bathymetry, thus influencing the flooding and the erosion of the coastal zone.

2.3 Long waves

The long or shallow water waves are the waves with wave length equal to more than twenty times the water depth. Some examples of long waves are the tsunamis, the river flood waves, the tidal waves, the seiches and the infragravity waves.

The infragravity waves (first observed by Munk; in Tucker 1950] have been observed in the nearshore zone with frequencies shorter than the incident waves, ranging from 0.001Hz to 0.05Hz. According to Longuet-Higgins and Stewart [1962, 1964] (in Van Dongeren et al. 2007) when the wave groups propagate over a horizontal bottom, they force a second-order bound wave which is in anti-phase with the short wave envelope. Over a slopping bottom the phase lag between the bound and the short waves is 180 degrees. This phase shift induces the energy transfer from the short waves to the bound wave, increasing the amplitude due to shoaling [Van Dongeren1997b in Van Dongeren et al. 2007]. In the breaker zone two mechanisms are proposed for the generation of the infragravity waves, due to the short waves dissipation; the moving position of the breaker point [Symonds et al. 1982] and due to the induced wave groupiness at the surf zone [Foda and Mei, 1981; Schaffer and Svendsen, 1988, in Van Dongeren et al. 2007].

The infragravity waves may influence the bottom profile or due to resonance the port operations. Aagaard and Greenwood [2008] mention that while the sediment is suspended by

the incident waves' orbital velocities and the infragravity waves act as the sediment transport mechanism, the lateral may dominate the total transport of the suspended sediment in the inner half of the surf zone.

2.4 Empirical, physical and numerical approximations of the coastal profile variations

In order to identify the response of the coastal system due to extreme or mild conditions and to assess the safety of the coastal system, a number of approaches have been summoned:

a) simple equations originating from curve-fitting, field observations and theoretical considerations [12],
b) physical [e.g. Vellinga [1983] and numerical models (e.g. Roelvink and Broker 1993),
c) more advanced real time storm forecast model schematizations (e.g. Baart et al. 2009),
d) the remote sense techniques (e.g. Argus [12]) in combination with numerical models (e.g. Van Dongeren et al. 2008).

2.4.1 Empirical beach and dune profile equations

The relatively stable coastal profile under similar conditions has been the subject of numerous studies (Bruun 1954; Saville 1957; Edelman 1968, 1972; Swart 1974; Dean 1977; in Kriebel and Dean 1985). As equilibrium profile can be defined the cross-shore profile of constant shape which is reached if it is exposed, for a sufficiently long time to constant wave and water level conditions [Van de Graaf 2006].

First, Bruun [1954] developed a model for the equilibrium beach profile by studying the coastal profiles of the coasts in Denmark and California. This power law relates the water depth as a function of the offshore distance [Van de Graaf 2006] as:

$$h = Ay^{(2/3)} \qquad [2.1]$$

where h = water depth
A = non-dimensionless constant related to the bed stability characteristics
y = offshore distance

Later on, Bruun [1962] expanded this statement also concerning the beach erosion in relation with the slow sea level rise under the absence of the longshore sediment transport. Graphically this could be presented by shifting the equilibrium profile upwards equal to the sea level rise, and landwards until the volume eroded from the beach face to be equal to the volume eroded offshore to the closure depth. This statement is known as Bruun's rule and is expressed as:

$$R_{\infty} = S\frac{L_a}{(h_a + B)} \qquad [2.2]$$

where R_∞ = equilibrium shoreline response to sea level rise
S = sea level rise
L_a = active length
h_a = active depth
B = freeboard

While this method is widely applicable concerning the small sea level rise over long periods, its limitation lays at the fact that it assumes a uniform deposition at significant distance offshore beyond the breaker zone, and that the upper limit of the active profile is not well defined [Dean et al. 2008]. According to Hayes [1967], during short period events (e.g. hurricanes), this sediment fluctuation should be limited to a short distance offshore of the surf zone.

Edelman [1968] proposed a similar to Bruun's rule graphical representation of the storm induced erosion and established the so called post-storm profile, in correlation with the breaking wave height, the maximum storm surge level and the equilibrium pre- and post storm profiles. Chiu [1977, in Kriebel and Dean 1985] states that as Edelman's theory does not interrelate the evolution of the profiles during the storm period, but with the maximum steady state surge level, it better describes the maximum potential storm induced erosion and not the time dependent sediment transport mechanism.

Later on, Edelman [1972] modified Bruun's rule for larger values of increased water level and for time varying storm surges. The time varying storm-induced profile is expressed as:

$$R(t) = W_b \ln\left(\frac{h_b + B_0}{(h_b + B_0 - S(t))}\right) \qquad [2.3]$$

with

$$B(t) = B_0 - S(t) \qquad [2.4]$$

where $R(t)$ = time varying profile
W_b = surf zone width
h_b = breaking depth
B_0 = original berm height
B_t = instantaneous berm height
$S(t)$ = storm surge level

Dean [1977] proposed three dominant destructive forces that would affect the equilibrium profile:

a) the wave energy dissipation per unit water volume
b) the wave energy dissipation per unit surface area
c) the uniform average longshore shear stress over the surf zone.

The observations from more than 500 profiles at the east coast and the Gulf of United States supported Bruun's law concerning the first dominant force, and proposed the exponent of 0.4 of [2.1] for the two lateral.

On the seaward limit of the long term (yearly or seasonal scales) profile fluctuation, Hallermeier (1978, 1981) proposed two depths and introduced the term of the closure depth h_c. The shallowest one (which is of higher applicability importance) was related with the limit of intense bed activity and the deepest one with the area seaward of which the lowest transport due to waves is observed [Dean et al. 2008]. Hallermeier related the closure depth with relatively rare wave conditions (0.14% of the time) as:

$$h_c = 2.28H_e - 68.5\left(\frac{H_e^2}{\left(gT_e^2\right)}\right) \qquad [2.5]$$

$$\text{with } H_e = \bar{H} + 5.6\sigma_H \qquad [2.6]$$

where h_c = closure depth
H_e = effective significant wave height
g = acceleration of gravity
T_e = effective wave period
$\bar{H}$ = mean annual significant wave height
σ_H = standard deviation of significant wave height

or independent of the wave period as:

$$h_c = 2\bar{H} + 11\sigma_H \qquad [2.7]$$

2.4.2 Physical experiments

As part of the dune safety assessment in the Netherlands Vellinga [1983 and 1986; also in WL| Delft Hydraulics 1978] performed a series of physical tests in the Delta flume concerning the impact at the Dutch coast of the 1953 and the 1976 storm surges. He extended the previous work implemented by Van de Graaf [1977] and concluded for the safety effectiveness concerning the erosion process related with the fall velocity scaling law [Van de Graaf 2006].

$$\frac{n_l}{n_h} = \left(\frac{n_h}{n_w^2} \right)^{0.28} \quad [2.8]$$

where n_l = ratio of the horizontal distance between the prototype and the model
n_h= ratio of the water depth between the prototype and the model
n_w= ratio of the bottom material fall velocity between the prototype and the model

and the profile curve

$$h = Ay^{0.78} \quad [2.9]$$

$$\text{with } A = 0.70 \left(\frac{H_0}{\lambda_0} \right)^{0.17} w^{0.44} \quad [2.10]$$

where A = non-dimensionless shape factor
H_0= deep water wave height
λ_0 = deep water wave length
w = bed material fall velocity

Based on the deep water significant wave height H_s during storm events, he correlated the breaking depth h_b as the limit at which the effective deposition may take place as:

$$h_b = 0.75 H_s \quad [2.11]$$

In case of no dune overtopping, Vellinga [1983] proposed that the slope above where the runup takes place and the dune scarp is formed is equal to 1:1. At the same study, it was observed that the profile deposition during storm conditions continues upon higher depths and with decreasing rate as approaching to the equilibrium state.

2.4.3 Numerical models

Kriebel and Dean [1985] proposed a numerical model in order to estimate the time varying storm surge and wave height during extreme storm events, showing its validity on idealized cases and by studying the effect of hurricane Eloise in Florida. They associated the surge level with the potential erosion mentioning that, while the surge level contributes implicitly (higher water level 'transfers' higher wave energy on the upper parts of the beach) to the erosion process it does not govern the time scales of response. Additionally, the increasing wave height increases the time of response as the surf zone becomes wider. Finally, they attest that, faster beach response is associated with the smaller grain size and larger potential erosion with the steeper beach face slope.

Steetzel [1993] developed a time-dependent numerical model for the simulation of the cross shore profile development during extreme events. The model DUROSTA has been tested on prototype, large and small scale conditions for varying storm conditions, and estimated favourably the profile development of coastal profiles with bars, with dunes or revetments, while the erosion volume above the storm surge level was underestimated.

In the report TUD 2009, the correlation between the numerical results from the DUROSTA model (see the report Deltares 2008) and the process-based XBeach numerical model (Roelvink et al. 2009) is investigated, by studying the dune erosion reduction during extreme storm surge conditions under the presence of large submerged tankers in the area of Delfland, the Netherlands. Both of the models estimated that the erosion volume was decreasing up to 55-65% (of the induced erosion volume without tankers), while differences were observed concerning the actual setback and the amount of the dune erosion (Tables 2.1 and 2.2).

Case	Dune erosion per running m (m^3/m)	Setback (m)	Erosion w.r.t D02 (%)	Hs (m) at 2m depth
D02 (no tankers)	240	80	100	4.9
D03 (6 tankers 75m gap, wind waves)	210	65	80	3.74
D06 (6 tankers 75m gap, swell)	230	75	95	4.49
D07 (5 tankers 150m gap)	230	75	95	4.38
D08 (7 tankers 50m gap)	180	50	65	2.92

Table 2.1: Numerical results of the DUROSTA model, concerning the dune erosion per running m (m^3/m), the setback (m), the percentage of erosion with respect to the 'no-tankers scenario' and the estimated Hs (m) without (case D02) and under the presence (cases D03 to D08) of the submerged tankers (data obtained from the report Deltares 2008).

Case	Dune erosion (m^3)	Dune erosion per running m (m^3/m)	Setback (m)	Erosion w.r.t D02 (%)	Hrms (m) at 2 m depth
D02 (no tankers)	404110	165	40	100	5.43
D03 (6 tankers 75m gap, wind waves)	270750	123	30	75	3.71
D06 (6 tankers 75m gap, swell)	282100	136	35	83	3.76
D07 (5 tankers 150m gap)	255700	132	35	80	4.25
D08 (7 tankers 50m gap)	171700	88	20	55	3.30

Table 2.2: Dune erosion amount (m^3), dune erosion volume per running m (m^3/m), setback (m), percentage of erosion with respect to the 'no-tankers scenario' and estimated Hrms (m) as computed from the XBeach model, without (case D02) and under the presence (cases D03 to D08) of the submerged tankers.

On the nearshore zone features development, Roelvink and Stive [1989] studied the effect of wave asymmetry, undertow, wave breaking induced turbulence and the short-infragravity waves' interaction, by comparing laboratory and numerical experiments. The results showed good agreement on the development of a barred beach and the importance of a more accurate simulation of these factors on the sediment transport processes.

Van Rijn et al. [2001] present the results of five numerical models in comparison with laboratory as well as field observations at Egmond, the Netherlands. The models were tested on their capability to estimate the morphological change due to storm and seasonal hydrodynamic conditions. Van Rijn et al. mention the reasonable capability of the models to simulate the profile evolution on the storm scale, while the models showed low skill when the larger seasonal experiments were performed.

The Argus program has been developed by the Coastal Imaging Laboratory of Oregon State University [14], in order to provide a safer and for longer periods (in comparison with the field measurements) monitoring technique for the coastal areas, especially during storm events. By collecting different types of digital images along the beach and the nearshore area, it has been demonstrated as a more feasible method to detect the evolution of the geological features located in the nearshore zone, by means of the waves and currents deformation. Van Dongeren et al. [2008] presented a model-data assimilation technique to estimate the nearshore bottom profile. They applied this method on a small-scale case, as well as on prototype scale for the areas of Duck in U.S.A for a short time span which included a storm event and in Egmond in the Netherlands for a period of 1.5 years. This technique proved to accurately represent the profile change and the applicability to estimate the sub and intertidal bathymetry by using remote data from radar and video observations.

3. DESCRIPTION OF THE STORM EVENTS AND THEIR IMPACT

3.1 Introduction

The history of the Netherlands is interrelated with the fight against floods. Kraker [2000] describes the human response from the disastrous storm surge in 1530 and the sporadic dyke repairing until the 20th century central and technically advanced setup of the flood defense system. This chapter starts with the description of the impact due to the 1953 storm surge which rearranged the flood protection perspective in the Netherlands. Then, the impact of the storm surge of 1976 is described. In section 3.4 we present the volumetric analysis and accordingly the areas where the 1976 storm surge event will be studied, while examining the characteristics of each area.

3.2 The Big flood of 1953 in the Netherlands

At the weekend from January 31st to February 1st in 1953 strong winds occurred at the North Sea approaching Faeroe Islands from the West to West-Southwest and then plunged southeastwards to the German Bight. The highest winds were recorded around midnight of 31st to 1st January, ranging from 100-130 knots which were regarded as 'phenomenal' at the time [Lamb 1991].

Gerritsen [2005] states that it was the track of the storm and its slower propagation that was different among the predecessor storms of 1894, 1906 and 1916. Because of this track, prevailing northwest winds led to higher and more intense surge.

The forecast of the storm was reasonably accurate and gave the authorities 18 hours lead to take mitigation actions [Van den Dool et al. 2001]. The Netherlands' storm tide warning service (SVSD) that was funded in 1921 and in cooperation with the Royal Netherlands Meteorological Institute (KNMI) should have issued warnings for high water level threat by telegrams (30 subscriptions at this time among them limited at the delta area) and radio broadcasts. The fact that the peak of the storm took place at the weekend between 03:00 and 04:00 in the morning on Saturday left these services unavailable.

The most dangerous wind conditions threatening the Dutch coast are the North-Northwestern gales. The 1953 storm surge was the result of severe winds in excess of more than 50 knots (approximately 26m/sec) for more than 24 hours, and at this event they were the winds that were more important than the pressure and caused the surge [Van den Dool et al. 2001]. Wolf and Flather [2005] state that the elongation of the storm to the North resulted to long fetch and generated large wind waves.

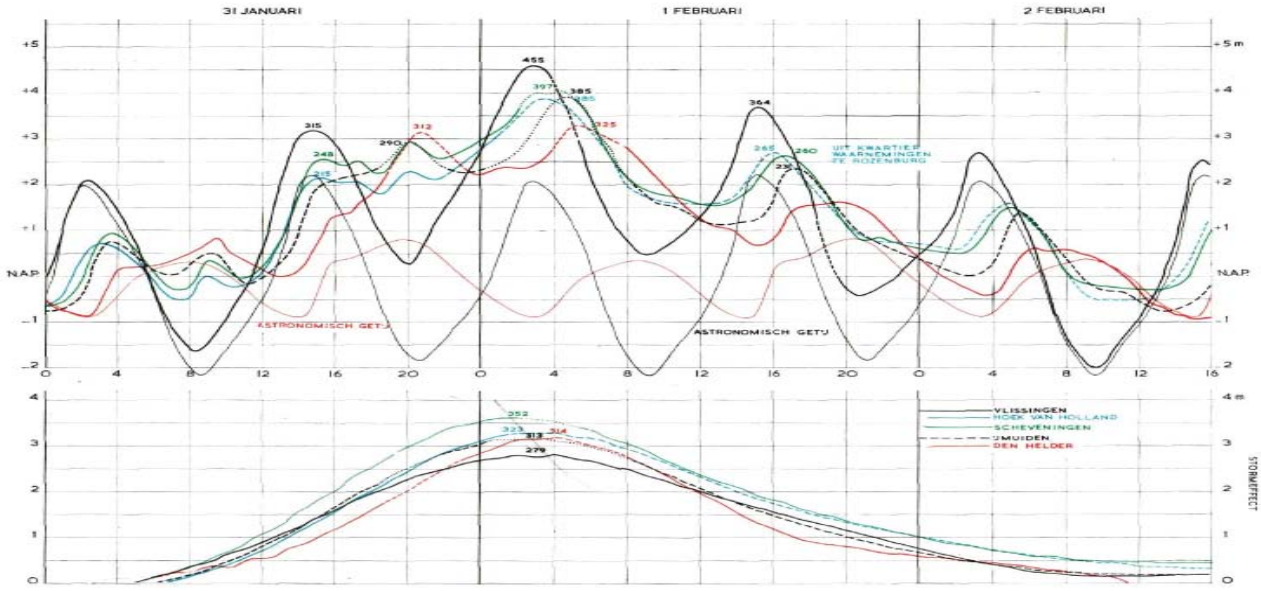

Figure 3.1: Measured water level (upper panel) and surge level (lower panel) during the 1953 storm surge in Vlissingen (black line), Hoek van Holland (blue line), Scheveningen (green line), IJmuiden (dashed black line) and Den Helder (red line) [from the report Verslag over de stormvloed van 1953, KNMI and Rijkswaterstaat].

The surge level has been recorded at many locations in the North Sea. In the inlet of Oosterscheldt the actual water elevation was N.A.P. +5 m [Donker 1993 in Van de Dool et al., 2001]. Fig. 3.1 depicts the water level as recorded by the KNMI and Rijkswaterstaat. The highest surge level was measured in Vlissingen equal to N.A.P. +4.55 m, followed by Scheveningen where the tidal surge raised up to N.A.P. +4 m. While, no available wave data were found, some sparse data over the North Sea show that the significant wave height was up to 12 feet (approximately 4.1 m) at the first high tide and 9 feet (approximately 2.7m) on the second high tide [Smith 1954 in Wolf and Flather, 2005] at the Low Countries. The 1953 event was assumed as an at least 1 in 50 year wave event [Wolf and Flather 2005].

The maximum surge level coincided with high spring tide, exceeded the design load that the dykes could withstand and led to 150 dyke breaches, mainly because of overtopping of the primary sea defense dykes (Fig. 3.2). In the Netherlands alone 1835 people died, 100000 were evacuated and 136500 ha of land were inundated [Gerritsen 2005]. The total damage was estimated at that time at 895 million Dutch guilders. Higher impact was recorded at the southern part of the country, due to the lack of warning, the geometry of the North Sea and the nature of the delta area, where the increased water level got trapped.

According to Van de Graaff [1977] (also in WL| Delft Hydraulics 1978), the amount of eroded material which triggered due to the 1953 storm surge would have reached the $100m^3/m$, meaning that the dune erosion would be equal to 20-30m, as the water level was approximately 1.0m below the maximum level assumed in the design conditions. For further information, the reader is referred to the T.A.W. archives, which describe the pre-storm and

the post storm profiles concerning the impact of the 1953 storm surge. Measurements for historical storm events or the coastal position during normal conditions may be found since the late 19th century. Over the cross-shore direction, these measurements are extended from the shallow nearshore zone until the level above the dune foot and over the longshore

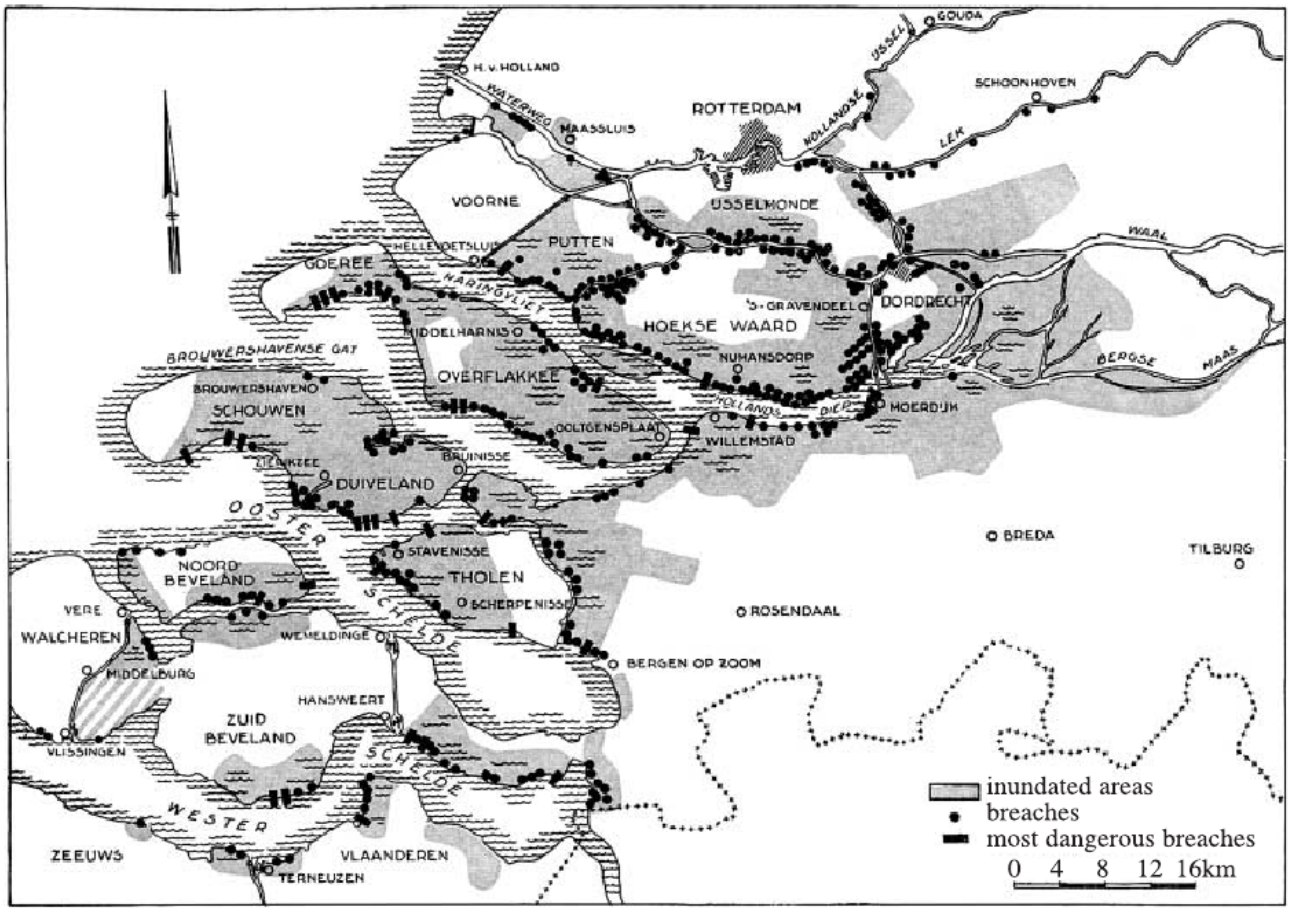

Figure 3.2: The aftermath of 1953 storm surge at the southern part of the Netherlands (source: Rijkswaterstaat, in Gerritsen 2005).

direction may describe the pre and post storm condition of an area and the damage that have been recorded (e.g. breaches).

As a lesson for civil action, it is worth mentioning that at places were the inhabitants and the water boards reacted immediately the catastrophe was limited, while at neighboring areas where indecisiveness dominated the calamities were extended. The struggle against water (in places even 3 meters above the normal tidal level) continued for many days after the storm surge had passed, as the tide was penetrating and receding twice a day causing further damage [Gerritsen 2005].

3.3 The 1976 storm surge

In the last days of December 1975 a series of warm front wave depressions broke away and traveled quickly eastwards from the Atlantic system to central Europe. A strong depression moved from the British Isles to the west coast of Denmark in the night hours on the 2nd of January to the 3rd, and caused the wind at the North Sea and over the Netherlands to gain hurricane force [from the weather report of KNMI considering this event]. The strongest gradient winds reached almost 100 knots (approximately 51m/sec) from the North - West over the central and eastern parts of the North Sea in the morning hours of January 3rd [Lamb 1991]. In the Netherlands, the strongest gales during this storm event were recorded in Vlissingen (station 310) ranging up to 25.8 m/sec and originating from the South-West (Fig. 3.3); these gales were the seventh highest measured gales for the period 1962 to 2002 (KNMI).

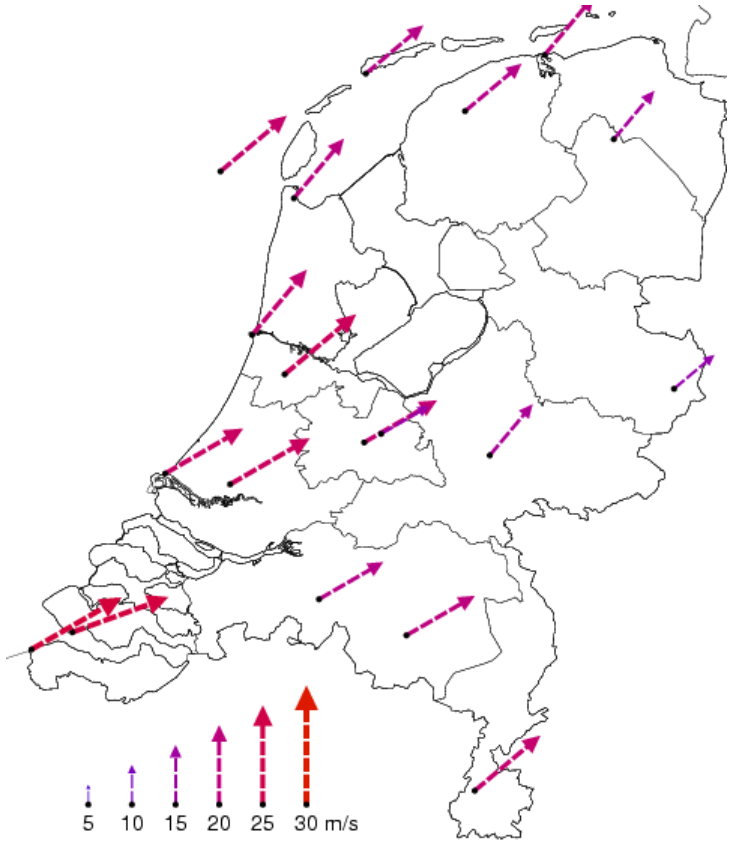

Figure 3.3: Wind field during the 1976 storm at 2-1-1976 24:00 GMT. The highest measured gales concerning this storm event were recorded in Vlissingen during this time span (bottom left corner of the figure). Figure obtained from KNMI.

In the Netherlands, the average probability of occurrence of the water level had been estimated equal to 1/20 years, slightly exceeding the level of the dune foot (about N.A.P.+3m) [WL| Delft Hydraulics 1978]. Figure 3.4 demonstrates the storm surge level obtained from five tidal records along the Dutch coast. First, the surge hit the northern part of the Netherlands

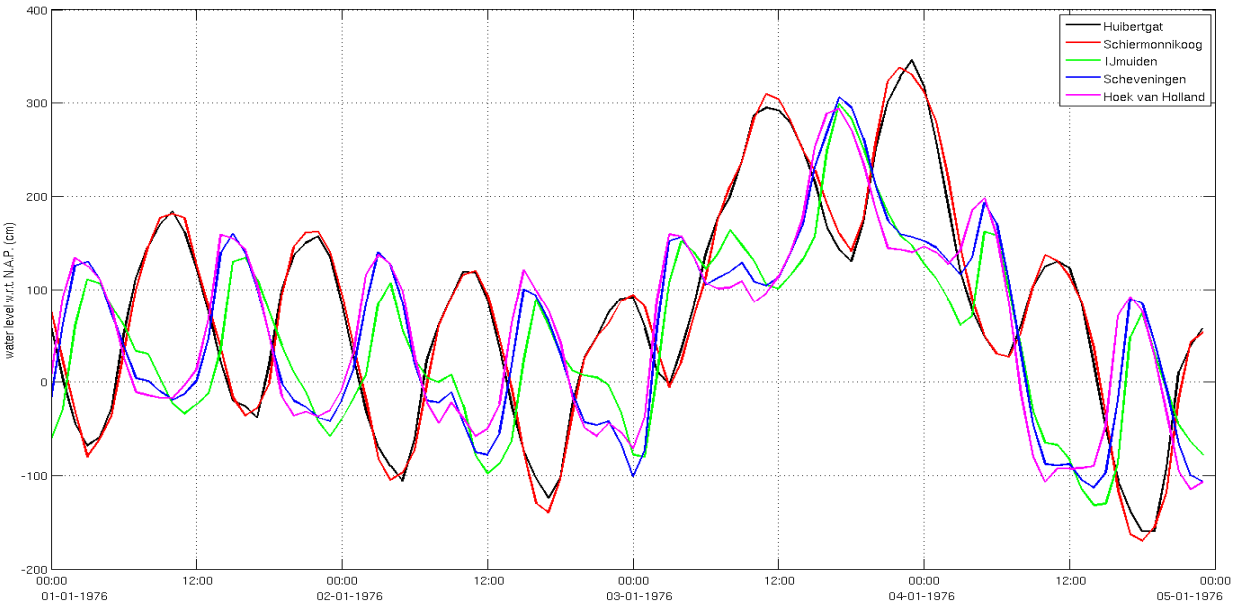

Figure 3.4: Measured water level from the 1-1-1976 until the 5-1-1976. Starting from the North where the 1976 storm surge was more severe; Huibertgat (black line), Schiermonnikoog (red line), IJmuiden (green line), Scheveningen (blue line) and Hoek van Holland (magenta line).

where the impact was more severe (in contrast with the 1953 storm surge) and after half an hour, hit the central part of the North Holland province. Often in the literature, many upcoming storm surge events are investigated and correlated with the consequences due to the 1976 storm surge [Etri and Mayerle 2006].

While the impact in the Netherlands was not of the same magnitude as in 1953, it recalled of the disaster that occurred 23 years before. The storm found the government-state more prepared and the citizens on position to reinforce the dykes. The fatalities were not absent; 11 people died when a vessel sank off the Dutch coast and 2 people died on land. The average amount of erosion above the maximum storm surge level was $32m^3/m$ over the whole Dutch coast [Steetzel 1993] with an average dune retreat of 10m.

3.4 Overview of the dune erosion during the 1976 storm surge

Since 1963 the Dutch coastline is monitored twice a year (once in summer and once in winter) as part of the Jarkus project of Rijkswaterstaat. Measurements are performed in average every 200 m over the longshore direction and from the 10m depth contour until the top of the first dune. Additionally, every five years accessional measurements are performed

up to 5 km offshore [Damsma 2009]. Prior to the initiation of the Jarkus project, the measurements were limited from a nearshore depth of N.A.P.-2m until above the dune foot.

At the period between October of 1975 and the late January 1976, Ir. Rakhorst performed a series of measurements in nine areas of the North Holland province following the Jarkus transects. Starting from the North they are; Julianadorp (568 to 648), Groote Keeten (1085 to 1175), Bergen aan Zee (3400 and 3700), Egmond (4000 to 4100), Castricum aan Zee (4500), Wijk aan Zee (4900 to 5000), Bloemendaal (5900 to 6100) and two sites in Zandvoort (6500 and from 7000 to 7100). Depending on the area three or four sets of measurements were performed, one or two in late 1975 and two between the 4th and the 26th of January 1976. In this study, the most recent measurements before and after the storm were selected, which cover the period between the 19th of December 1975 to the 8th of January 1976.

On average, the range of the pre-storm measurements extends between the low water line to an area above the dune foot (e.g. from N.A.P.-2m to N.A.P.+8m). Concerning the post storm profile, the data range varies, depending on the impact at each area and the slope of the dune profile. In many cases the steep post storm profile precluded the survey even above N.A.P.+3m. Due to the post storm data restriction and in order to obtain a reflection of the measured amount of erosion, the post storm data are related with the pre-storm ones, and the

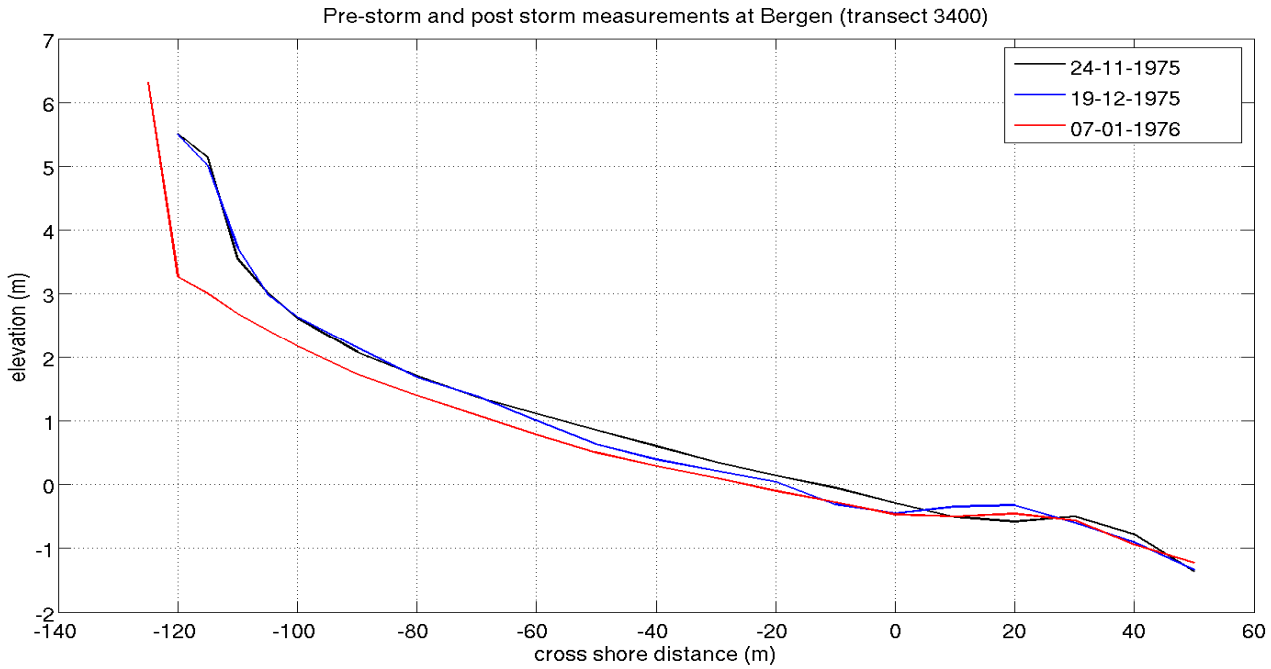

Figure 3.5: Pre-storm and post storm measurements of Jarkus transect 3400, in Bergen as performed by Ir. Rakhorst at 24-11-1975 (black line), at 19-12-1975 (blue line) and at 07-01-1976. For a preliminary assessment of the storm induced volume change, the deposited volume is calculated from the highest pre-storm landward point (x=-120m) until the deepest seaward point between the pre-storm and the post storm profiles (x= 50m).

erosion volume is calculated from the highest landward point of the pre-storm profile, until the minimum most seaward point between the two profiles (e.g. the volume described between the cross shore points x=-120m to x=50m in Fig. 3.5).

Table 3.1 presents the cumulative effect of the 1976 storm surge at the nine sites along the North Holland province. It is observed that over the longshore direction, the volume change difference varies; in Julianadorp the maximum volume change equals to 32m^3/m (transect 588) while in a distance of 200m (both to the North and to the south) the volume difference is reduced to less than 10m^3/m (transects 568 and 608). In Bergen aan Zee, two measurements

Table 3.1: Measured volumes in nine sites of the North Holland province prior and after the 1976 storm surge. The last three columns present the difference at the elevation and the cross-shore distance.

		volume (m^3)			pre storm	post storm	
	transect	pre storm	post storm	Difference (m^3)	hup-hlow	hup-hlow	xup-xlow (m)
Julianadorp	568	309.88	319.55	9.67	7.97	5.01	150
	588	270.10	238.10	-32.00	5.97	4.26	150
	608	265.60	273.30	7.70	6.95	4.48	150
	628	324.30	337.30	13.00	7.2	4.61	165
	648	556.83	562.05	5.22	7.01	6.83	210
Groote Keeten	1085	252.40	269.88	17.48	6.1	4.83	145
	1115	251.18	276.90	25.73	6.61	4.9	150
	1175	255.20	261.28	6.07	6.29	4.61	135
south of Bergen Aan Zee	3400	358.85	312.55	-46.30	6.84	4.61	170
	3700	299.73	293.10	-6.63	6.31	4.29	175
Egmond	4000	207.80	210.30	2.50	7.46	4.33	105
	4050	334.80	291.15	-43.65	6.68	4.55	130
	4100	239.30	234.68	-4.63	7.61	4.49	105
Castricum aan Zee	4500	254.05	259.20	5.15	6.51	4	130
North of Wijk aan Zee	4900	245.15	224.40	-20.75	6.74	4.12	105
	4950	336.13	298.30	-37.83	6.18	4.24	145
	5000	241.68	248.35	6.67	6.41	4.3	125
Zeeweg Bloemendaal until Parnassia beach	5900	294.97	288.95	-6.02	8.21	6.11	140
	5925	266.40	295.35	28.95	7.85	4.93	145
	5950	309.48	306.63	-2.85	8.86	5.72	130
	5975	242.58	226.68	-15.90	8.38	4.33	120
	6000	226.65	244.30	17.65	8.48	4.23	125
	6025	240.60	269.38	28.78	7.26	4.5	135
	6050	275.75	268.55	-7.20	9.04	4.7	130
	6075	232.83	245.50	12.68	7.47	4.42	120
	6100	215.58	240.20	24.63	7.31	4.43	125
North of Zandvoort, Boulevard Barnaart	6500	400.90	360.55	-40.35	6.57	6.8	195
Zandvoort	7000	270.50	255.30	-15.20	7.15	4.73	130
	7050	286.63	259.95	-26.68	7.46	4.74	160
	7100	286.13	267.03	-19.10	7.93	4.69	105

had been performed over a distance of 3000m. The overall highest volume difference has been calculated in this site in transect 3400 (46.30m^3/m) as an effect of the 1976 storm surge, followed by the transect 4050 in Egmond (43.65m^3/m) and the transect 6500 in North Zandvoort (40.35m^3/m). In total nine measurements had been performed in the area close to Bloemendaal, with an interval of 250m over the longshore direction. In this site the volume difference varies from 3m^3/m (transect 5950) up to 29m^3/m (transect 5925). Due to this longshore variability along the North Holland province (Fig.A.1 in App. A), three sites are going to be studied: the site in Julianadorp where the volume difference ranges considerably; the site in Bergen aan Zee with the highest measured impact and the site in Castricum, which is ranked among the areas with the lowest impact.

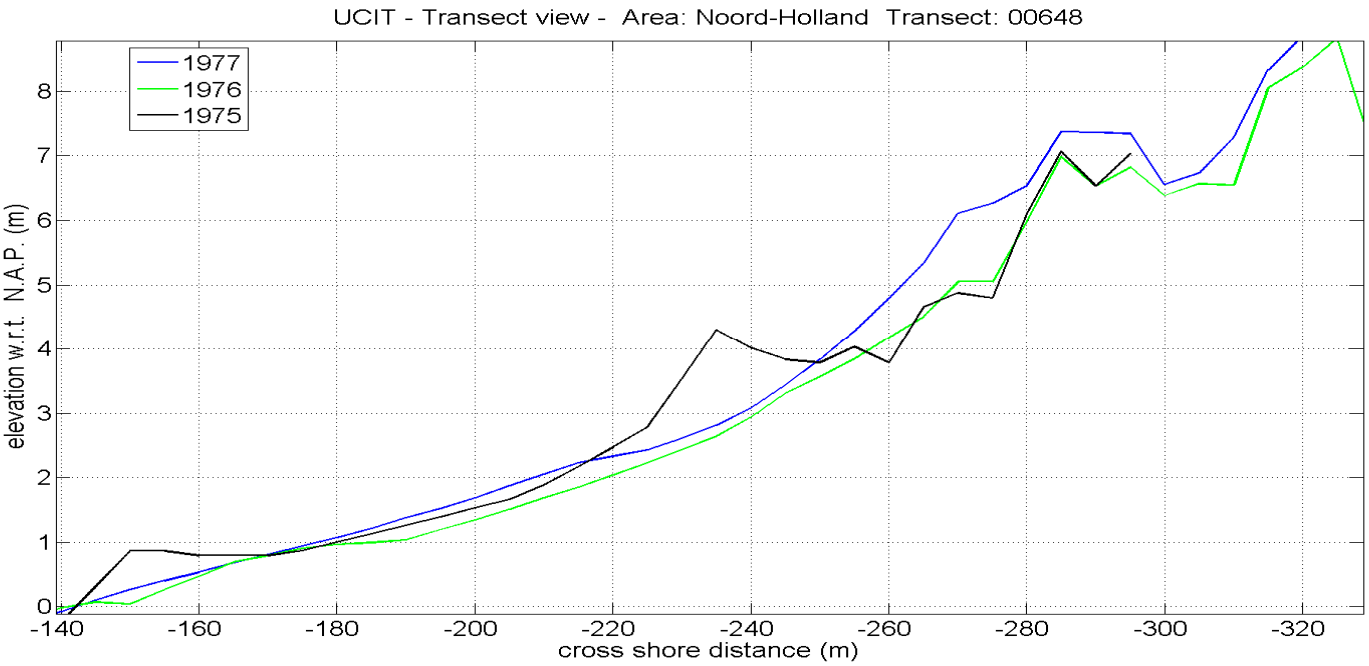

Figure 3.6: Summer profiles of the transect 648 in Julianadorp, in 1975 (black profile), 1976 (green profile) and 1977 (blue profile). For an extended view see Fig. A.3, App. A.

The site in Julianadorp is located close to the tip of the Holland coast. This area is prone to continuous erosion due to the strong ebb tidal currents originating from the Marsdiep inlet, and therefore series of groins have been constructed along the coastline. The beach profile consists of four dune rows with the seaside one extending up to N.A.P.+7m, the second one up to N.A.P.+9m, the third one up to N.A.P.+10 and the most landward one up to N.A.P.+16m (see also Fig. A.3 in App. A). The offshore area is described by an non-uniform bottom profile (see Fig. A.2 in App. A for a relative comparison of the longest available bottom profiles concerning the three study areas, as measured at the summer of 1976) which is interrupted by a system of bars and troughs due to the strong tidal currents. The 1976 summer profile of transect 648 (green profile in Fig. 3.6), demonstrates that the maximum dune retreat was approximately 25m; the backshore berm was completely eroded (the area around x= -240m), while the area above N.A.P.+4.5 was not affected significantly. Furthermore, the foreshore area has been eroded (x= -150m) and the offshore bar (around x= 100m) was shifted offshore 5m. During the next year (blue profile) the system tends to restore the pre-storm condition showing a trend for onshore migration of the geological features (e.g. the berms at x= 450m and x= 600m, Fig. A3 in App. A). Heading to the North, the dune retreat was measured equal to 8m in transect 628 (Fig. A.7) and 10m in transects 608 and 568 (Fig. A.4 and Fig. A.6 respectively). Similar response with the area around transect 648 was recorded at the measured profile of transect 588; under the presence of the backshore berm the dune erosion was restricted to 5m, while the backshore berm was eroded (Fig. A.5).

In contrast with the profile in Julianadorp, the offshore bottom profile of the Jarkus transect 3400 in Bergen is significantly smoother (Fig. A.2). The offshore area is described by a flat

bottom profile which is interrupted by the presence of an offshore bar and trough close to the N.A.P.-5m depth contour (x= 500m, see Fig. A.9 in App. A) and a second system of a bar and trough at the inner surf zone (around x= 100m). Two series of dunes are present with the seaside dune extending up to N.A.P.+16m and the second one up to N.A.P.+12m. According to the most recent to the storm measurements performed by Ir. Rakhorst, the dune retreat was measured equal to 10m (Fig. A.10 in App. A) and the backshore zone has been deepened up to 0.8m. The summer profile of 1976 (green profile in Fig. 3.7) presents that significant deposition took place at the foreshore and partial degradation of the offshore bar, due to the presence of the storm in early January. The degradation of the profile continued and the next year (blue profile), with the bar which is located close to the shoreline to be shifted further offshore and the bar located at the end of the surf zone to appear more degraded.

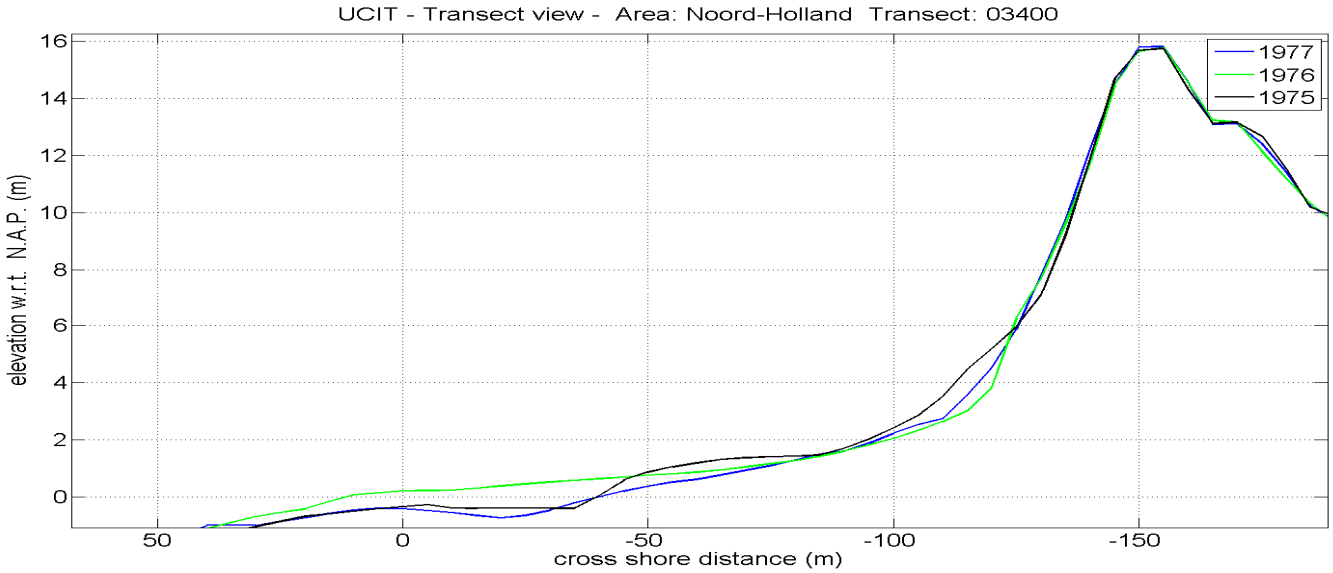

Figure 3.7: Summer profiles of the transect 3400 in Bergen aan Zee in 1975 (black profile), 1976 (green profile) and 1977 (blue profile). For an extended view see Fig. A.9, App. A.

Further to the south the post storm profile of transect 3700 demonstrates that the backshore zone was submerged 0.7m in comparison with the measured pre-storm profile and that significant deposition took place at the wet foreshore zone (Fig. A.11).

The 1976 summer profile of the Jarkus transect 4500 in Castricum (blue profile in Fig. A.2) is characterized by a flatter and shallower offshore profile. In the area around 700m from the MKL, a wide trough is present, followed by a system of bar and trough as approaching to the inner surf zone (Fig. A.12 in App. A). Due to the storm, significant deposition has taken place at the nearshore trough (at x= 230m; Fig. A.12 green profile), while the adjacent bar is shifted offshore, resulting to sedimentation of the offshore trough (x= 700m). During the next year (blue profile in Fig. A.12), a wide trough was present at this area as the previously formed nearshore bar was shifted offshore. Moreover, the trough located further offshore became

narrower due to the landward accretion that took place around this area. Slower deformation appears at the backshore zone. According to the measurements (between December 1975 and five days after the storm, see also Fig. A.13 in App. A), the dune retreat has been measured equal to 10m, and significant amount of sediment has been deposited over the foreshore; the maximum beach face elevation is estimated up to 0.70m. As no data are available above the N.A.P.+6m, the summer profiles of 1975 and 1976 (Fig. 3.8) witness that the dune had been eroded up to N.A.P.+12m, a pattern that did not alter one year later.

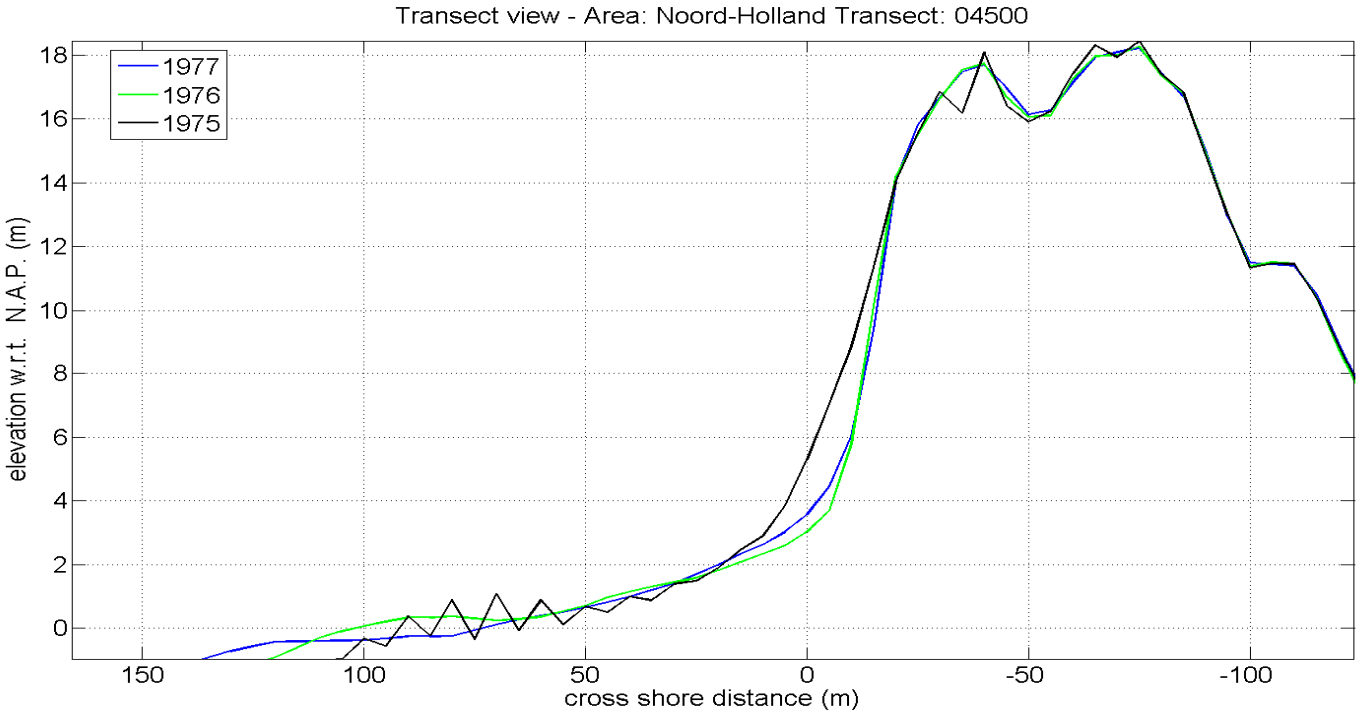

Figure 3.8: Three summer profiles of the Jarkus transect 4500 in Castricum aan Zee in 1975 (black line), 1976 (green line) and 1977 (blue line).

Figure 3.9 presents the natural variability of the selected sites over the years 1974, 1975, 1976, 1980 and 1981, including the most recent measurements before and after the storm. Prior to the 1976 storm surge, the general pattern of the volume change demonstrates an abrupt fall in most of the cases, with the profile 3700 in Bergen to appear as the most prone site to erosion after 1980. In contrast, before the 1976 storm surge the profile 648 in Julianadorp shows a tendency to shrink, but during the winter of 1975 the volume change remained constant, which is not the case for the rest of the studied areas.

After the storm event of 1976 and until 1981, the most non-uniform volumetric pattern appears in Julianadorp, probably due to the presence of the groins. The Jarkus profiles 588 and 628 regained a significant amount of the eroded sediment until the summer of 1976 and retained this volume change until 1981. It must be noted that the eroded amount of sediment

at the profile 588 was one of the highest among the available measurements (see Table 3.1). At the transect 648, the volume change due to the storm was minor, but significant sediment has been eroded until the summer of 1976. Later on the volumetric pattern changes and this transect shows a tendency to accrete, while after 1980 the volume change is further reduced. Due to the bathymetry and the presence of the groins, this area is recommended in order to examine the validity of the XBeach model. It is not only the interaction of the coastal structures that makes this area interesting for numerical validation scenarios. Due to the rich bathymetry and the longshore induced gradients due to the presence of the groins, it is recommended to perform both 1D and 2D morphodynamic simulations in order to evaluate

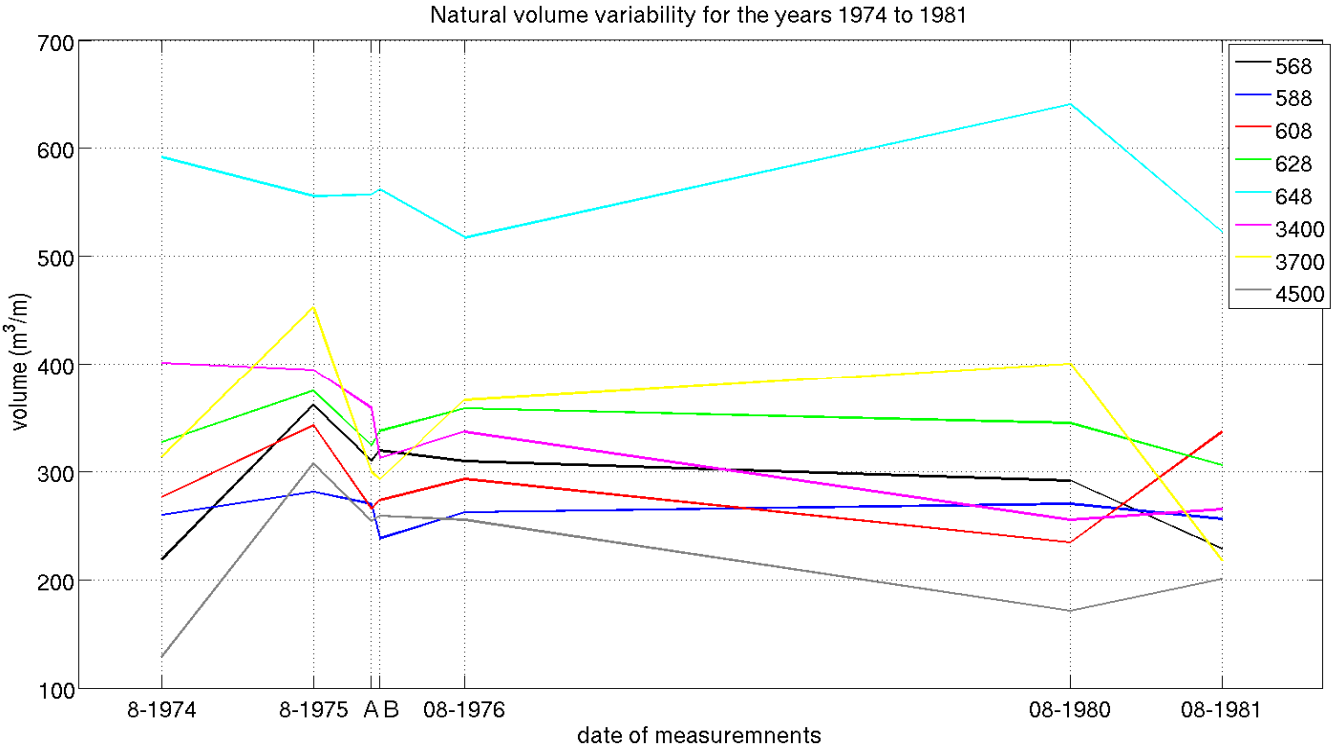

Figure 3.9: Natural volume variability for the sites in Julianadorp (transects 568 to 648), Bergen (transects 3400 and 3700) and Castricum (transect 4500), from 1974 to 1981. The points A and B demonstrate the state of the dunes before (December 1975) and after (January 1976) the 1976 storm surge.

the different storm induced profile patterns. The profile 648 with the entire degraded backshore berm and the relatively unaffected short dune, will be examined in order to address the performance of the XBeach model and the operational model chain.

Both of the measured profiles in Bergen appear accreted after the summer survey of 1976. While the volume change of the profile 3400 was the highest that had been measured, a relative rapid sediment recovery is observed until the summer of 1976, followed by a steep negative rate of the volume change until the summer survey of 1980. In contrast, the

volumetric change of transect 3700 seems to increase until the summer of 1980 and afterwards a rapid drop of the volume change is observed. Further to the south, the profile 4500 in Castricum was characterized by a continuously and steep negative volume change until the summer of 1980, while later on the volume change appears increased.

The volume variability (Fig. 3.9) of the sites in Bergen (transect 3400) and in Castricum (transect 4500) demonstrate a similar pattern on the evolution of the coastal response. Both of the sites consist of a system of bars and troughs next to the offshore zone. This system may lead to dissimilar coastal patterns along the coastline. Most important, the erosion volume magnitude of the two sites, pointed out for Castricum low volume loss and for the site in Bergen, one of the highest recorded volume loss during the 1976 storm surge. For a model validation skill, these two areas are going to be examined, in order to conclude on the capability of the model to estimate different responses of the coastal zone.

4. DESCRIPTION OF THE DELFT3D AND THE XBEACH MODELS

4.1 Introduction

In the current study two numerical models have been used in order to simulate the 1953 and the 1976 storm events, while the operational model suite is designed to include additional numerical models for weather forecasting (GFS [13]) and the calculation of ocean swell (WAVEWATCH III™ [Tolman 1997, 1999, 2009]). The Delft3D model will be applied to simulate the surge due to the pressure and wind disturbances locally at the North Sea for the 1953 storm, and globally for the 1976 storm. The dune impact as a result of the 1976 storm event is simulated with the XBeach model by accounting for the varying flow and wave conditions at the final nested grid of the operational model train (a further description of the operational model setup is presented at Chapter 5).

4.2 Delft3D model suite

The Delft3D model has been developed by WL|Delft Hydraulics and Delft University of Technology. It is a model suite capable of simulating the hydrodynamics and morphodynamics on coastal, fluvial, lake and estuarine environments, integrating the simulation of tasks for water quality and ecology. In this study two modules were applied in order to investigate the hydrodynamic conditions during the 1953 and the 1976 storm events in The Netherlands; the Delft3D-Flow [Lesser et al. 2004] and the Delft3D-Wave [the SWAN model, Booij et al. 1999] modules.

4.2.1 Delft3D-Flow module

4.2.1.1 Hydrodynamic implementation

The Delft3D-Flow module solves the 2D or 3D unsteady shallow water equations, derived from the three dimensional Navier Stokes equations for incompressible free surface flow on a Cartesian rectangular, orthogonal curvilinear or spherical grid. The model provides the option for non-hydrostatic or hydrostatic simulations, the latter when the gravitational acceleration is assumed larger than the vertical accelerations.

$$\frac{(\partial P)}{(\partial \sigma)} = -\rho g h \qquad [4.1]$$

where P = pressure [Pa]
σ = vertical sigma coordinate
ρ = local fluid density including salinity, temperature and sediment [kg/m^3]
g = gravitational acceleration [m/sec^2]
h = water depth [m]

The horizontal momentum equations over the x and y directions are given respectively as:

$$\frac{\partial U}{\partial t} + U\frac{\partial U}{\partial x} + V\frac{\partial U}{\partial y} + \frac{\omega}{h}\frac{\partial U}{\partial \sigma} - fV = \frac{-1}{\rho_0}P_x + F_x + M_x + \frac{1}{h^2}\frac{\partial}{\partial \sigma}\left(v_V \frac{\partial u}{\partial \sigma}\right) \qquad [4.2]$$

$$\frac{\partial V}{\partial t} + U\frac{\partial V}{\partial x} + V\frac{\partial V}{\partial y} + \frac{\omega}{h}\frac{\partial V}{\partial \sigma} - fU = \frac{-1}{\rho_0}P_y + F_y + M_y + \frac{1}{h^2}\frac{\partial}{\partial \sigma}\left(v_V \frac{\partial v}{\partial \sigma}\right) \qquad [4.3]$$

(1) (2) (3) (4) (5) (6) (7) (8) (9)

where U, V = Generalized Lagrangian Mean velocity components [m/sec]
ω = vertical velocity component in sigma coordinate system [sec^{-1}]
h = water depth [m]
f = Coriolis coefficient [sec^{-1}]
ρ_0 = reference water density [kg/m^3]
$P_{x,y}$ = horizontal pressure components under Boussinesq approximation [Pa]
$F_{x,y}$ = horizontal Reynold's stresses components [m/sec^2]
$M_{x,y}$ = external source or sink of momentum components [m/sec^2]
v_V = vertical kinematic viscosity [m^2/sec]

with $U = u + u_s$ [4.4]

$V = v + v_s$ [4.5]

where u, v = Eulerian velocity components
u_s, v_s = Stokes' drift components

The horizontal momentum equations consist of the following terms:

(1) = velocity gradients
(2), (3), (4) = advective acceleration terms
(5) = Coriolis force
(6) = barotropic pressure terms
(7) = horizontal Reynold stresses
(8) = external forces
(9) = vertical Reynold stresses

the depth averaged continuity equation is given by:

$$\frac{\partial \zeta}{\partial t} + \frac{\partial\left[h\bar{V}\right]}{\partial y} = S \qquad [4.6]$$

where S = contributions per unit area due to withdrawal of water, evaporation and precipitation
$\bar{V}$ = GLM velocity [m/sec]
ζ = water surface elevation above reference datum [m]

4.2.1.2 Boundary conditions

The boundary conditions may be defined as water levels, velocity, discharges, water level gradients (Neumann) or weakly reflective (Riemann) constituents. In order to account for the tidal level fluctuations at the larger of the nested numerical domains (see Chapter 5), in this study the boundary conditions are defined as uniform over the water depth, open, astronomical water levels by importing the amplitude and the phase of the tidal components. Additionally, the river discharges are defined as regular non-equidistant flows.

4.2.1.3 Physical parameters

As input the user may define a number of physical parameters as the acceleration of gravity, the water and air density, temperature, atmospheric pressure, wind drag coefficient, bed roughness and eddy viscosity. In this study the wind and pressure fields were the primary force in order to describe the atmospheric conditions during the storm events. The space varying wind and pressure fields obtained from the HIRLAM project and the ECMWF re-analysis database (see Chapter 5) were defined on the hydrodynamic grid of the Delft3D-Flow model. The storm surge level is the result of the wind and pressure fields in combination with the user defined astronomical tidal level.

4.2.2 Delft3D-Wave module

Along with the flow computation performed by the Delft3D-Flow module it is possible to combine the effect of waves. The wave module that is used in this study is a graphical user interface for the open source, third generation, spectrum model SWAN [Booij et al. 1999, Holthuijsen 2007, [9]]. The wave characteristics are computed and interrelated with the flow module, in order to account at each timestep for the interaction between the depth, the flow velocities, the water level and the waves without including the bed update. The SWAN model may run at the same rectilinear grid of the flow, allowing for a more convenient simulation of the hydrodynamic conditions.

The SWAN model solves the conservation of the action density, instead of the energy density, as the action density is conserved under the presence of currents, while the energy density does not. The action density is equal to the quotient of energy density over the relative radian frequency:

$$N = \frac{E}{\sigma} \qquad [4.7]$$

where N = action density
E = energy density
σ = relative radian frequency

and the action balance equation in Cartesian co-ordinates is equal to:

$$\underset{(1)}{\frac{\partial N}{\partial t}} + \underset{(2)}{\frac{\partial c_x N}{\partial x}} + \underset{(3)}{\frac{\partial c_y N}{\partial y}} + \underset{(4)}{\frac{\partial c_\sigma N}{\partial \sigma}} + \underset{(5)}{\frac{\partial c_\theta N}{\partial \theta}} = \underset{(6)}{\frac{S_{total}}{\sigma}} \qquad [4.8]$$

with $c_x = c_{g,x} + U_x$ [4.9]

$c_y = c_{g,y} + U_y$ [4.10]

where N = action density
c_x , c_y = propagation velocities in x and y direction
$c_{g,x}$, $c_{g,y}$ = group velocities in x and y directions
θ = wave direction
σ = relative radian frequency
S_{total} = source term of energy density

The action balance equation consists of the following terms:

(1) = action balance change
(2), (3) = propagation of action balance in x and y directions (shoaling)
(4) = frequency shift due to variations in depths and currents
(5) = depth and current induced refraction (diffraction is optionally included)
(6) = source term including wave generation, dissipation and non-linear wave-wave interactions.

4.3 XBeach model

The XBeach model [Roelvink et al. 2009] is an open source, process based, morphodynamic numerical model which can be used as a standalone model or in combination with other operating suites (e.g. MOPRHOS-3D) for an integrated storm induced coastal hazard mitigation (e.g. the operating system in The Netherlands [Baart et al. 2009]; and in Southern California, U.S.A. [Barnard et al. 2009]). The model solves the 2D horizontal equations for wave propagation, flow and sediment transport, accounting for varying wave and flow boundary conditions and the varying wave height (surf beat) in order to estimate the dune erosion during extreme events.

4.3.1 Coordinate system and grid setup

The coordinate system of the XBeach model is defined on a world coordinate reference system, with the x-axis oriented perpendicular and the y-axis parallel to the shoreline, by defining the origin (x_{ori} and y_{ori}), and the orientation alpha counter-clockwise with the x-axis (Fig. 4.1).

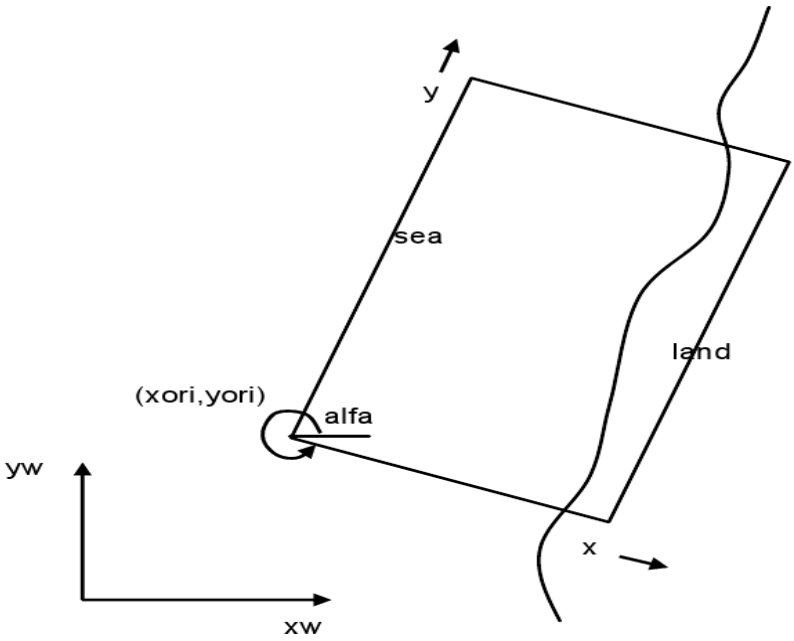

Figure 4.1: The coordinate system of the XBeach model (re-printed after Roelvink et al. 2009).

The numerical domain is a rectilinear, non-equidistant, staggered grid where the bed levels, water levels, water depths and concentrations are defined at the center of the cells and the velocities and sediment transports at the cell interfaces. Additionally, in the wave energy balance, the energy, the roller energy and the radiation stress are defined at the center of the cells and the radiation stress gradients at the cell interfaces.

The numerical discretization of the flow is an upwind explicit scheme (similar to Stelling and Duinmeijer 2003] with first order accuracy. With this schematization it is ensured a proper calculation of the space and time gradients in the nearshore and the swash zone, avoiding the shock-like hydrodynamic and morphodynamic instabilities.

4.3.2 Hydrodynamic implementation

The wave calculation is computed with the time dependent wave - action balance equation:

$$\frac{\partial N}{\partial t} + \frac{\partial c_x N}{\partial x} + \frac{\partial c_y N}{\partial y} + \frac{\partial c_\theta N}{\partial \theta} = -\frac{D_w}{\sigma} \qquad [4.11]$$

where D_W is the total wave energy dissipation:

$$D_w(x,y,t,\theta) = \frac{S_w(x,y,t,\theta)}{E_w(x,y,t)} \bar{D}_w(x,y,t) \quad [4.12]$$

and c_θ the propagation velocity in θ-space:

$$c_\theta(x,y,t,\theta) = \frac{\sigma}{\sinh(2kh)}\left(\frac{\partial h}{\partial x}\sin\theta - \frac{\partial h}{\partial y}\cos\theta\right) + \cos\theta\left(\sin\theta\frac{\partial u}{\partial x} - \cos\theta\frac{\partial u}{\partial y}\right) + \sin\theta\left(\sin\theta\frac{\partial v}{\partial x} - \cos\theta\frac{\partial v}{\partial y}\right) \quad [4.13]$$

At the total wave energy dissipation [4.12] the component $\bar{D}_w$ is the energy dissipation due to wave breaking [Roelvink 1993]:

$$\bar{D}_w = \frac{\alpha}{\pi} Q_b \sigma E_w \,, \quad [4.14]$$

Q_b the percentage of breaking waves:

$$Q_b = 1 - \exp\left(-\left(\frac{H_{rms}}{H_{max}}\right)^n\right) \quad [4.15]$$

with $H_{rms} = \sqrt{\frac{8E_w}{\rho g}}$, [4.16]

$$H_{max} = \frac{\gamma \tanh(kh)}{k} \quad [4.17]$$

and E_w the total wave energy:

$$E_w(x,y,t) = \int_0^{2\pi} S_w(x,y,t,\theta)\,d\theta \quad [4.18]$$

The components of the radiation stress are:

$$S_{xx,w}(x,y,t) = \int\left(\frac{c_g}{c}\left(1+\cos^{2\theta}\right) - \frac{1}{2}\right)S_w d\theta \quad [4.19]$$

$$S_{yy,w}(x,y,t) = \int\left(\frac{c_g}{c}\left(1+\sin^{2\theta}\right) - \frac{1}{2}\right)S_w d\theta \quad [4.20]$$

$$S_{xy,w}(x,y,t) = \int \sin\theta\cos\theta\left(\frac{c_g}{c}S_w\right)d\theta \quad [4.21]$$

where N = action balance
σ = relative frequency
S_w = energy density in each directional bin
c_x, c_y = wave propagation in x and y directions, similar as equation [4.9] and [4.10], with the Lagrangian velocity components u^L and v^L respectively
c_θ = propagation velocity in θ-space
θ = angle of approach with respect to x-axis
$\bar{D}_w$ = total wave energy dissipation due to wave breaking according to Roelvink [1993]
D_w = total wave energy dissipation
Q_b = fraction of breaking waves
H_{rms}, H_{max} = rms and maximum wave height
E_w = total wave energy
γ = breaking index
k = wave number
h = water depth
S_{xx}, S_{yy}, S_{xy} = radiation stress due to wave action

At the wave-action balance the roller energy is accounted as the wave energy dissipation. The roller energy balance is calculated as:

$$\frac{\partial S_r}{\partial t} + \frac{\partial c_x S_r}{\partial x} + \frac{\partial c_y S_r}{\partial y} + \frac{\partial c_\theta S_r}{\partial \theta} = -D_r + D_w \qquad [4.22]$$

with the total roller energy dissipation:

$$D_r(x,y,t,\theta) = \frac{S_r(x,y,t,\theta)}{E_r(x,y,t)} \bar{D}_r(x,y,t) \qquad [4.23]$$

in which the roller energy dissipation is calculated according to Reniers et al. [2004], Deigaard [1993] and Svendsen [1984] :

$$\bar{D}_r = \frac{2g\beta_r E_r}{c} \qquad [4.24]$$

The radiation stress components are calculated as:

$$S_{xx,r}(x,y,t) = \int \cos^2\theta S_r d\theta \qquad [4.25]$$

$$S_{yy,r}(x,y,t) = \int \sin^2\theta S_r d\theta \qquad [4.26]$$

$$S_{xy,r}(x,y,t) = \int \sin\theta \cos\theta S_r d\theta \qquad [4.27]$$

where S_r = roller energy in each directional bin
D_r = roller energy dissipation
E_r = total roller energy
c = phase velocity
$S_{xx,r}$, $S_{yy,r}$, $S_{xy,r}$ = radiation stress due to roller action

The total radiation stress F_x, F_y due to wave forcing is calculated as the summation of the wave and roller radiation stress components:

$$F_x(x,y,t) = -\left(\frac{\partial S_{xx,w} + S_{xx,r}}{\partial x} + \frac{\partial S_{xy,w} + S_{xy,r}}{\partial y}\right) \quad [4.28]$$

$$F_y(x,y,t) = -\left(\frac{\partial S_{xy,w} + S_{xy,r}}{\partial x} + \frac{\partial S_{yy,w} + S_{yy,r}}{\partial y}\right) \quad [4.29]$$

For the calculation of the low-frequency and the mean flows the model solves the shallow water equations into a depth-averaged Generalized Lagrangian Mean formulation [Andrews and McIntyre 1978; Walstra et al., 2000]. The GLM momentum equations are calculated as:

$$\frac{\partial u^L}{\partial t} + u^L\frac{\partial u^L}{\partial x} + v^L\frac{\partial u^L}{\partial y} - fv^L - u_h\left(\frac{\partial^2 u^L}{\partial x^2} + \frac{\partial^2 u^L}{\partial y^2}\right) = \frac{\tau_{sx}}{\rho h} - \frac{t_{bx}^E}{\rho h} - g\frac{\partial \eta}{\partial x} + \frac{F_x}{\rho h} \quad [4.30]$$

$$\frac{\partial v^L}{\partial t} + u^L\frac{\partial v^L}{\partial x} + v^L\frac{\partial v^L}{\partial y} + fu^L - u_h\left(\frac{\partial^2 v^L}{\partial x^2} + \frac{\partial^2 v^L}{\partial y^2}\right) = \frac{\tau_{sy}}{\rho h} - \frac{t_{by}^E}{\rho h} - g\frac{\partial \eta}{\partial y} + \frac{F_y}{\rho h} \quad [4.31]$$

$$\frac{\partial \eta}{\partial t} + \frac{\partial hu^L}{\partial x} + \frac{\partial hv^L}{\partial y} = 0 \quad [4.32]$$

in which the Lagrangian velocity equals to the summation of the Eulerian velocity and the Stokes drift over the horizontal directions:

$$u^L = u^E + u^S \quad [4.33]$$

$$v^L = v^E + v^S \quad [4.34]$$

The Stokes drift [Phillips 1977] over the two horizontal directions is equal to:

$$u^S = E_w\frac{\cos\theta}{\rho hc} \quad [4.35]$$

$$v^S = E_w\frac{\sin\theta}{\rho hc} \quad [4.36]$$

where u^E, v^E = Eulerian velocities over x and y directions
u^S, v^S = Stokes drift over the x and y directions
t_{bx}, t_{by} = bed shear stresses
τ_{sx}, τ_{sy} = wind stress over the x and y directions
u_t = horizontal viscosity
f = Coriolis coefficient
η = water level

4.3.3 Boundary conditions

The wave offshore boundary conditions may be described by the parametrized JONSWAP (option by specifying H_{m0}, f_p, angle of incidence, peak enhancement factor of the JONSWAP spectrum, directional spreading, step size frequency and Nyquist frequency) or the directional SWAN spectrum. This method is based on Hasselmann [1962] theory and implemented by Van Dongeren et al. [2003].

At the lateral boundaries the wave gradients are set to zero in order to avoid the shadow zones deformed at this part of the numerical domain.

Concerning the flow boundaries, at the seaward and the landward side of the domain 2D absorbing boundary conditions are prescribed taking into account the incoming bound long waves [Van Dongeren and Svendsen 1997]. The lateral boundaries may be Neumann (for the 2D test cases) or no-flux boundaries (for the profile mode test cases).

4.3.4 Morphological implementation

The sediment transport is modelled with a depth-averaged advection-diffusion equation [Galappatti and Vreugdenhil 1985]:

$$\frac{\partial hC}{\partial t}+\frac{\partial hCu^E}{\partial x}+\frac{\partial hCv^E}{\partial y}+\frac{\partial}{\partial x}\left[D_h h\frac{\partial C}{\partial x}\right]+\frac{\partial}{\partial y}\left[D_h h\frac{\partial C}{\partial y}\right]=hC_{eq}-\frac{hC}{T_s} \qquad [4.37]$$

in which the adaptation time T_s (low values represent instantaneous deposition) for the entrainment of sediment is calculated as:

$$T_s=\max\left(0.05\frac{h}{w_s},0.2\right) \qquad [4.38]$$

where C = depth-averaged sediment concentration
D_h = sediment diffusion coefficient
T_s = adaptation time
h = water depth
w_s = fall velocity

The bed updating is calculated as:

$$\frac{\partial z_b}{\partial t}+\frac{f_{mor}}{1-p}\left(\frac{\partial q_x}{\partial q_y}\right)=0 \qquad [4.39]$$

in which the sediment transport rates at the x and y directions are calculated as:

$$q_x(x,y,t) = \left[\frac{\partial hCu^E}{\partial x}\right] + \left[\frac{\partial}{\partial x}\left[D_h h \frac{\partial C}{\partial x}\right]\right] \quad [4.40]$$

$$q_y(x,y,t) = \left[\frac{\partial hCv^E}{\partial y}\right] + \left[\frac{\partial}{\partial y}\left[D_h h \frac{\partial C}{\partial y}\right]\right] \quad [4.41]$$

where f_{mor} = morphological acceleration factor [Reniers et al. 2004]
p = porosity

The equilibrium sediment concentration is calculated by the Soulsby - Van Rijn formulation [Soulsby 1997] :

$$C_{eq} = \frac{A_{sb} + A_{ss}}{h}\left(\left(\left(u^{E^2}\right) + 0.018\frac{u_{rms}^2}{C_d}\right)^{0.5} - u_{cr}\right)^{2.4}\left(1 - \alpha_b m\right) \quad [4.42]$$

where A_{ss}, A_{sb} = suspended and bed load coefficients
C_d = drag coefficient due to flow velocities
u_{rms} = near bed short-wave orbital velocity
u_{cr} = critical velocity for the sediment motion initiation, due to mean and orbital velocities
m = bed slope
α_b = calibration factor

For further information the reader is referred to the XBeach user manual [Roelvink et al. 2009b] and at the public domain of XBeach [11]. The parameters and formulations investigated in this study are further discussed at Chapter 6.

5. THE CONTINENTAL SHELF MODEL COUPLED WITH THE XBEACH MODEL

5.1 Introduction

A dependable model train for the real-time storm surge simulation, may consist of four stages; the accurate wind and pressure field forecast, the generation of the surge and wave conditions, the propagation from deep to shallow water and finally the morphological impact at the shoreline. In line with this approach, this chapter starts with the presentation of the operational model and the computed boundary conditions. Then, we present the evaluation of the computed hydrodynamic conditions with the available measured data. In practice when the operational model has been used, the forecasted hydrodynamics were tested with the available data and the computed results were corrected (Verlaan et al. 2005). In this study, the validation of the operational model may highlight the uncertainties of the computed hydrodynamics, which influence the computed results of the XBeach model. This chapter ends with the XBeach model input data construction, which will be used for a dune erosion model study.

5.2 The operational model

The real-time forecast system that is going to be established needs to satisfy the requirement for an early hazard assessment. Verlaan et al. [2005] describe the development of the operational model from the middle 1980s until the latest developments in 2005. Nowadays, the three stages of generation, propagation and the inundation together with the morphological change due to the storm surge are decomposed at a system of three model schematizations with finer grid resolution as approaching to lower depths (Fig. 5.1).

The Continental Shelf Model (CSM) is the first part of the model train decomposition. It consists of two interrelated fragments where the surge and the waves are calculated by the Delft3D Flow and the Delft3D Waves (the lateral is the SWAN model as discussed by Booij et al. 1999] modules respectively. Concerning the computation of the surge, a domain which covers the entire area of the North Sea is constructed (see paragraphs 5.3 and 5.4 for a detailed description of the numerical domains of the 1953 and the 1976 storm surges respectively), where the tidal constituents and the wind and pressure fields are applied as input factors for the generation and the propagation of the surge. The calculation of the wind induced waves is performed on an individual domain which describes the Eastern part of the North Sea. The short waves calculation is the product of the wind force in combination with the swell, where there is the option for calculating the lateral by an external numerical model. While the surge and the wind waves are calculated separately, the internal bilateral communication allows for the prudent computation of their interaction.

The next part of the operational model train, the Kuststrook model (KST) is utilized in order to simulate the propagation of the hydrodynamic conditions until the coastal area of the

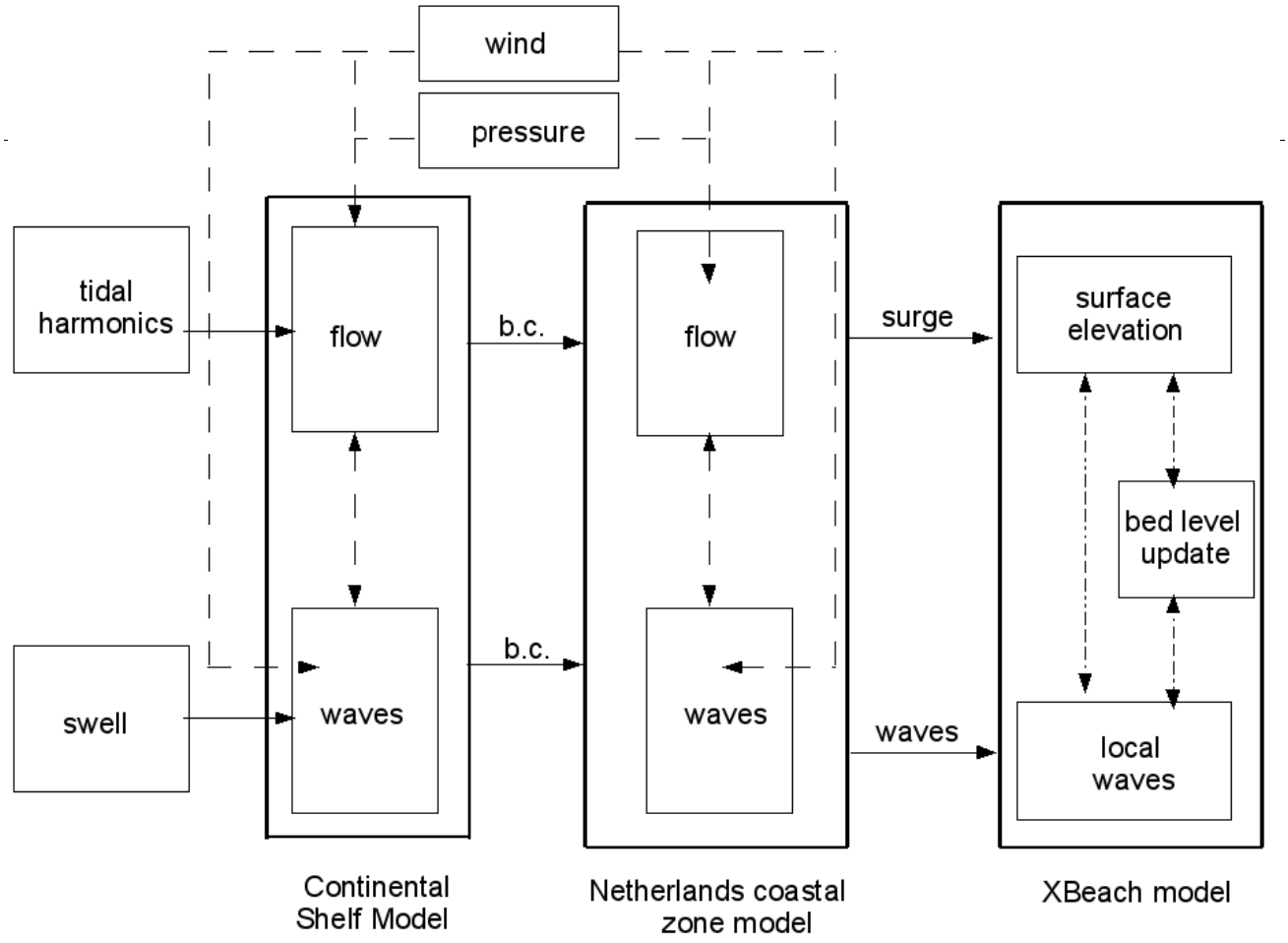

Figure 5.1: Graphical schematization representing the current form of the operational model.

Netherlands. It consists of two model domains of the Delft3D Flow and Wave modules, which are nested at the corresponding model domains of the CSM. The refined bathymetry at the model domains where the surge and the short waves are computed, accounts for an accurate simulation including the bathymetric features that are often present at the nearshore area, while the smaller grid domains than the CSM, contribute to less time demanding computations.

The final model setup is applied in the area with the interest at the morphodynamic change. It may consist of an 1D or 2D numerical grids with varying or constant resolution. As hydrodynamic input the model receives the storm tide timeseries and the parametrized or the SWAN spectra that have been calculated by the KST model. At the CSM and the KST numerical domains the morphodynamic influence is not accounted, due to the high depth and therefore the hydrodynamic change is prone only to variations of the meteorological disturbances (wind and pressure) and the initial bottom profile. At the XBeach model domain, the updated bathymetry at each time step may vary, affecting the profile of the currents and the waves of the next time step.

5.3 Model setup and the meteorological conditions during the 1953 storm surge

The 1953 storm surge, due to its severity and the loss that triggered, has been the objective of a numerous case studies (Gerritsen 2005, Wolf and Flather 2005). The model decomposition of this study is based on the schematization by Ir. Van der Kaaij in 1998, concerning a case study for the site near Egmond in the Netherlands. In total, six different numerical domains have been constructed simulating the surge and the wind waves from the open sea to the seaside zone. The numerical domain of the Delft3D-Flow module consists of three nested grids as the above described CSM and KST models, and the grid describing the nearshore zone around Egmond (Fig. 5.4 left side from bottom to top respectively). The first one is a rectilinear grid covering the North Sea area with 201x173 grid points on a spherical co-ordinate system with uniform resolution of approximately 8.4x9.3km. The deformation and the propagation of the surge is computed at the entire domain by the U_{10}, V_{10} wind components and the pressure field which are obtained from the re-analysis dataset of the HIRLAM programme (Fig. 5.2 and 5.3). The 6-hourly interval HIRLAM data cover the Northwestern European Atlantic continental shelf from 15^0 W to 15^0 E and from 48^0 N to 62.3^0 N, with spatial resolution of 9.3x9.3km, for the period from the 25th of January 1953 at 18:00 to the 2nd of February 1953 at 00:00. This long period of simulation is required in order to eliminate the numerical errors of the hydrodynamic conditions due to the computational spin up time, and in order the storm to be described thoroughly. The nature of the storm surge requires an extended domain for the complete simulation of the phenomena while the resolution may remain low. In combination with the pressure and the wind field, the astronomical tidal level is required to calculate the storm deformation and the propagation until the next nested grid.

While the waves and the surge approach shallower waters, the interaction with the bottom becomes more intense, affecting their propagation. Therefore the resolution of both of the numerical grids should be finer in order to account for these changes and to ensure the correct propagation of the hydrodynamic conditions. The numerical domain for the computation of the surge describes the offshore area of the Netherlands, extending from the depth of N.A.P. -30m until a minor elevation of N.A.P. +3m. Over the longshore direction, it runs from Hoek van Holland until the island of Ameland. It is characterized by a rectilinear grid in a spherical coordinate system with a constant resolution of approximately 5x2km.

The morphological influence of the storm surge is calculated at the third nested grid. For the case study in Egmond, the area is covered by a grid of 72x216m resolution. Over the cross shore dimension, the domain runs from the 20m depth contour until the N.A.P.+13m elevation. In order to avoid the noise from the boundaries at the area of interest, the model domain is extended over the longshore direction, while the active site is monitored in terms of the hydrodynamic and the morphodynamic conditions. At this schematization, the morphological calculation was performed by the Delft3D model.

Furthermore, the wind waves are computed in a triad of nested numerical domains (Fig. 5.4 right side). For the wave simulation the fetch is important, while the resolution can be coarse.

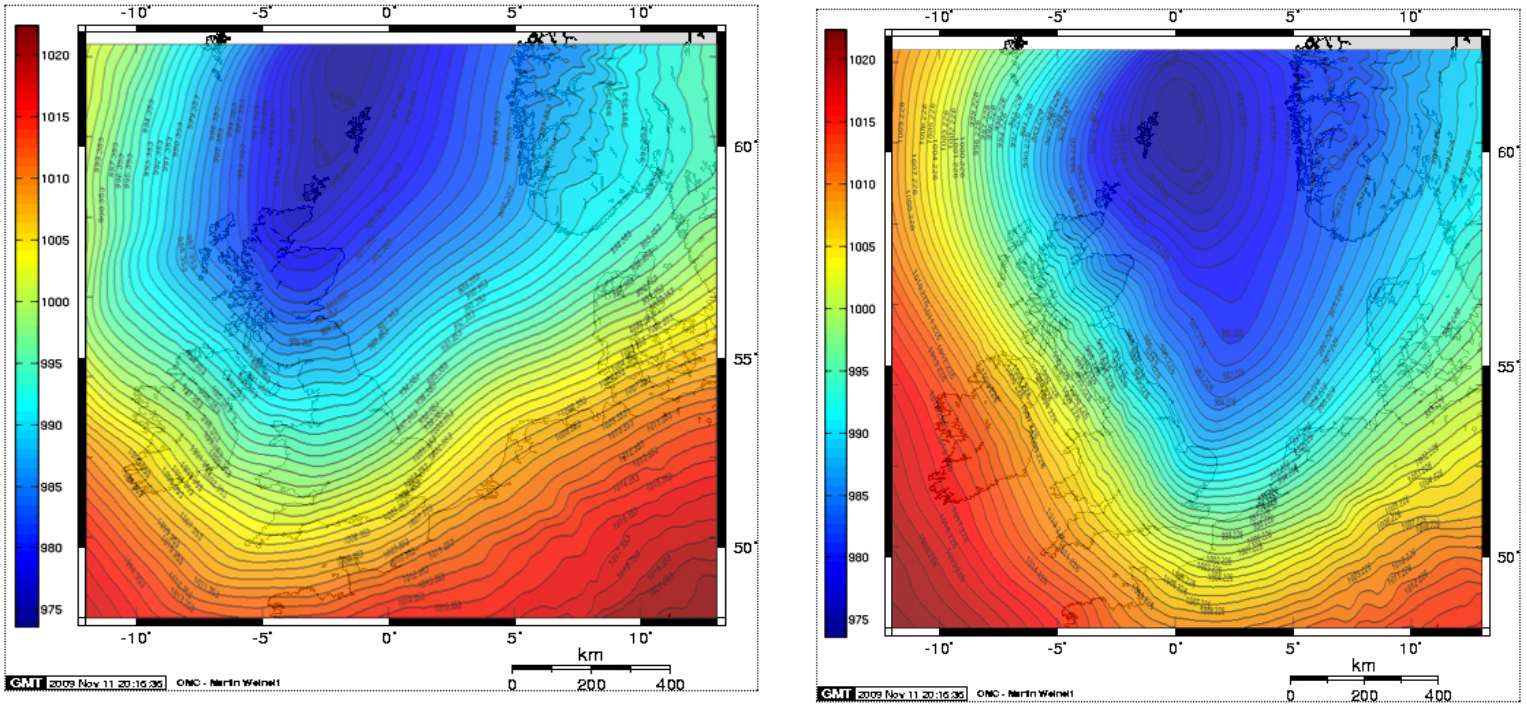

Figure 5.2: Computed pressure field (mbars) over the Northwestern European Continental Shelf during the peak of the storm at 31-1-1953 at 00:00 (left panel) and 31-1-1953 at 06:00 (right panel).

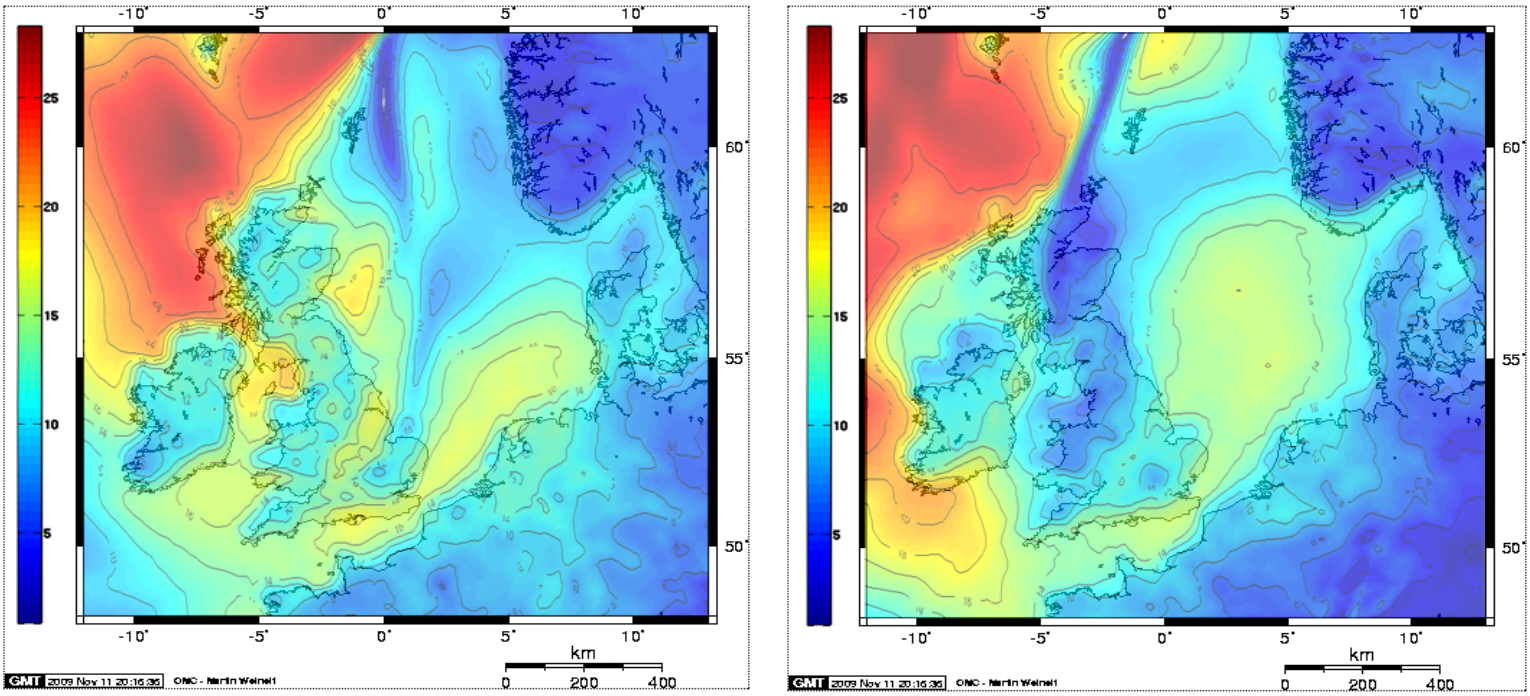

Figure 5.3: Computed wind velocities (m/sec) over the Northwestern European Continental Shelf at 31-1-1953 00:00 (left panel) and at 31-1-1953 at 06:00 (right panel).

Starting from the coarser grid of the Delft3D-Wave module, the resolution increases from 18x27km for the grid which describes the Eastern part of the North Sea, to 3.6x5.4km for the offshore area of the Netherlands and finally the area around Egmond is nested at a grid of 72x216m. The tidal and the storm surge timeseries, as well as the gales are obtained as boundary conditions computed from the CSM flow model. Additionally, the model accounts for the quadruplet wave-wave interaction as well as the energy dissipation at deep water due to white-capping.

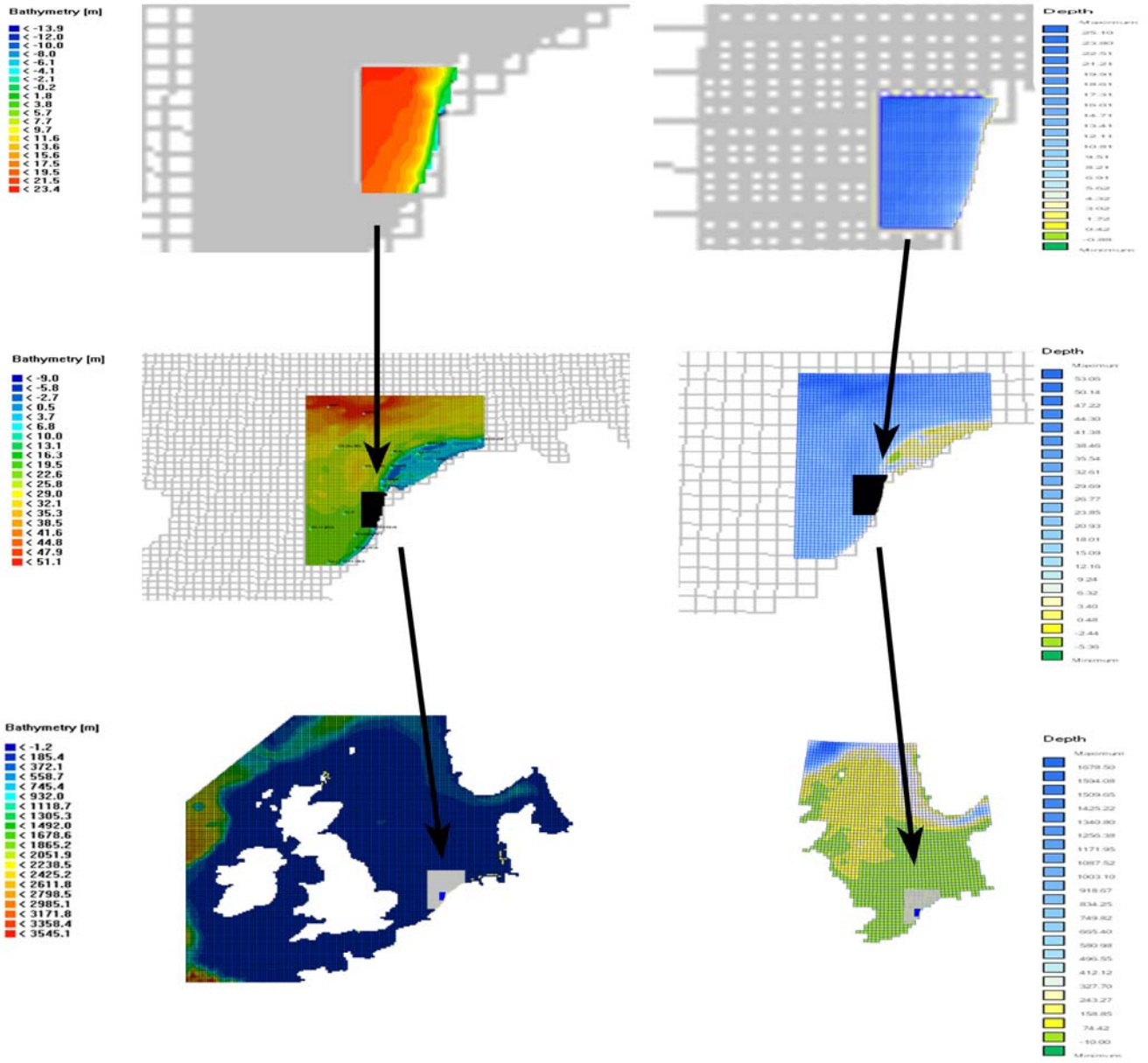

Figure 5.4: The numerical grids of the Delft3D-Flow (left side) and Delft3D-Wave modules (right side): the site near Egmond (top panels), the offshore area of the Netherlands displaying the KST model (middle panels) and the continental shelf model (bottom panels).

5.4 Hydrodynamic conditions during the 1953 storm surge

The validation process of the operational model is conducted in terms of the computed storm surge level, as no measured wave data were found (also discussed in paragraph 3.3) for the storm surge event of 1953. Therefore, the quantitative comparisons will be restricted between the computed and the measured storm surge levels.

Figure 5.5 depicts two representative measured and computed water level records in Vlissingen and in IJmuiden (see Appendix B, figures B1 to B5 for the available measured storm surge level data with the corresponding computed ones in Hoek van Holland, Scheveningen and Den Helder). The recorded impact during the 1953 storm surge was more intense on the southern part of the Netherlands. According to the measurements, the storm surge level in Vlissingen was recorded up to N.A.P. +4.5m (black dashed line in Fig. 5.5) and it is the highest among the available data. The model estimates well the arrival time and the phase of the surge, while it gives some minor deviations concerning the surge peak at the order of 0.30m. Higher order of discrepancies is observed from the comparison of the measured and computed surge level in IJmuiden (blue lines in Fig. 5.5). While the arrival time is in good agreement with the measured data, the computed surge level is underestimated more than 0.6m and the phase lag is more than 45 minutes.

Possible reasons for these dissimilarities appear due to the lower resolution of the numerical domains, or due the geological features that are not included at the bottom profile of the numerical grid. These dissimilarities should be considered critical, as they can lead to serious errors when approaching to shallow water; consequently leading to underestimations of the storm induced morphological impact at the shoreline.

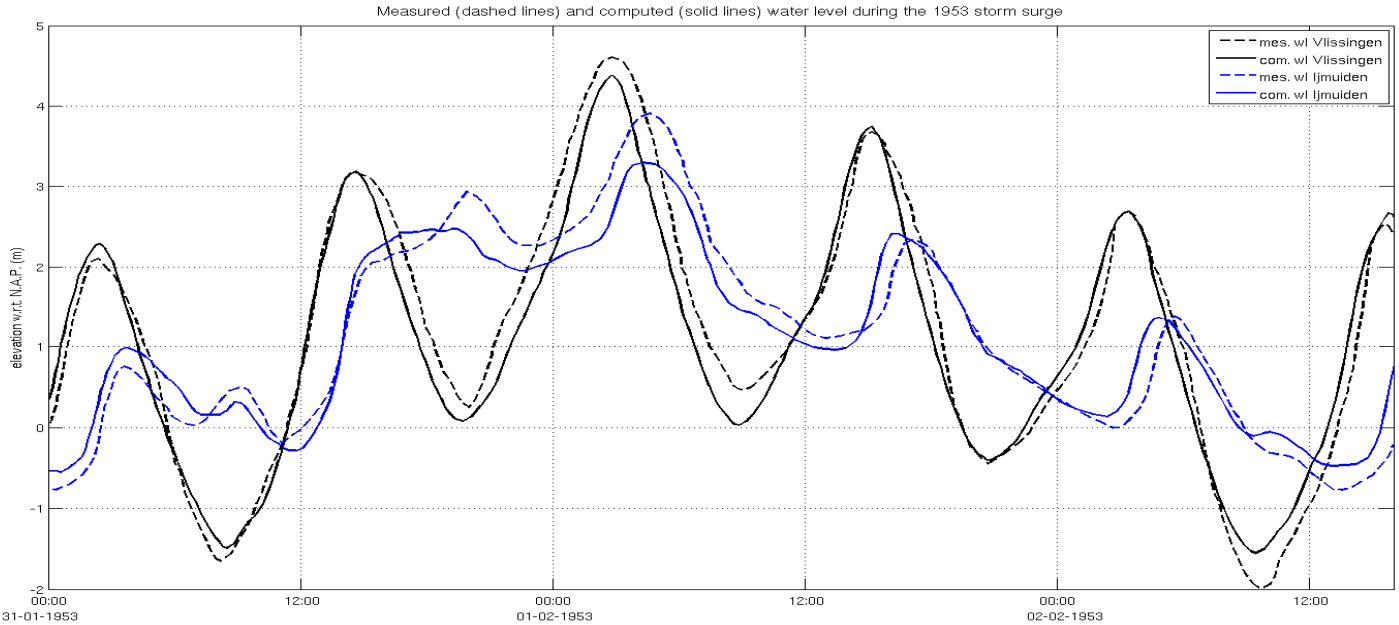

Figure 5.5: Measured (dashed lines) and computed (solid lines) in Vlissingen (black lines) and in IJmuiden (blue lines) during the 1953 storm surge.

5.5 Model setup and the meteorological conditions during the 1976 storm surge

The simulation approach of the storm event of January 1976 follows a similar approach with the one described for the 1953 storm. The current form of the operational model is based on the schematization by Ir. Van Ormondt (here only some of the differences are presented between the current and the previous described operational model schematizantion as implemented by Ir. Van der Kaaij), compounding the Delft3D modules for the generation and the propagation of the storm surge, and the XBeach model as the final constituent for the calculation of the hydrodynamic conditions and the morphological change in the nearshore area.

The simulation of the surge and the wind waves is divided into two sets of numerical grids each one consisting of two nested grids with reducing resolution. The coarser ones describe the area of the North Sea, and the finer ones the offshore belt of the Netherlands. The first grid (Fig. 5.6 top left panel) consists of 201x173 grid points on a rectilinear domain with regular resolution of approximately 8.4x9.3km. The meteorological boundary conditions are computed over this domain, deforming and propagating the storm surge and the short waves until the next nested grid. In order to examine the validity of the operational model, another source of meteorological data is applied. The wind and pressure fields are derived from the ERA-40 re-analysis database of the ECMWF (European Centre for Medium-Range Weather Forecasts), as described by Uppala et al. [2005]. This dataset contains the re-analysis of the global atmospheric conditions from 1957 to 2002, with spatial resolution of 2.5x2.5 degrees. For the generation of the surge, the 6-hourly wind velocity field and the pressure field (Fig. 5.7 and 5.8 respectively) covering the period from the 1st of January 1976 until the 4th of January 1976 are assimilated together with the timeseries of the tidal constituents. Additionally, the wind waves' energy is calculated on the coarsest grid (Fig. 5.6 bottom left panel) of the Delft3D-Wave module which describes the Eastern part of the North Sea.

The second set of numerical grids covers the offshore part of the Netherlands. The Kuststrook model (KST) consists of two numerical grids, each one applied for the calculation of the storm surge and the wind waves. The first domain (Fig. 5.6 top middle panel) is a curvilinear grid of 63x181 grid points with varying resolution as approaching to shallower depth. The domain extends over the longshore direction from Middelkerke in Belgium until the island of Norderney in Germany and over the cross-shore direction from the N.A.P. -30m depth contour until the N.A.P. +1m elevation. The initial tidal timeseries in combination with the computed surge level due to the wind and pressure fields are propagating into this domain with finer resolution, in order to account for the higher energy dissipation due to the lower depth. The domain for the calculation of the wind waves (Fig. 5.6 bottom middle panel) describes the same area and with the same resolution. The difference between the two domains is that at the bifurcation of the river Scheldt, only the flow conditions are accounted and the wind waves are not considered.

At the current form of the operational model, the morphological influence due to the storm surges is computed by the XBeach model. The last nested grid with the highest resolution

among the model constituents, describes this area over an 1D or 2D numerical domains (right panel in Fig. 5.6). The storm surge timeseries and the wave energy spectra from the KST model are applied at the offshore boundary, and therefore the bottom depth at this location should meet the requirements for the smooth propagation of the boundary conditions. The same requirement is necessary to be fulfilled at the lateral boundaries. In order to account for the bed level update and the consequent change of the hydrodynamic conditions both at the dry and at the wet nearshore area, it is recommended to preserve low resolution, despite the time demanding calculations (see paragraph 5.7).

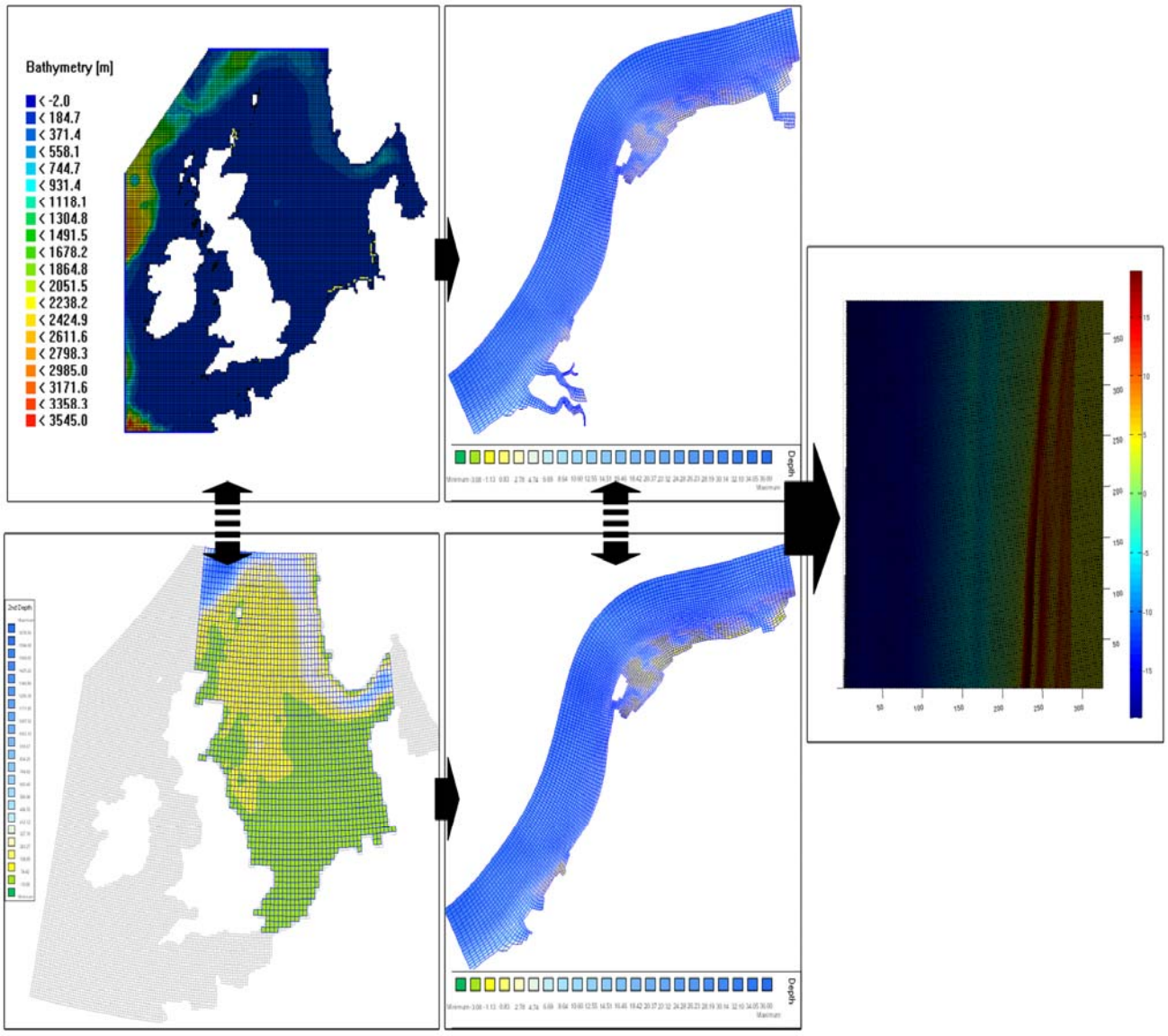

Figure 5.6: Model schematization of the 1976 storm surge. Top panels illustrate the Delft3D-Flow models, the bottom panels the Delft3D-Wave models and at the right panel the model domain for the XBeach model.

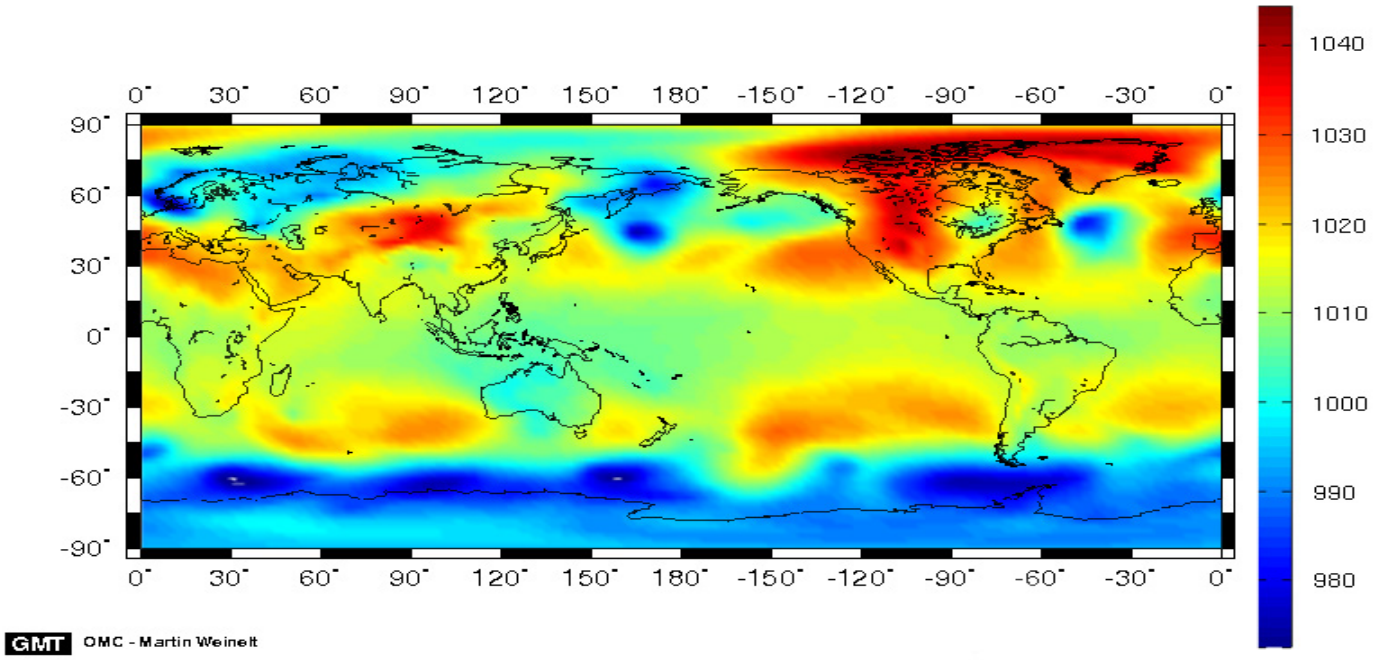

Figure 5.7: Global pressure field (mbars) on Saturday 3-1-1976 at 12:00, as computed from the operational model. The low atmospheric pressure that resulted to the 1976 storm is depicted at the top left of corner of the figure.

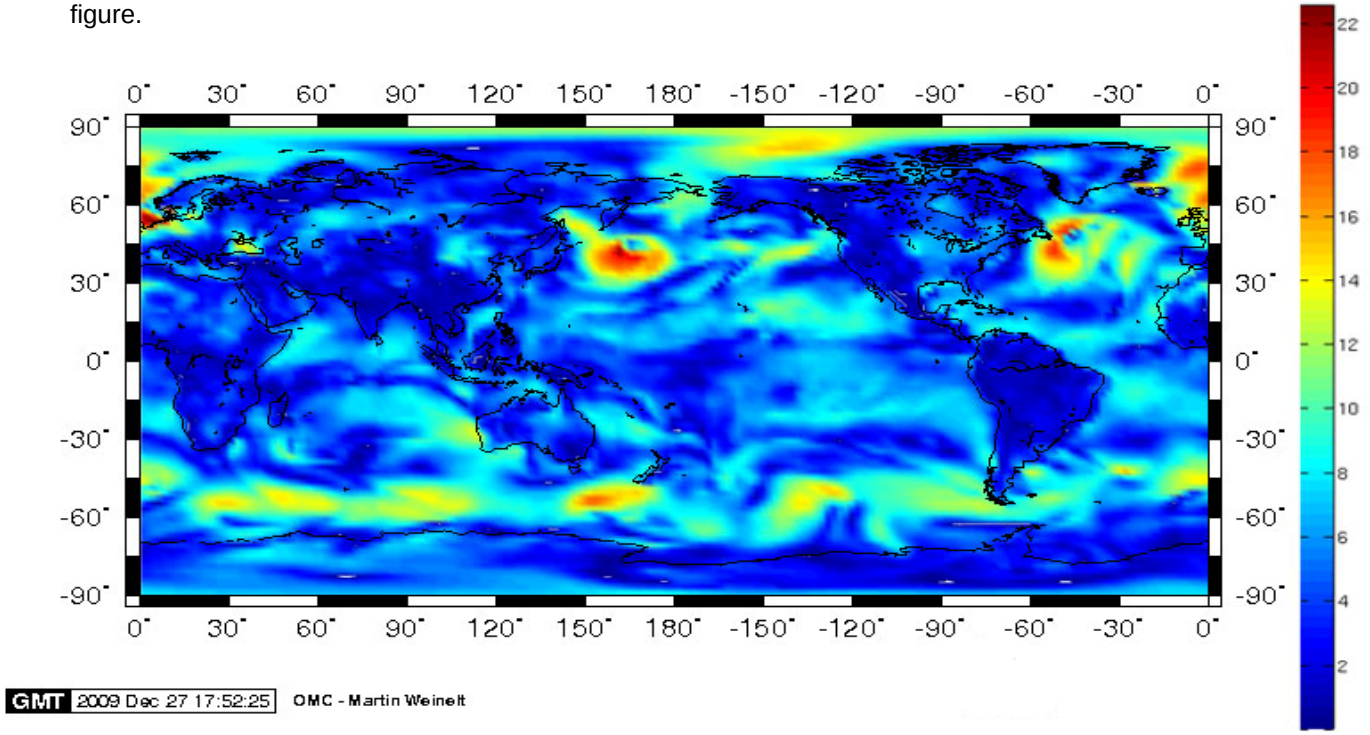

Figure 5.8: Global wind field on Saturday 3-1-1976 at 12:00. Note the high gales at the top left corner of the figure.

5.6 Hydrodynamic conditions during the 1976 storm surge

In contrast with the predecessor storm of 1953, the storm event of 1976 has been better recorded in terms of the wave and storm surge level conditions. Because of the available pre-storm and post storm coastal profile recordings, the morphological validity of the operational model can be assessed.

Concerning the North Holland province, the available wave measurements (black circles in Fig. 5.7 and 5.8) closer to the area of interest were obtained from a buoy located 10 km North-West of IJmuiden at 52^o 32' 25" North and 4^o 25' 37" East at 16m depth (source: WL| Delft Hydraulics R587 1978). The measurements cover the period from the 19:00 on the 1st of January 1976 until the 19:00 on the 4th of January and were interpolated at the same time interval with the available data (read below). The original data are presented in table B.1 in appendix B. The wave records in figures 5.7 and 5.8 demonstrate that the storm had arrived at the evening hours of the 2nd of January, reached a peak at the evening hours of the 3rd of January (around 18:00), with maximum H_s of 6.2m and T_{mean} of 9.1 seconds. The trend of the data shows the end of the storm during the early evening hours of the 4th of January.

Caires et al. [2008] reconstructed the wave field from January 1st of 1958 to December 31st of 2001 for the nearshore buoy MP1 near Petten (Fig. 5.9), by deploying the offshore ERA-40 re-analysis wave model. Accounting for shallow water conditions with a refined time-step of 20 minutes and three configurations (nominally WAM3, Van der Westhuysen [2007] and Rogers et al. [2003], in Caires et al. [2008]), for the model SWAN [Simulation of Waves in Nearshore areas, Booij et al. 1999], they reconstructed the hindcasts for the period from 1958 to 2001. The wave data presented in Fig. 5.7 and 5.8 (blue crosses) show the same trend with the measurements (black circles), indicating the storm surge period between the evening hours of the 2nd of January to the late evening of the 4th of January.

The significant wave height and the mean wave period offshore of Bergen aan Zee as computed from the SWAN energy spectra of the KST model are presented in Fig. 5.7 and 5.8 respectively (red stars). While the trend of the data shows a similar pattern with the measurements and the hindcasted significant wave height and mean wave period, it is obvious that in Bergen aan Zee the computed wave conditions are considerably lower. Over the entire offshore boundary of the KST model, where the two domains are nested, the H_s does not exceed 3m, and it needs to be further identified which are the numerical parameters that restrict to this uniform pattern (see also Fig. B6 in App. B). Additionally, the numerical parameters concerning the wind simulation as performed by the model, may address another possible reason of these deviations. Furthermore, considering that at the location of the measurements (Fig. 5.9) the waves are well developed and the depth (N.A.P. -16m) shallow enough, the differences that are observed may be due to the energy dissipation while approaching shallower waters.

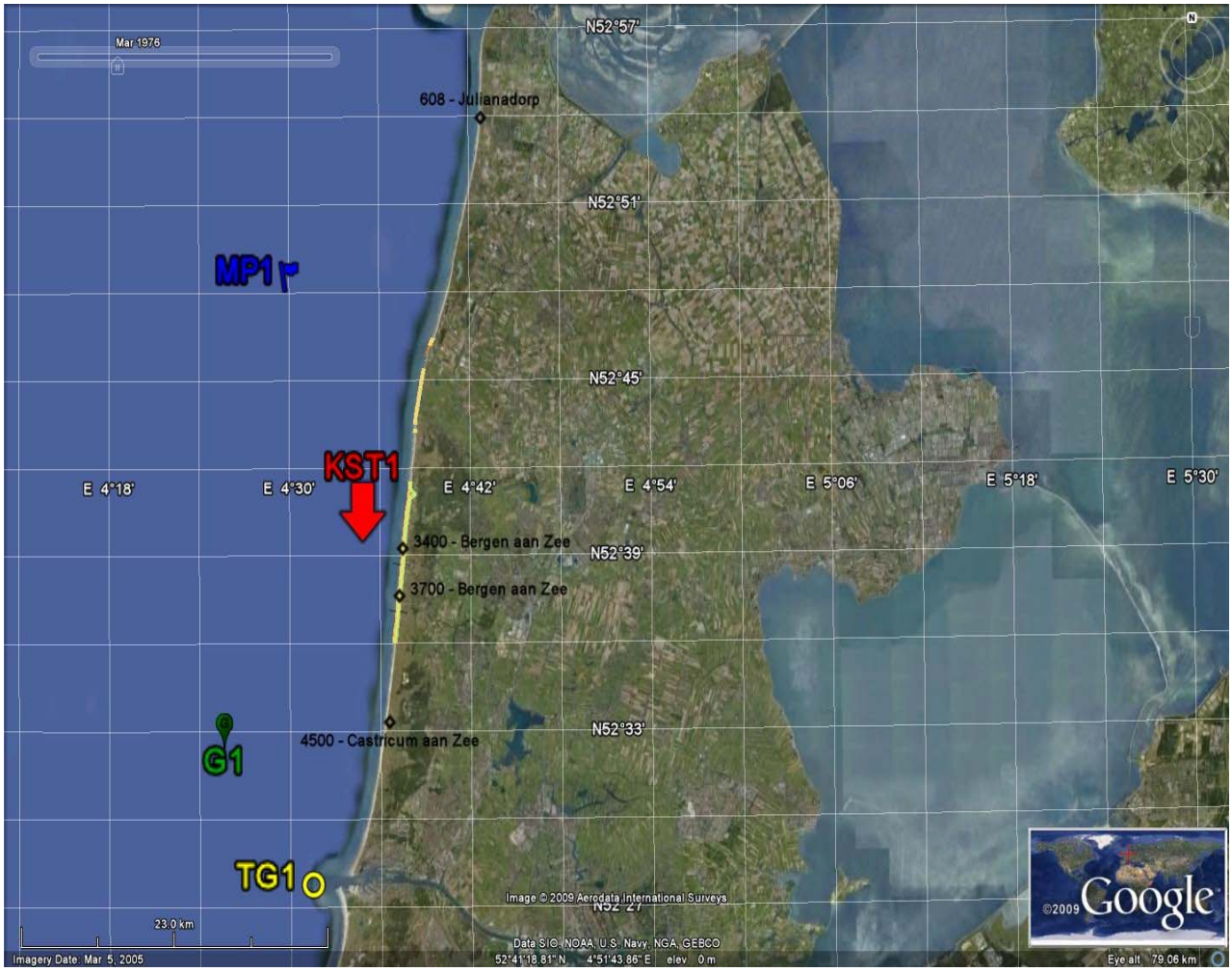

Fig. 5.9: The location of the nearshore buoy MP1 in Petten (after Caires et al. 2008), the buoy G1 (after the report R587, WL| Delft Hydraulics) from where the measurements during the 1976 storm surge were obtained, the location at the offshore area of Bergen aan Zee (KST1) and the tidal gauge in IJmuiden (TG1).

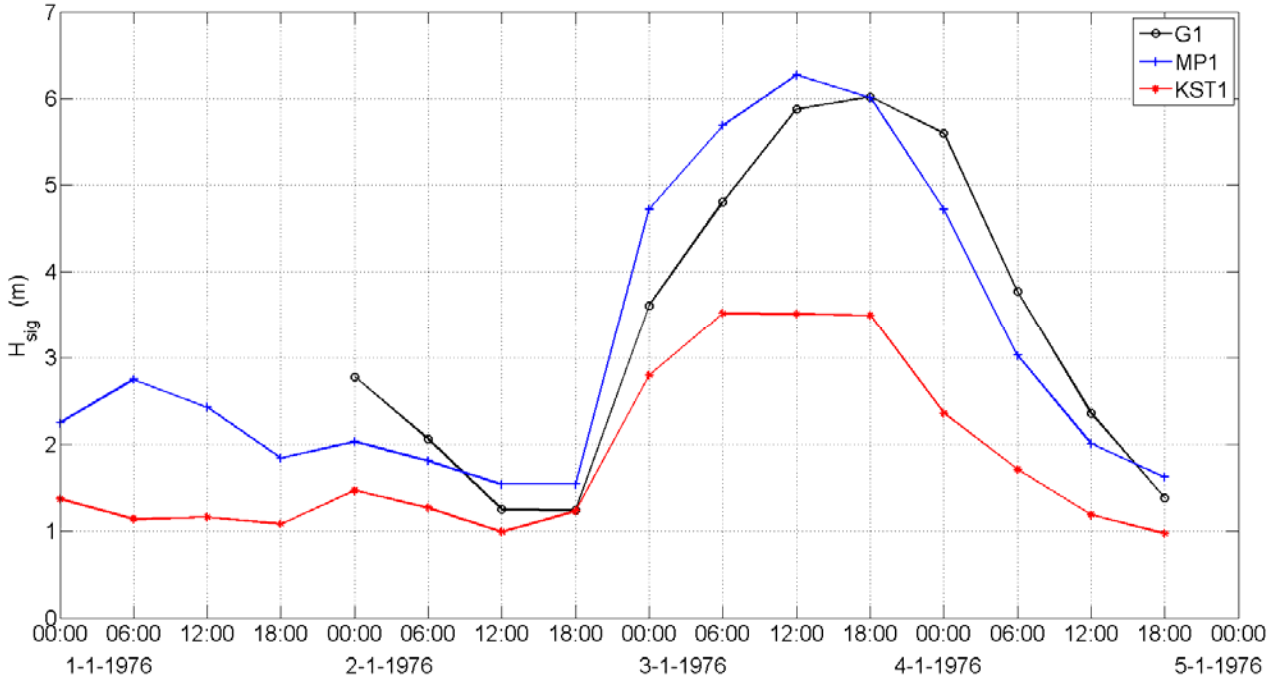

Fig. 5.10: Measured Hs at the site G1 during the 1976 storm surge (circles), hindcasted Hs at MP1 (after Caires et al. 2008) (crosses) and computed Hs at KST1 (stars).

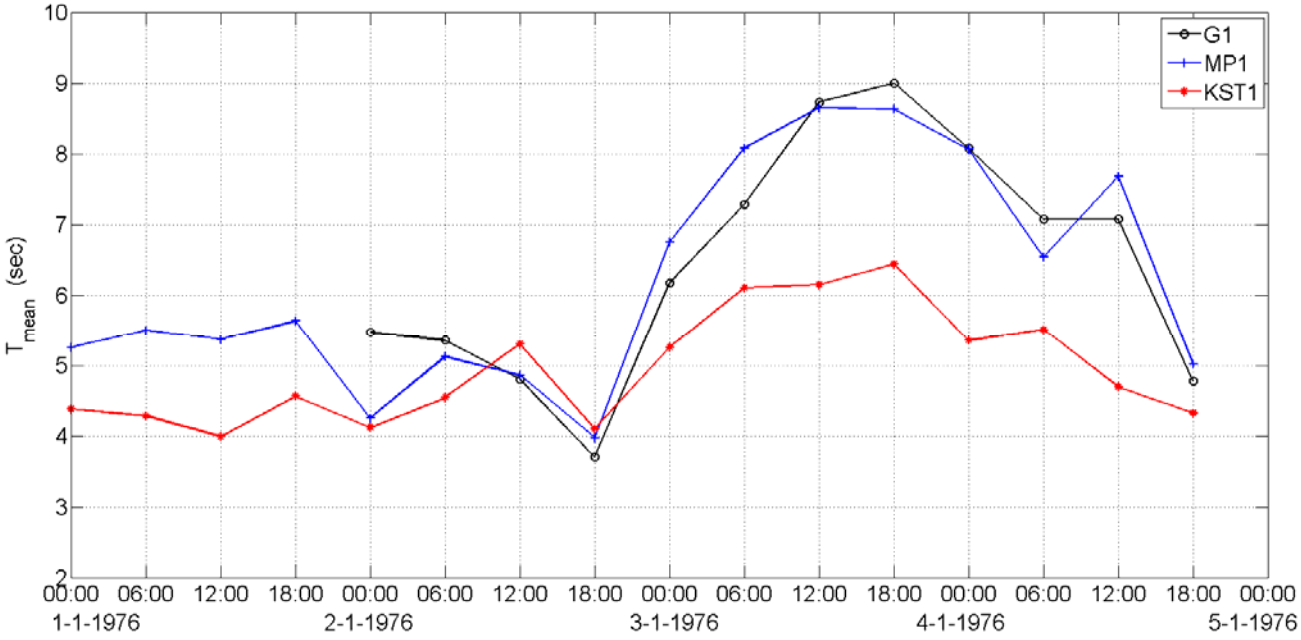

Fig. 5.11: Measured T_{mean} at the site G1 during the 1976 storm surge (circles), hindcasted T_{mean} at MP1 (after Caires et al. 2008) (crosses) and computed T_{mean} at KST1 (stars).

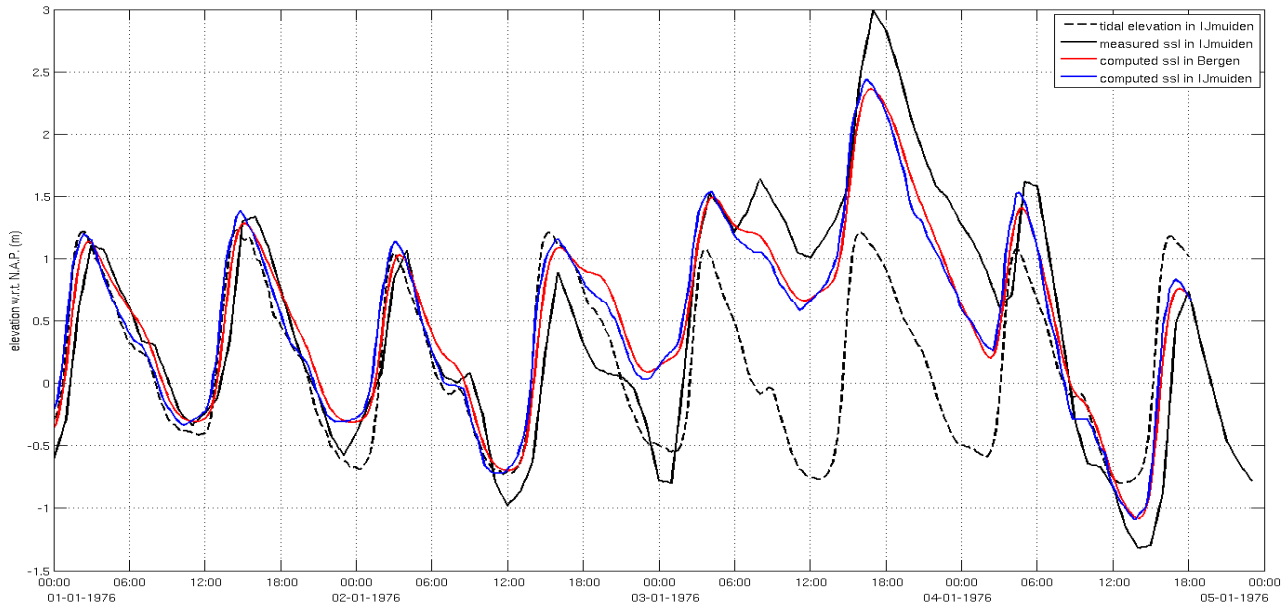

Figure 5.12: Tidal elevation (dashed black line) and measured storm surge level in IJmuiden (solid black line). Computed storm surge level in IJmuiden (blue line) and computed storm surge level in Bergen.

Differences are observed between the measured and the computed storm surge level, as obtained from the tidal gauge in IJmuiden (black solid line in Fig. 5.12) and the KST model (blue line in Fig. 5.12), which can be due to the lower grid resolution of the lateral (possible errors of the wind drag coefficient of the Delft3D-Flow module have not been examined). The maximum difference is observed during the peak of the surge (at the 3rd of January at 18:00) and is equal to 0.60m. The surge in IJmuiden arrives at the first morning hours of the 3rd of January 1976. It appears to be weakened after 08:00 o'clock at the 4th of January 1976 and that after 11:00 o'clock of the same day it does not appear to affect significantly the area.

The computed storm surge level in Bergen has the same elevation as the one in IJmuiden. As no available measured data exist for the storm surge level in Bergen, no profound quantitative estimation of the computed surge level can be argued. It can be stated that some deflections may occur of the same range as between the measured and computed surge level in IJmuiden. The track of the storm was East to North East, as computed from the DCSM, which means that the surge affected first the coastal areas of Bergen and then arrived in IJmuiden. Therefore, it would be safe a first assessment of the storm surge in Bergen to be performed starting from the 00:00 at the 3rd of January until the 18:00 of 4th January. The peak surge level appears around 16:30 at the 3rd of January. According to the measurements, the effect of the storm should not be considered significant after the 08:00 morning hour of the 4th of January.

5.7 XBeach model grid construction

The numerical profiles for the 1D simulations are constructed as follows:

- The measurements performed by Ir. Rakhorst at late December (see Appendix A, figures A.4 to A.8 for the area in Julianadorp, A.10 to A.11 for the area in Bergen and A.12 for Castricum) are selected and extended over the seaward and the landward cross-shore direction as indicated by the latest Jarkus measurements in 1975.
- The longest Jarkus transect of each area is applied in order to extend the profiles from the N.A.P. -10m depth contour until the N.A.P. -15m depth contour. The morphological changes below the N.A.P. -10m depth contour are assumed minor and if any, uniform over the longshore direction of the same area.
- The Jarkus measurements describe the profile after the end of the first dune and rarely until the second dune. This length is decent for the storm event of 1976 as no dune overtopping took place. This is also indicated by the rather steep profiles after the last landward post storm measurement.
- The offshore boundary is constructed horizontal and with uniform resolution.

For the 2D simulations (Fig. 5.13 and Fig. 5.14), the profiles of the 1D simulations are used after the following changes are applied:

- The profiles are converted and oriented from the RSP to the RD coordinate system.
- Over the longshore direction the southern and the northern profiles are mirrored at a distance equal to the length of the longest transect, in order to avoid the numerical noise form the boundaries inside the area with the morphological interest.
- These prolonged grids are expensive in terms of the computational time. Therefore, a non-equidistant grid is constructed with the cross-shore resolution varying from 2m to 20m and over the longshore direction from 2m to 50m, with decreasing resolution outside of the reference morphological area.

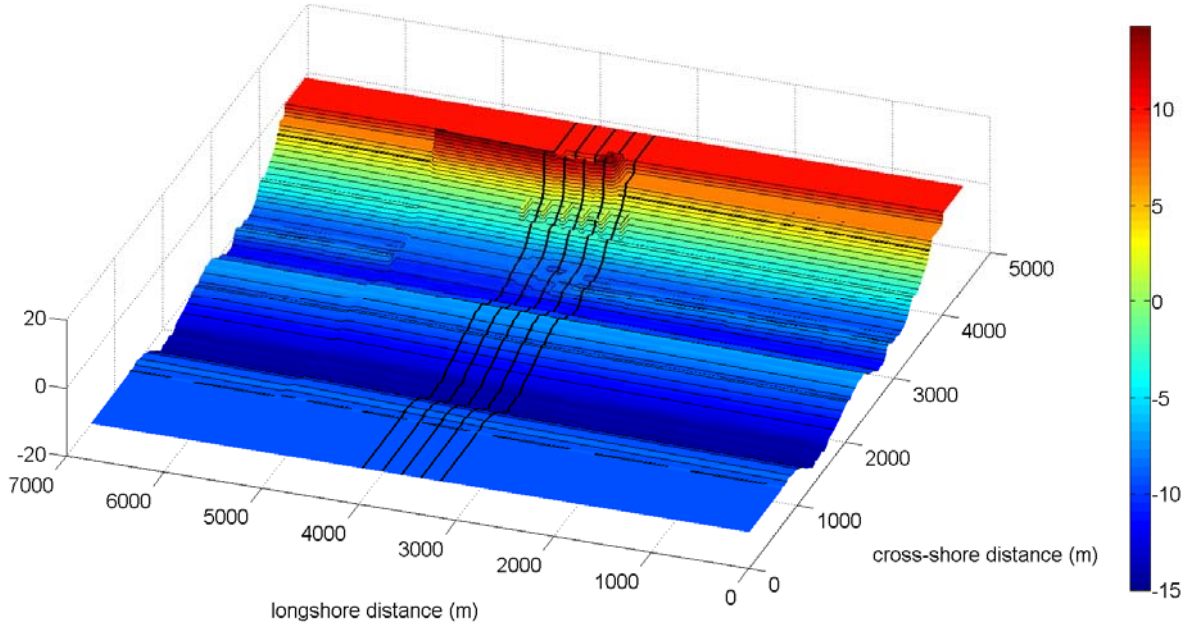

Figure 5.13: Numerical domain with varying resolution over the cross-shore and the longshore direction in Julianadorp and the groins as non-erodible structures. The black lines indicate the Jarkus transects, from North to South they are: 568, 588, 608, 628, 648.

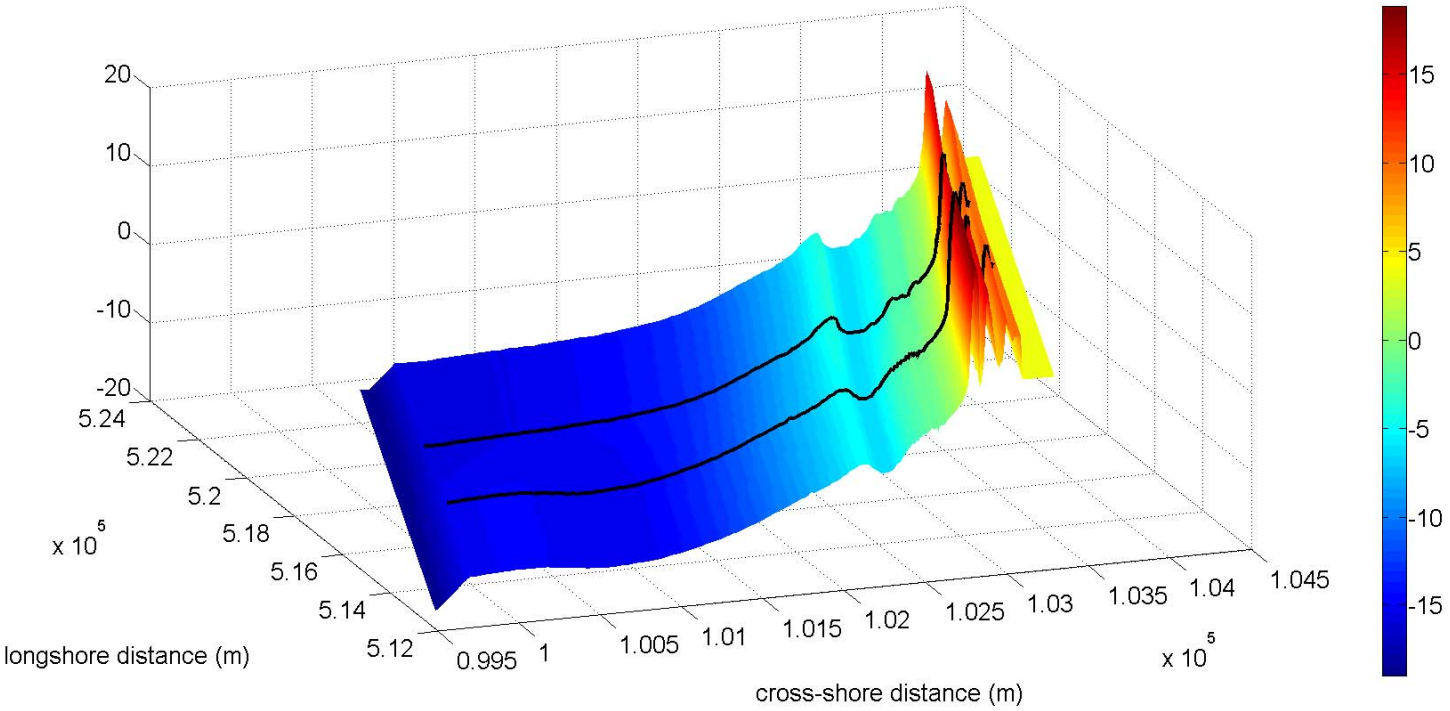

Figure 5.14: Numerical domain with varying resolution over the cross-shore and the longshore direction in Bergen. From North to South the black lines indicate the Jarkus transects 3400 and 3700.

6. Modelling and analysis of the dune erosion during the 1976 storm surge

6.1 Introduction

The volumetric analysis presented in Chapter 3 gave evidence of the non-uniform longshore amount of erosion, as an effect of the 1976 storm event. The highest amount of erosion was measured in Bergen at the Jarkus transect 3400, while in Castricum the erosion was limited. In this chapter, the XBeach model will be used to investigate this longshore variability. First, the sensitivity of the model is tested on the internal physical parameters, as well as on physical quantities. The simulated post storm erosion is examined in terms of the profile and volume change, both in Bergen and in Castricum, attempting to identify the reason of the different response. Finally, the effect of the 1976 storm is examined in the area of Julianadorp.

6.2 Sensitivity of the XBeach model

The sensitivity of the XBeach model has been examined qualitatively and quantitatively on a series of tests both on laboratory [Roelvink et al. 2009, Van Thiel de Vries 2009] and on prototype scale [McCall 2008; Pool 2009, Roelvink et al. 2009] for a number of extreme event conditions. In this study, uncertainties may arise from the fact that the internal physical parameters as well as their combinations influence the post storm profile. Additionally, the divergence between the measured and computed boundary conditions is examined. Finally, the limited profile data concerning the 1953 storm surge and the assumptions concerning the grid construction for the 1976 storm surge, point the need for the following sensitivity study.

First, an 1D base case is introduced concerning the Jarkus transect 3400 in Bergen, where the highest volume change was measured. As part of the operational model chain validation, the storm surge level is imposed as computed by the KST model at the observation point offshore of Bergen. The effect of the storm is examined from the 00:00 at the 3rd of January (assuming that 0.50m of water surface elevation is among the computational error limits) until 08:00 o' clock at the 4th of January when the effect of the storm appears marginal (red profile at Fig. 5.12 in chapter 5). However, the morphological change will be examined up to 18:00 of the same day, as the post storm surveys had been carried out three or four days after the storm had passed. Thereby, the performance of the model is examined on extreme and calm conditions, by quantifying the morphological impact at both of these time intervals.

The sensitivity analysis and the 1D validation of the XBeach model are performed only over the cross shore direction; therefore the directional distribution of the waves cannot be accounted. At the following numerical experiments, the wave record as derived from the operational model will be examined, as part of its validation process (Fig. 5.10 and 5.11).

The internal numerical parameters (see Appendix C) for the base case are set as

recommended by Roelvink et al. [2009]. The influence at the final profile is examined at the following cases by interchanging the parameters according to the best fit with the measured post storm survey. The experiments are presented in Table 6.1. The examined internal physical parameters concern the waves' non-linearity, the critical wet slope for avalanching and the long waves' induced sediment stirring. The model sensitivity to the physical quantities is tested with two water level records (computed and measured) and by increasing the wind setup. The post storm erosion volume is measured at the same reference frame as explained in Chapter 3 and is calculated as:

$$V = \sum(|b_{orig} - b_{final}| \times dx) \qquad (6.1)$$

where b_{orig} : pre-storm profile
b_{final} : computed post storm profile
dx : grid resolution

Here the upper limit is accounted as the highest elevation where the erosion takes place at each monitoring period, and the lower limit coincides with the deepest measured point according to the measurements performed by Ir. Rakhorst.

Table 6.1: Aggregated tests and numerical parameters for the 1D simulations of Jarkus transects 3400 in Bergen, 648 in Julianadorp and 4500 in Castricum.

	parameter				
test case	**wave asymmetry**	**critical wet slope**	**lws**	**surge**	**wind**
t34.13	0	0.3	0	comp.	-
t34.10	0.5	0.3	0	comp.	-
t34.15	0	0.15	0	comp.	-
t34.17	0	0.15	1	comp.	-
t34.19	0	0.15	1	measured	-
t34.20	0	0.15	1	comp.	20m/sec
t45.04	0	0.15	1	measured	-
t648.07	0	0.15	1	comp.	-

6.1 Base case study

The first considered profile is the Jarkus transect 3400 in Bergen. The pre-storm profile consists of a dune of N.A.P.+16m with slope of 1:2.2. At the end of the upper backshore area a berm of 6m height is present with a slope of 1:6.7 and width equal to 20m. As it is observed from the measured post storm profile (red profile at the top left panel in Fig. 6.1), the presence of the backshore berm prevented the erosion of the dune face, while the berm was eroded up until the N.A.P.+3m. It is expected that the profile above the berm was affected as well, as the data seem to attest. However the steep profile of the berm (1:1.4) after the storm, made the surveying impossible above the N.A.P.+6m elevation. Until the depth of N.A.P.-1.5m, the

measurements describe a flatter and slightly eroded profile, which means that the degradation has been continued until lower depths.

The top right panel of Fig. C.1 in App. C presents the storm induced profile until the peak of the storm. The berm (at x= 2450m) appears deepened and smoother, and the migration of the sediment at the offshore side of the berm induced the shoaling in this area. In contrast, the trough located at x= 2600m appears unaffected, in contrast with the trench around x= 2800m, which was elevated as it started trapping sediment. As approaching to shallower depth more intense wave breaking takes place which may resulted to the observed offshore transport of the sediment at this area (x= 2900m). As the peak of the surge coincided with the HHW level, the total volume change calculated at the reference frame (the area between the highest pre-storm measured point and the minima between the deepest measured points) is estimated equal to 48m^3/m. Until this period the computed profile (top right panel in Fig. 6.1) shows that the backshore berm is partially degraded until the elevation of N.A.P.+3m (blue line with crosses in Fig. 6.2 bottom panel) and most of the sediment is deposited from the backshore area. Due to the higher waves observed during this period and the low water depth, the maximum elevation that the erosion took place is observed at the end of the backshore berm up to N.A.P.+5m (blue line with circles in Fig. 6.2 lower panel). This point indicates the highest runup of the simulation (no avalanching took place during this period) and the maximum inundated area which extends to approximately 90m from the MKL. The combination of higher waves and the relative low water depth explains the high volume rate during this period (top panel in Fig. 6.2).

The second period describes the storm induced impact correlated with the second tidal circle up until 08:00 of the 4th of January (bottom left panel in Fig. 6.1). In the beginning, the combination of the HW slack tide and the high storm surge continued the degradation of the shore and the backshore berm. The deposited sediment was transported further offshore during the following neap tide due to the shallower depth and the increased shear stress, raising the rate of the volume change during this period.

Then, the second spring tide raised the storm tidal level until the 1.5m, increasing the amount of the foreshore eroded volume to approximately 72m^3/m. The subsequent ebb tide combined with the fainted storm surge, continued eroding the foreshore area with the same rate. At the end of the storm surge period, the measured and the simulated profiles show dissimilarities. The backshore berm has not been affected as much as recorded at the measurements. The backshore area has encountered significant degradation, showing a very flat post storm profile, contrary with the steeper corresponding measured area. Most of the sediment is transported from the area below the original backshore berm (x= 3105m), in total leading to 5m retreat (until x= 3100m) and 2m retreat above N.A.P.+3m, while the measurements indicate 15m retreat and almost entire degradation of the backshore berm. Apart from the wrong position of the sediment source, the amount of the displaced volume is overestimated, with the computed volume change to be equal to 75m^3/m while the measured volume change is approximately 52m^3/m.

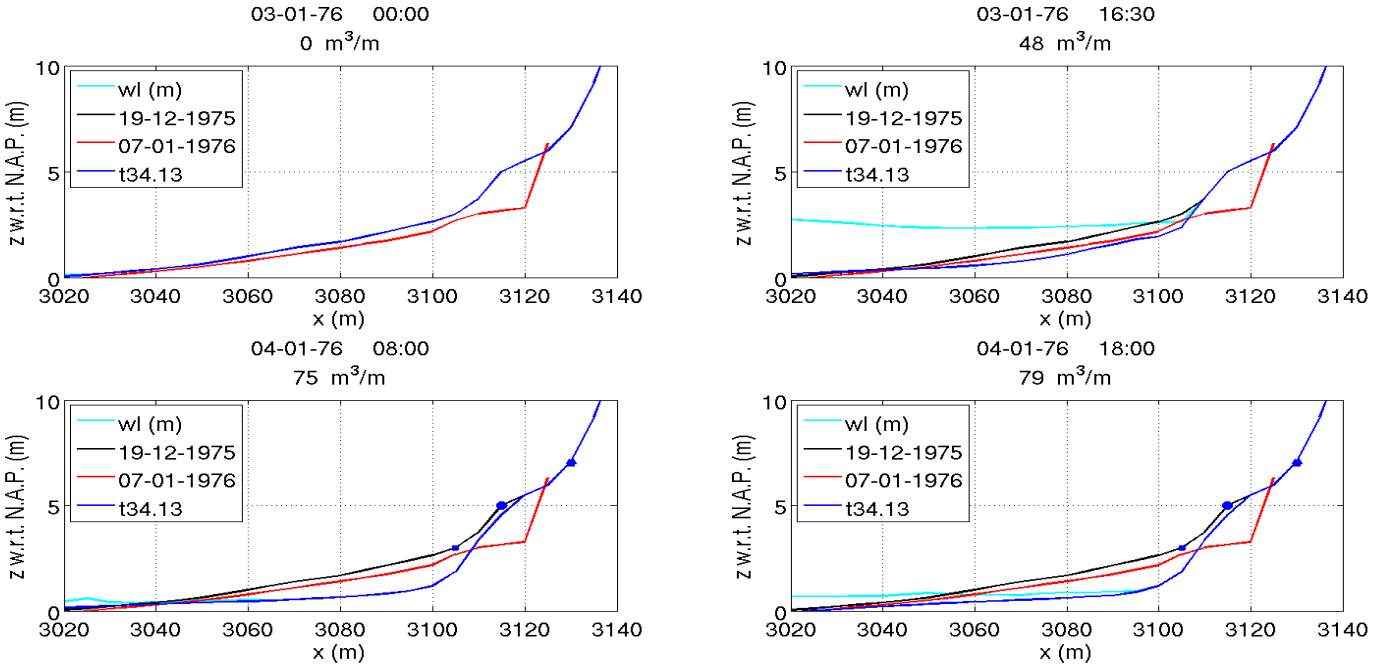

Figure 6.1: Measured pre-storm (black line) and post storm (red line) profile and computed profile (blue line) for the base test case t34.13 in the beginning of the simulation (top left panel), at 16:00 of 3-1-1976 (top right panel), at 08:00 of 4-1-1976 (bottom left panel) and at 18:00 of 4-1-1976 (bottom right panel).

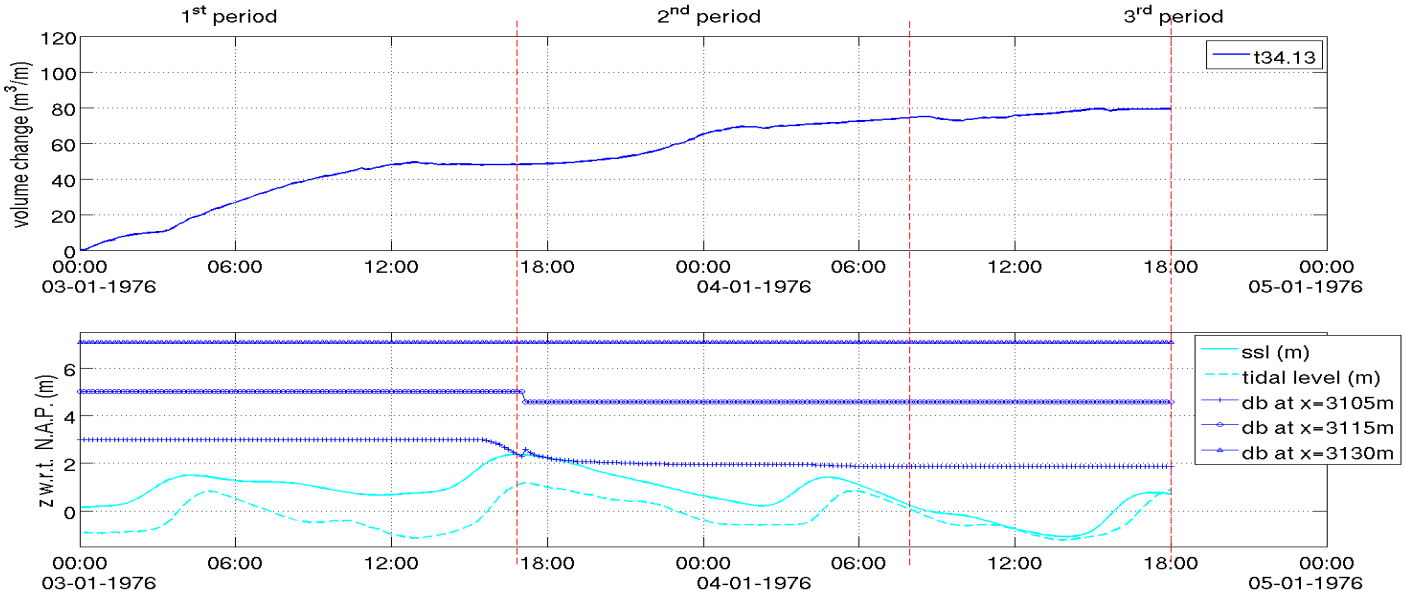

Figure 6.2: Top panel; Volume change as function of the storm evolution for the reference case t34.13. Bottom panel; Computed storm surge level (cyan line) and tidal elevation (cyan dashed line) in Bergen. Two points at the backshore berm from where the sediment is transported; at N.A.P.+5m (blue line with circles) and at N.A.P.+3m (blue line with crosses) and a point on the dune face at N.A.P.+7m (blue line with triangles), where no degradation was observed; see Fig. 6.1 for the location of the observation points. The red lines indicate the three periods of the storm as described in the four panels in Fig. 6.1.

Possible reasons of these differences are the lower estimated hydrodynamic conditions in combination with the numerical parameters which define the avalanche process at the model. The contribution of these parameters is the subject of paragraphs 6.2.2.2 and 6.2.3.

After the storm surge has passed, the deposited sediment at the foreshore area is transferred further offshore under the influence of the ebb tide alone. At the end of this period, the volume change is calculated equal to 79m^3/m, with increasing rate during the ebb tide and almost zero amount of erosion due to the following neap tide.

6.2.2 Sensitivity analysis to internal physical parameters

6.2.2.1 Wave asymmetry

At the nearshore area the sediment transport is affected by the nonlinear shape of the waves. In order to account for the transport due to wave skewness (narrow crests and wide troughs) and wave asymmetry (forward leaning) the flow velocity is calculated respectively as:

$$u_{A1} = u_a S_k u_{rms} \quad (6.2)$$

$$u_{A2} = - u_a A_s u_{rms} \quad (6.3)$$

where
u_{A1} : sediment advection velocity due to wave skewness [m/sec]
u_α : calibration coefficient for wave skewness and wave asymmetry
S_k : parametrization with the Ursell number for wave skewness (Ruessink and Van Rijn (2009), in Van Thiel de Vries (2009))
u_{rms} : root mean square flow velocity [m/sec]
u_{A2} : sediment advection velocity due to wave asymmetry [m/sec]
A_s : parametrization with the Ursell number for wave asymmetry (Ruessink and Van Rijn (2009), in Van Thiel de Vries (2009)).

The coefficient u_a (keyword facua) is implemented at the XBeach model as a calibration parameter for the sediment transport related to the wave shape, receiving values between 0.0 and 1.0. High values of the u_a parameter result to higher onshore velocities leading to onshore sediment transport. During extreme events the sediment transport is basically due to the long waves induced suspended sediment transport, so the contribution of the wave shape influence may be assumed minor. In case t34.10, the u_a parameter is set to 0.5 and the morphological evolution during and after the storm is examined with the default value of u_a=0.0 (base test case t34.13).

In the beginning of the first period, due to the increasing water level the lower backshore area started eroding (top right panel in Fig. 6.4). The sediment is deposited below the accounted

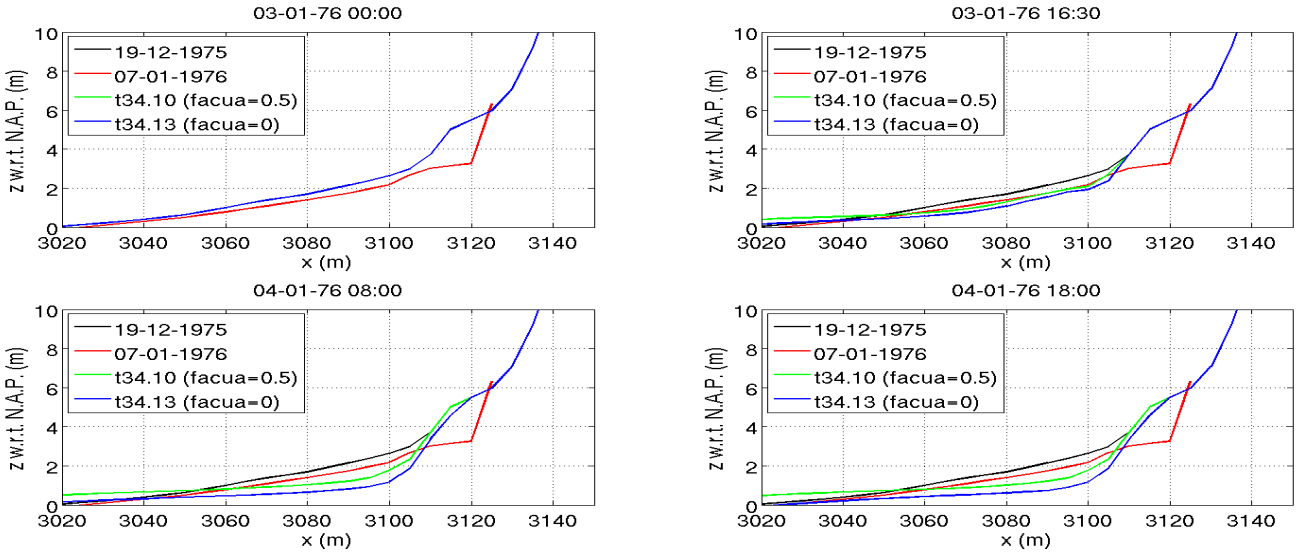

Figure 6.4: Measured pre-storm (black line) and post storm (red line) profile and computed profile for u_a=0.5 (green line) and u_a=0.0 (blue line) in the beginning of the simulation (top left panel), at 16:00 of 3-1-1976 (top right panel), at 08:00 of 4-1-1976 (bottom left panel) and at 18:00 4-1-1976 (bottom right panel).

reference frame, increasing the volume difference between the initial and the computed profile during this period. The rate of the volume change is higher, leading to approximately 57m^3/m (in contrast with the 48m^3/m in test t34.13). This pattern is more obvious at deep water (Fig. C2 in App. C), where the offshore bar and trench are shifted onshore. Closer to the shoreline, this forward shifted pattern induces the wave dissipation, which then accounts for lower degradation of the dune and the backshore berm, compared with the resulted profile at test case t34.13.

During the peak of the storm surge, the backshore berm was further eroded. The forthcoming ebb tide flattened the backshore zone by depositing sediment to the foreshore and the swash zone, while the deposition below this area was limited. In contrast with the continuous raising volume change that was observed during the test case t34.13, this case (top right panel in Fig. C2, App. C) presents an incorrect pattern for the nature of the studied events, as also discussed by Hoefel et al. [2003]. The increased onshore directed velocities combined with the low flow velocities during the slack water brought sediment landwards and accretion was recorded at the area where the volume difference is examined (green profile in Fig. C.2, bottom left panel). Additionally, the offshore bar and the trench located at the surf zone were further shifted landwards. When the next spring tide arrived, the shoreward directed offshore shoals and primarily the elongated beach profile, amplified the wave dissipation preventing extended dune erosion.

The measured and computed post storm profiles diverge considerably. The computed profile (green profile in the bottom left panel in Fig. 6.4) is characterized by low degradation of the backshore berm. In contrast with the measured foreshore profile, this area appears flattened

and elevated, due to the significant amount of sand that has been deposited. As for the onshore migration of the submerged coastal features, no measured data appear from this data set. It can be stated that the higher offshore directed velocities at the bar crest during the storm surge, should exceed the onshore directed velocities due to waves' nonlinearity. Therefore the landward migration of the offshore berm and the trough at the surf zone should not be observed during the storm surge.

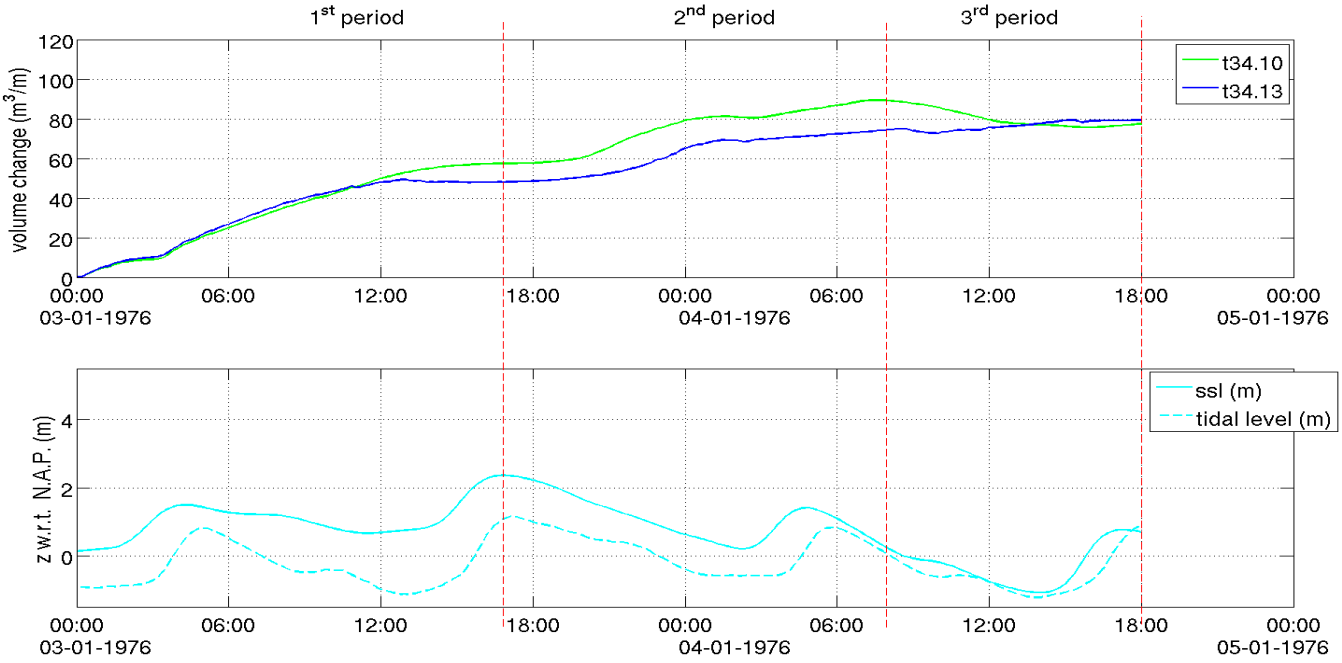

Figure 6.5: Top panel; Volume change as function of the storm evolution for the tests t34.10 (green line) and t34.13 (blue line). Bottom panel; storm surge level (cyan line) and the tidal elevation (cyan dashed line) in Bergen. The red lines indicate the three periods of the storm evolution.

At the third period (bottom right panel in Fig 6.4), the storm has ceased and the morphological impact is mainly due to the tidal influence. The beach profile is not affected significantly, while the swash zone became more flat, as the higher water level did not exceed the previously formed area of deposition.

Qualitatively, it can be argued that the value of 0.5 for the u_a parameter is more suitable for mild wave conditions, while zero or very low values (the same has been applied by Van Thiel de Vries [2009]) are preferable for storm events and for this range of grain diameter. Therefore, for this study, the u_a parameter will be set as u_a=0, in order to account for the significant higher flow velocities during the storm event.

6.2.2.2 Sensitivity to the wet slope parameter

At the dune erosion process, the collision regime contribution is accounted in the XBeach model through an avalanching algorithm. The bed level is updated through the amount of sediment that is deposited when a critical slope of the material is exceeded. Concerning the avalanching of the dry sand the critical slope (keyword dryslp) is set higher than the angle of repose of the dry sand and equal to 1. The slope above which the wet sand (keyword wetslp) is prone to avalanche is set equal to 0.3. Following the underestimated post storm profile of the backshore berm (which led at lower degradation of the backshore area) during the test case t34.13, in this section it is examined the effect of a lower wet slope value (wetslp=0.15) at the post storm profile.

Until the peak of the storm surge, the increasing water level (N.A.P.+3.1m) in combination with the lower wet slope value degraded the face of the backshore berm and the backshore area next to it (green profile in Fig. 6.6 top right panel). The difference at the profile with the two values of the wet slope parameter is located at this area, with the lower slope leading to 3m retreat of the backshore berm while in test case t34.13 (wetslp=0.3) the berm remains at its initial position. Further down shore the profiles show similar behavior with the sediment to be deposited at the initial shoreline (around the area of x= 3000m; Fig. C3 in App. C). Agreement between the computed profiles is observed as approaching to deeper water, where significant amount of sediment has been deposited at the landward side of the trough and the offshore bar has been sifted offshore (see also figure C.3 in App. C).

At the period till the pass of the storm (Fig. 6.6 bottom left panel), due to the lower water level (N.A.P. +2m) than the previous period, the main eroded area is the backshore zone. The degraded part of the backshore berm should be accounted due to sliding, given that the water level did not reach this level and the influence of the waves should not be considered significant at this area. The total retreat of the backshore berm is calculated equal to 4m for the test case t34.13 and equal to 9m for the test case t34.15, while the measured retreat at the 4-1-1976 was 14m. As a direct consequence of this limited retreat, both of the computed profiles present the backshore area more subducted in comparison with the measured post storm profile.

At the third period (Fig. 6.6 bottom right panel), no differences appear between the two computed profiles. Due to the ebb tide, the foreshore area continued eroding and the sediment has been deposited at the shallow runnel located at the nearshore zone (the area around x=2940m; Fig. C.3 in App. C).

In general it can be stated, that the lower value of the critical wet slope approaches better the measured post storm profile. It remains to be examined how much the underestimated computed hydrodynamic conditions contribute to the observed profile differences.

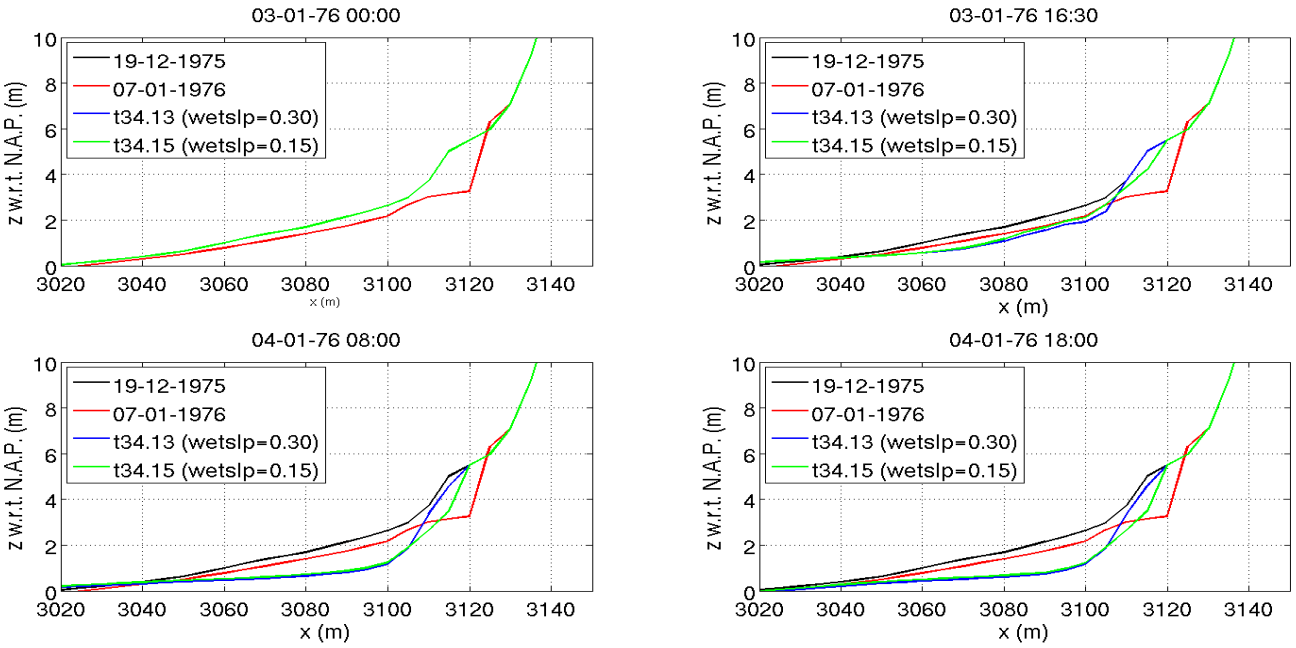

Figure 6.6: Centered view at the area where variance appears between the two computed profiles with wetslp=0.3 (blue line) and wetslp=0.15 (green line) in the beginning of the simulation (top left panel), at 16:00 of 3-1-1976 (top right panel), at 08:00 of 4-1-1976 (bottom left panel) and at 18:00 4-1-1976 (bottom right panel). The measured pre storm and post storm profiles are shown with the black and red line respectively.

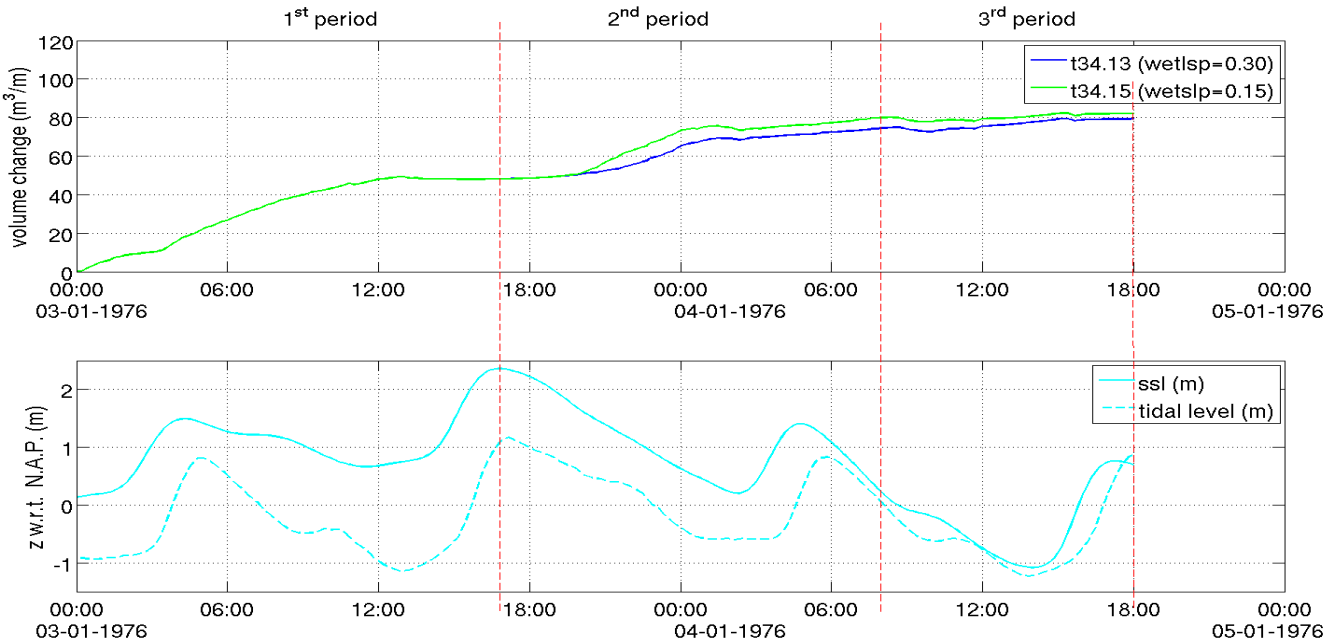

Figure 6.7: Top panel; Volume change as function of the storm evolution for the case t34.13 with wetslp=0.3 (blue line) and for the case t34.15 with wetslp=0.15 (green line). Bottom panel; storm surge level (cyan line) and tidal elevation (cyan dashed line) in Bergen. The red lines indicate the three different periods of the storm.

6.2.2.3 Sensitivity to the long waves' sediment stirring

Van Thiel de Vries [2009] studied the combined influence of the long and short waves, as well as their individual influence on the amount of dune erosion due to storm surges, through a series of physical and numerical tests with the XBeach model. He concluded that the amount of dune erosion only due to short waves, results approximately to 70% of the measured dune erosion volume, while the influence solely due to long waves is reduced to 50%. In the same study, Van Thiel de Vries mentions the contribution of the long waves on the dune erosion, and at shallow water the induced undertow and sediment stirring.

In the Soulsby - van Rijn formulation [4.42] [Soulsby 1997], the long waves' sediment stirring can be accounted explicitly in the suspended load coefficient A_{ss} and the bed load coefficient A_{sb}, or implicitly in the near-bed orbital motions [Reniers et al. 2004]. In order to account for the long waves' stirring, in the XBeach model (keyword lws) the velocity at each cell center of the numerical domain is computed by the averaged Eulerian velocities:

$$v_m = \sqrt{\overline{u_E}^2 + \overline{v_E}^2} \qquad (6.4)$$

where

v_m : velocity magnitude at the cell center [m/sec]
u_E : mean Eulerian velocity in the x-direction [m/sec]
v_E : mean Eulerian velocity in the y-direction [m/sec]

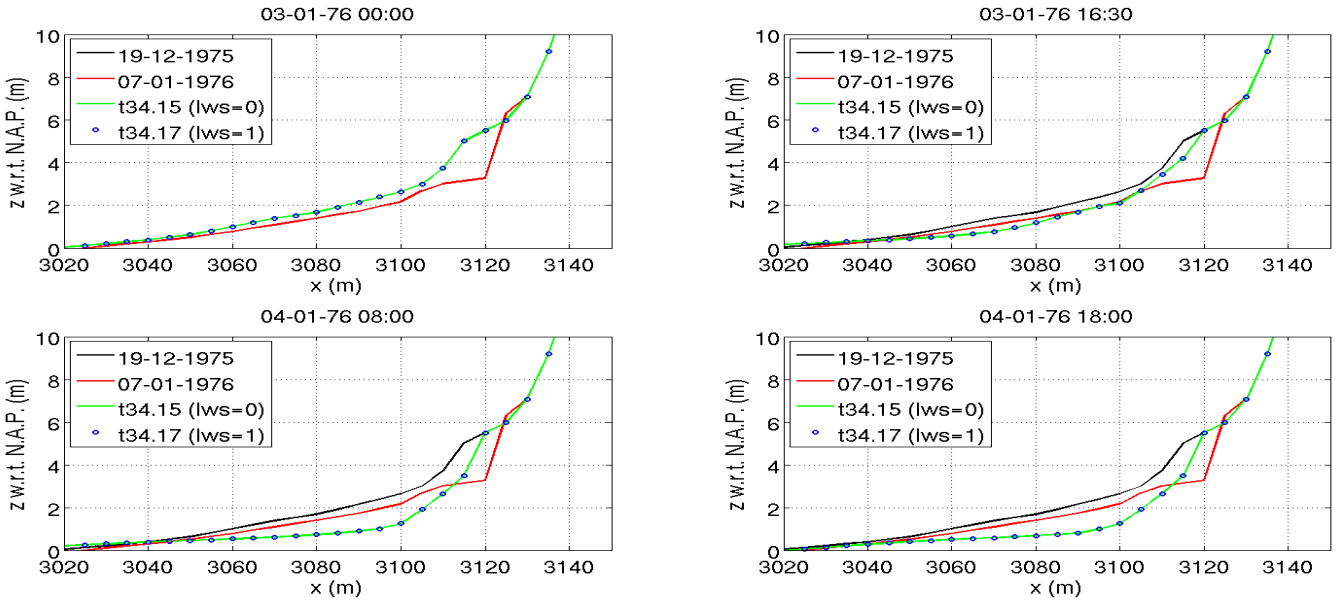

Figure 6.8: Measured pre-storm (black line) and post storm (red line) profile and computed profile for lws= 0 (green line) and lws= 1 (blue line) in the beginning of the simulation (top left panel), at 16:00 of 3-1-1976 (top right panel), at 08:00 of 4-1-1976 (bottom left panel) and at 18:00 4-1-1976 (bottom right panel).

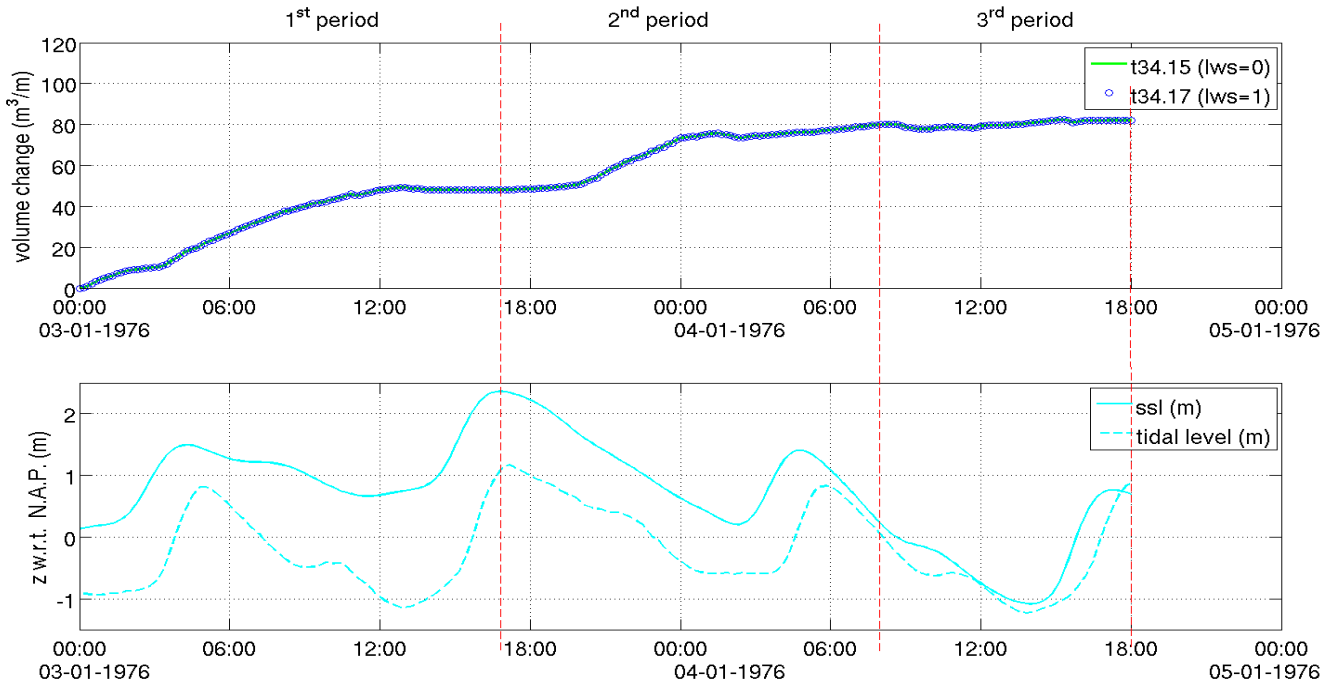

Figure 6.9: Top panel; Volume change over time without (blue line) and with the contribution of the long waves' sediment stirring (green line with circles) respectively. Bottom panel; tidal elevation and storm surge level in Bergen.

In this case the contribution of the long waves' sediment stirring does not change the post storm profile (green profile and the profile with the blue circles in Fig. 6.8 respectively). The volume change for the two cases is the same (top panel in Fig. 6.9) and the differences between the computed and the measured dune profile are not eliminated. However, it is expected that the orbital motion of the long waves may contribute to the suspended sediment transport. Therefore, the following simulations will be performed by applying this module (lws=1).

6.2.3 Sensitivity study due to the different measured and computed surge level

In this study, one of the main underestimations is the significant difference between the computed and the measured storm surge level (Fig. 5.12). The peak of the surge is underestimated up to 0.70m. McCall [2008] examined the effect of one hour time shift at the surge level caused by the hurricane Ivan at the Gulf of Mexico using the XBeach model. He concluded that the difference at the induced post storm profile is almost negligible. In this paragraph, it is examined the sensitivity of the model to higher storm surge level. For the test case t34.19, the storm surge level as measured near the breakwater of the port of IJmuiden is applied as the seaward water level boundary condition, while crudely neglecting the location of the measurements and the phase shift. The wave data are applied as computed by the DCSM, so that only the difference due to the varying water level to be examined.

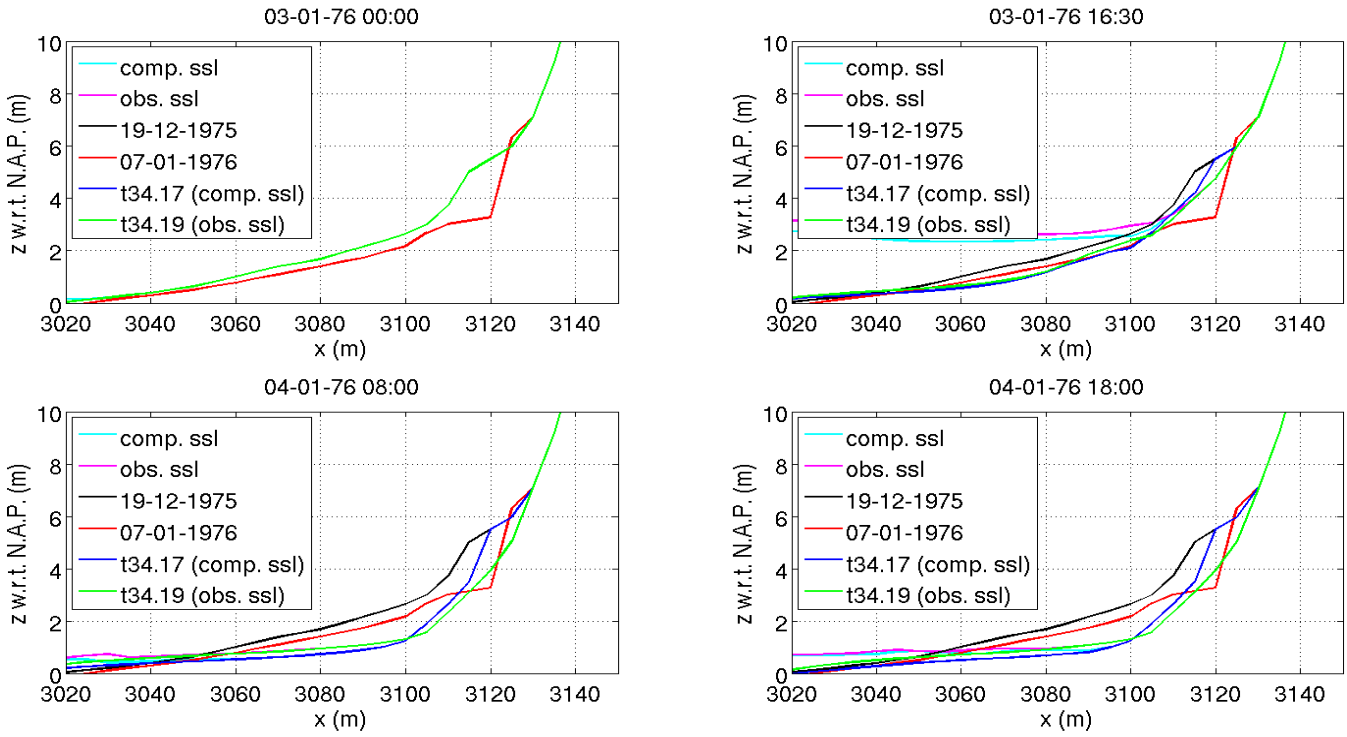

Figure 6.10: Beach and dune evolution during 42 hours from the arrival of the storm with the measured surge level from the tidal gauge in IJmuiden (magenta line) and the computed surge level in Bergen (cyan line). The black line indicates the pre-storm profile, the red line the post storm measured profile, the blue and green lines depict the computed profile with the two surge levels, in the beginning of the simulation (top left panel), at the peak of the storm surge (top right panel), at the end of the storm (bottom left panel) and 42 hours after the storm has arrived (bottom right panel).

At the first period until the peak of the storm surge, the difference between the measured and the computed water level is up to 0.70m. The higher water level as measured at the tidal gauge in IJmuiden results to higher degradation of the backshore berm in comparison with the degradation caused due to the computed water level from the DCSM (blue and green profiles respectively in the top right panel in Fig. 6.10). At the first case the retreat is estimated up to 10m, while at the second case the retreat did not exceed 5m. Differences between the two profiles are observed on the backshore berm and the marginal higher deposition at the backshore area (the area around x= 3100m). Further offshore, the two profiles are in good agreement estimating the same offshore migration observed at the offshore bar and at the landward side of the trough (around x= 2450m and x= 2750m in Fig. C5, App. C respectively).

During the second period the water level continued increasing until the 18:00 of the 3rd of January, when the highest elevation was observed. It can be stated that for the case t34.19 the flow depth 95m from the MKL (at x= 3115m) was measured equal to 0.45m resulting to an elevation of 5.5m above N.A.P., while this location remained dry, during the case t34.17. As a magnitude benchmark, during case t34.17 the flow depth at distance of 85m from the MKL (at x= 3105m) was measured equal to 0.5m, resulting to an elevation of 4.2m. The difference on

the morphological profile between the two cases is shown in Figure 6.10 (bottom left panel). At case t34.19 (green profile) the higher surge level wiped out the entire backshore berm (even more than the measurements records), while at case t34.17 (blue profile) the berm did not further retreat but scoured below the area of N.A.P.+4m. At the end of the storm, the backshore area appears extensively eroded in comparison with the measurements on the 4th of January 1976, as the eroded sediment from the berm removed from this area and deposited offshore.

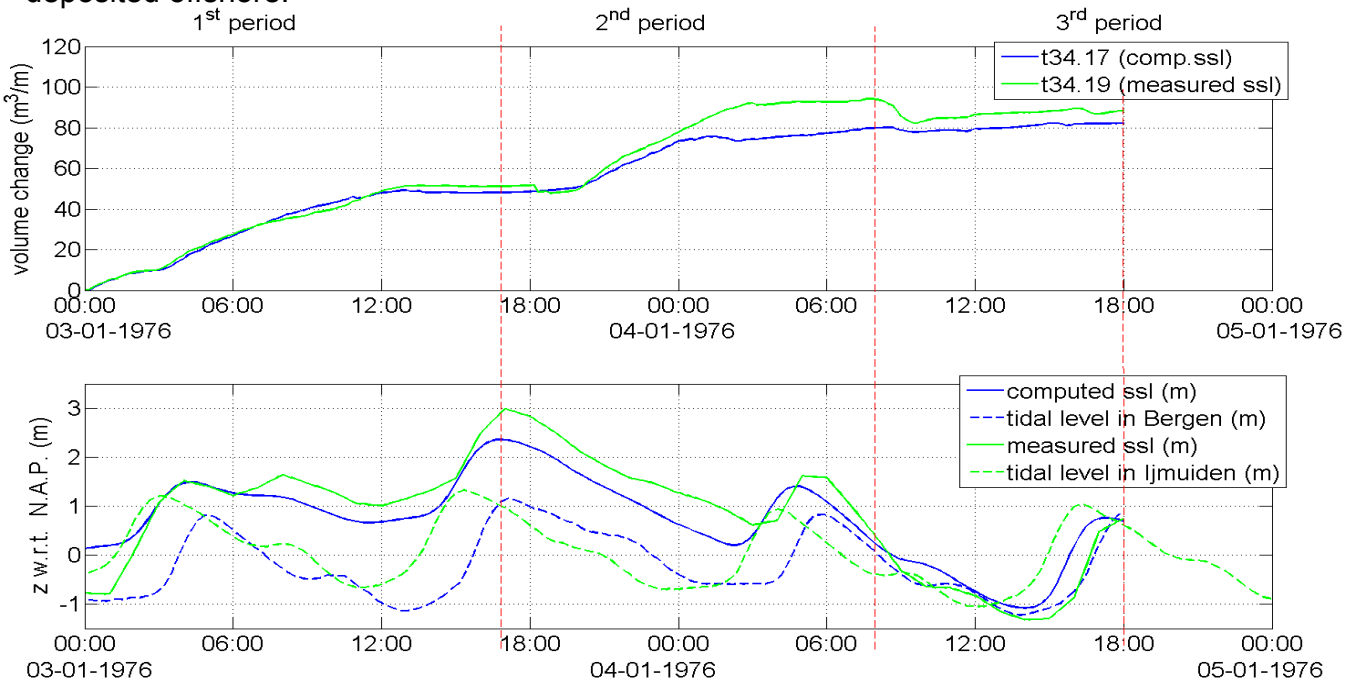

Figure 6.11: Top panel; Erosion volume change in Bergen, as computed by the measured storm surge level in IJmuiden (green line) and the computed storm surge level in Bergen (blue line). Bottom panel; Computed storm surge level (blue line) and tidal elevation in Bergen (dashed blue line), measured storm surge level (green line) and tidal elevation in IJmuiden (dashed green line).

At the last period due to the lower water level, the beach profile did not alter. A small amount of sediment was transported from the swash zone to the nearshore surf zone. For both of the cases the volume change is at the same range (Fig. 6.11 upper panel), with the case t34.13 showing marginal higher amount of erosion due to the higher water level.

In this section, it has been demonstrated that one of the main factors of the underestimated impact at the coastal profile, is the lower storm surge level. The test case t34.19 shows better agreement with the measured post storm profile. The profile evolution is estimated favorably and the model reacts as expected to different water level conditions. Differences are observed at the significant degraded backshore area, which leads to higher amount of the erosion volume.

6.2.4 The effect of wind setup

The test case of the previous section gave evidence of the dissimilarities due to the lower storm surge level. In order to examine further the sensitivity of the model to varying water level conditions and most important the contribution of the short waves on the dune face above the backshore berm, an additional setup of the storm surge is studied by increasing the wind stress. The wind stress is included at the XBeach model in the momentum balance equations [see eq. 4.30 and 4.31]. At this test case, the wind approaches normal to the shoreline with the velocity of 20m/sec. The wind setup is combined with the computed surge level in Bergen. The adapted internal model parameters are applied as discussed in the previous sections (see Table 3.1) and the rest of the parameters are explained in Appendix C.

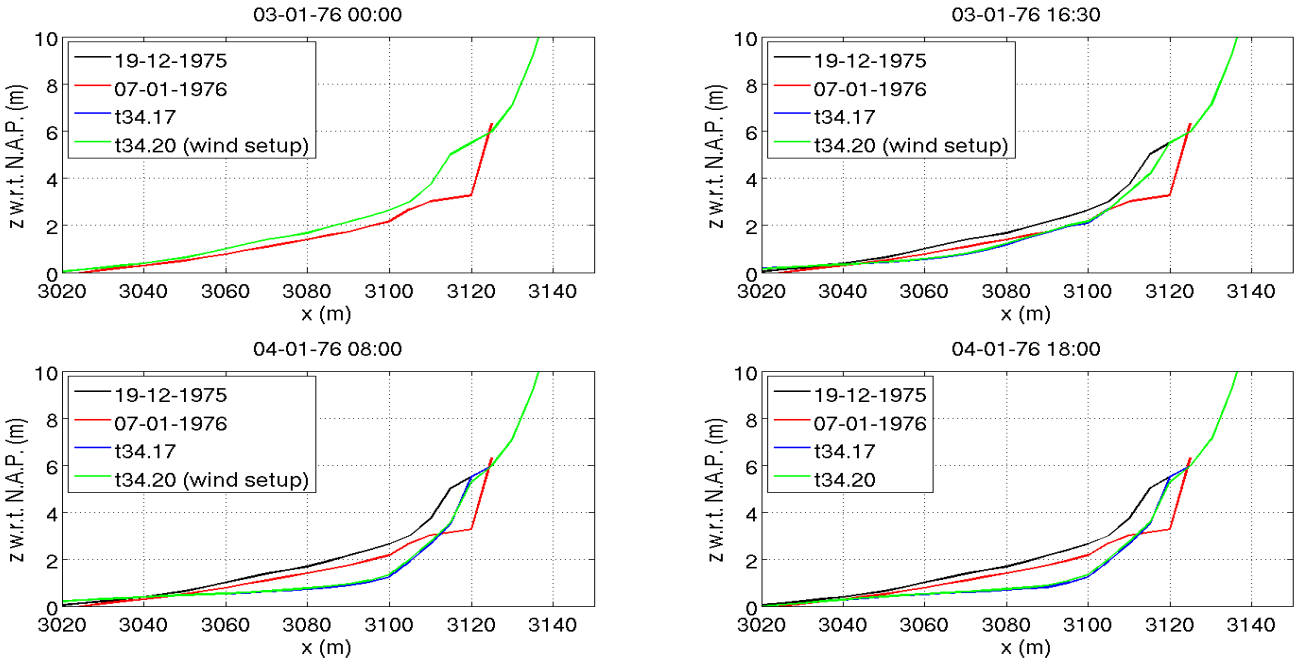

Figure 6.12: Pre-storm profile (black line), measured post storm profile (red line) and computed profile with (green line) and without the additional wind setup (blue line) respectively, in the beginning of the simulation (top left panel), at the peak of the storm surge (top right panel), at the end of the storm surge (bottom left panel) and 10 hours after the end of the storm (bottom right panel).

While the storm surge level increases, the impact on the dune face is minor, as observed in Fig. 6.12 (top right panel). Only after the end of the surge (green profile at the bottom left panel in Fig. 6.12), the upper level of the backshore berm started eroding more than at case t34.17, and a small amount of sediment was deposited at the backshore area. The difference between the computed erosion volume change (equal to $4m^3/m$, see top panel in Fig. 6.13) is marginal and does not improve the model performance.

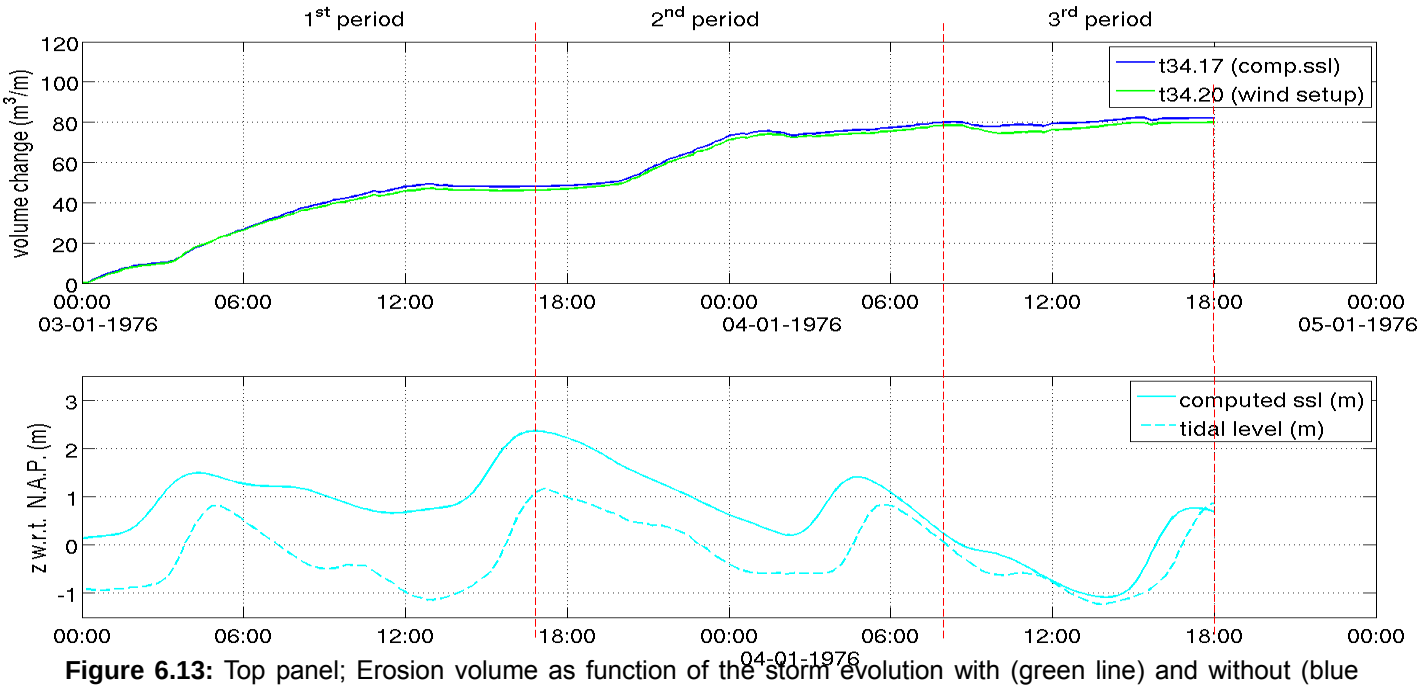

Figure 6.13: Top panel; Erosion volume as function of the storm evolution with (green line) and without (blue line) the additional imposed wind set up. Bottom panel; Computed storm surge level (solid line) and tidal level (dashed line) in Bergen.

6.3 Model verification - A test case in Castricum

The volumetric analysis of section 3.4 highlighted the lower volume change in Castricum after the storm surge event at the 3rd of January 1976. In this paragraph, this particular case is examined with the XBeach model by applying the above tested numerical parameters (Table 6.1) and the water level record from the tidal gauge in IJmuiden, as better performance was observed (see section 6.2.3). The pre-storm profile (blue profile in Fig. 6.14 upper left panel) consists of an offshore trough with maximum depth equal to 6.5m (top left panel in Fig. C.7, App. C). As approaching to the shoreline two more features are present, a second trough with maximum depth of N.A.P.-3.7m and a bar with height equal to N.A.P.-2m. The dune is extended until N.A.P.+18m above with a pre-storm slope of 1:2.6. The measured post storm profile (red profile in Fig. 6.14 upper left panel) is described by a steeper dune face with slope equal to 1:1.7 and significant deposition at the lower backshore area and at the swash zone.

At the period from the arrival of the storm surge until its peak, the degradation of the dune extended until N.A.P.+8.5m (top right panel in Fig. 6.14). Concerning the part of the dune above N.A.P.+4.5m, 21m^3/m were avalanched due to the initial steep profile. Part of the eroded sediment was deposited at the backshore area and part was moved further down shore. At the end of this period, in total 26m^3/m were eroded from the foreshore zone (from x=2885m to x=2960m). The total volume change at the measured reference frame (from the lowest measured point until the point where no erosion took place during the whole period of the storm) raised up to 62.5m^3/m, which provides an insight of the deposited amount of

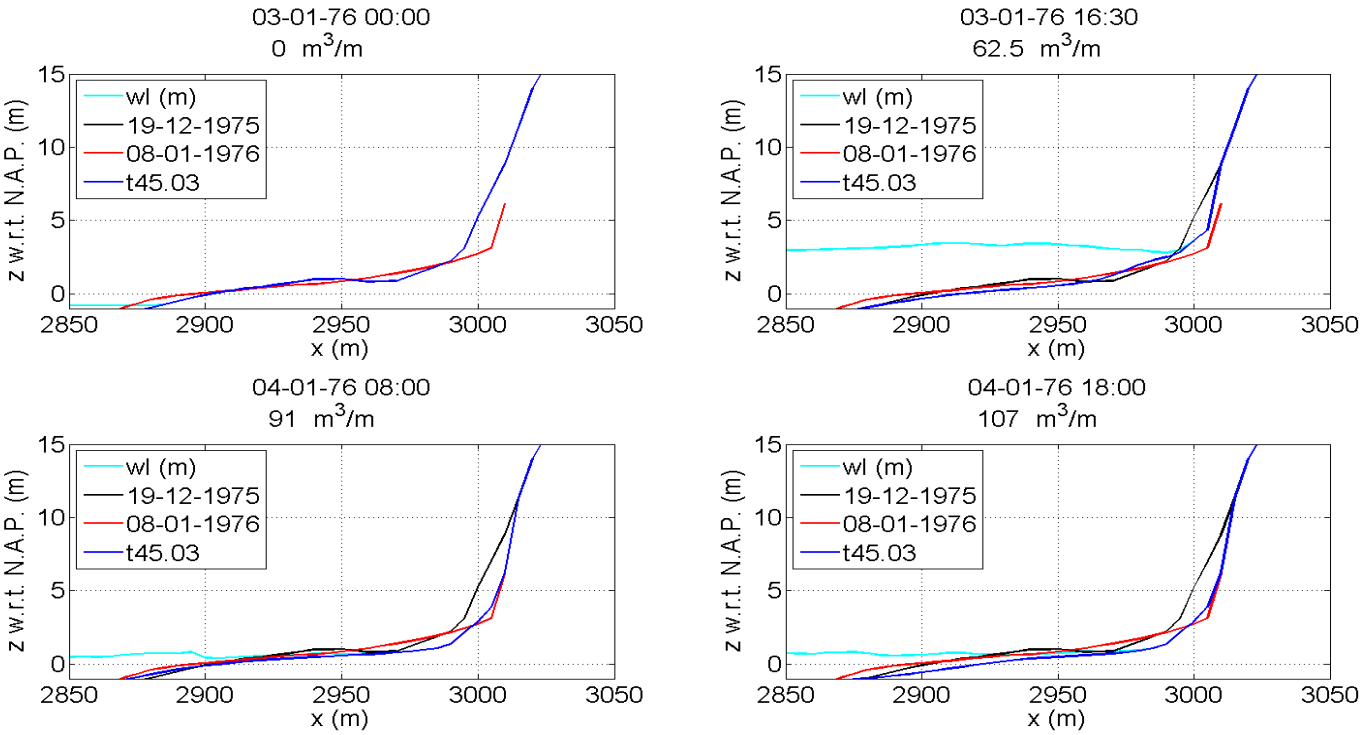

Figure 6.14: Measured pre-storm (black line) and post storm profile (red line) and computed profile (blue line) in Castricum at the beginning of the simulation (top left panel), at the peak of the storm surge (top right panel), at the end of the storm (bottom left panel) and 10 hours after the end of the storm (bottom right panel).

sediment that took place at this area. Significant degradation was observed at the nearshore bar (x= 2800m), while the nearshore runnel (at x= 2750m) and the offshore trough (at x=2860m) trapped the sediment and accreted (Fig. C.7 in App. C).

At the second period the dune face sustained more intense erosion. The total dune retreat is calculated equal to 6m, which is in good agreement with the measurements performed at the 8-1-1976 (blue and red profile respectively, at the bottom left panel in Fig. 6.14). While no measurements are available for the area above N.A.P.+6m, the trend of the data seems to agree with the model's estimations, that the erosion should have taken place at a level higher than N.A.P.+11m. At the end of the storm, the dune avalanching raised to almost 32m^3/m, while the total dune erosion was equal to 41 m^3/m (from x= 3000m to x= 3020m). Differences appear between the measured and the modelled post storm profile of the backshore zone. The model overestimates the erosion amount leading to a more scoured dune foot and flatter profile of the backshore area. Therefore the foreshore area appears more flat and the offshore trough has been further accreted.

At the last period after the storm has ceased the beach profile altered significantly. The sediment that has been deposited at the beach front during the storm, has been eroded with low rate (top panel in Fig. 6.15) due to the ebb tide and increased the bed level of the foreshore zone (blue profile at the bottom right panel of Fig. 6.14).

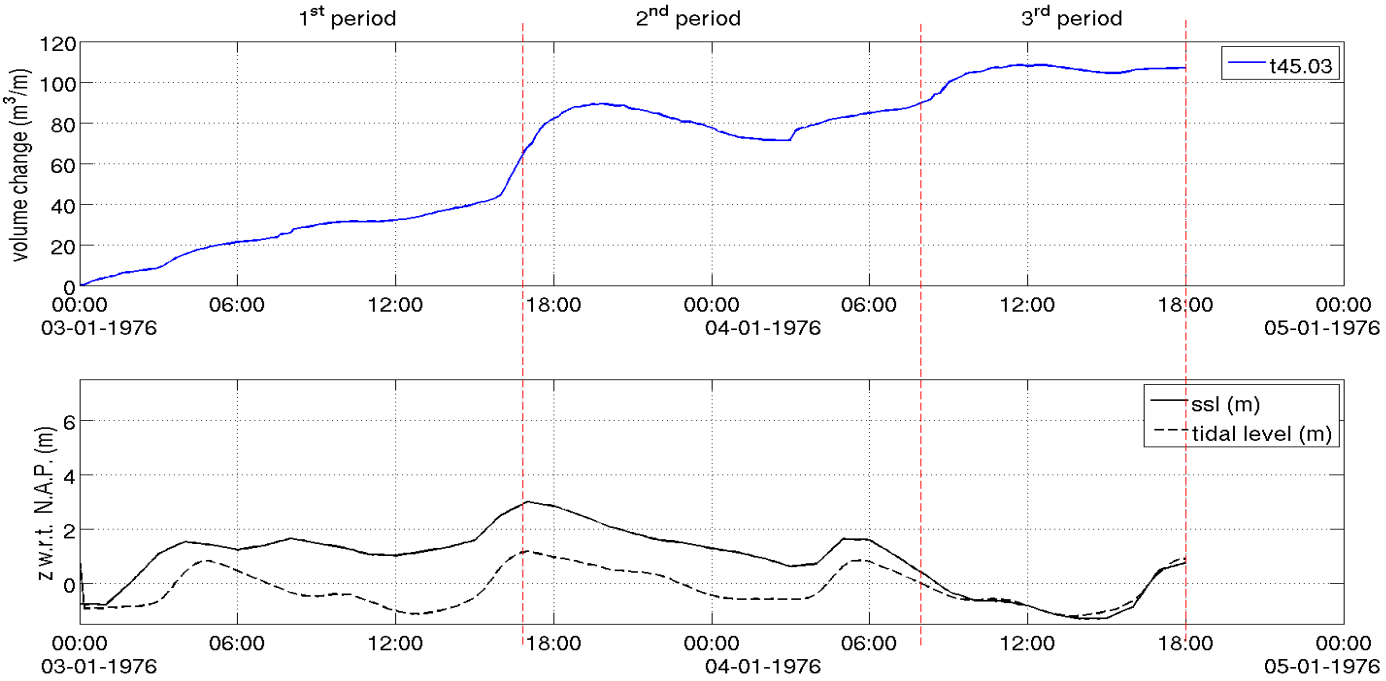

Figure 6.15: (Upper panel) Volume change at Castricum as calculated at the three periods of the study. (Bottom panel) Imposed storm surge level (solid line) and the tidal elevation (dashed line).

6.4 A test case in Julianadorp

The third case study concerns the impact of the 1976 storm surge in Julianadorp. As mentioned in Chapter 3, the area around this site is protected by series of groines in order to eliminate the transport due to the tidal currents originating from the Marsdiep inlet. At the current case, the effect of the groines will be neglected and the profile evolution is examined under the hydrodynamic conditions as computed from the KST model. The model parameters are listed in Table 6.1.

The Jarkus transect 648 in Julianadorp is a relatively shallow area where the offshore area is characterized by the presence of a bar with maximum height equal to N.A.P. -2.7m (around x= 2750, Fig. C8 in App. C). Two rows of dunes are present at the backshore zone with the most seaward one being the highest and extending until the N.A.P.+7m. As it observed from the measured post storm profile (red profile at the top left panel in Fig. 6.16), the first dune was completely eroded while the second one sustained lower damage.

At the end of the first period (top right panel in Fig. 6.16) which coincides with the maximum storm surge level, the first dune appears significantly eroded. During this period the maximum runup level raised up to N.A.P.+4.0m partially eroding the first dune. This dune recession allowed the penetration of the waves until higher level, resulting also to partially damage of

the second dune. The foreshore zone sustained significant erosion and became deeper approximately 0.60m with respect to the initial profile. Most of the sediment seemed to be trapped at the nearshore trough almost 200m from the shoreline (around x= 2800m, see Fig. C8 in App. C), while the nearshore bar appears fairly degraded and migrated further offshore. During this period, the volume change of the beach and the dune profile is estimated equal to 49m^3/m.

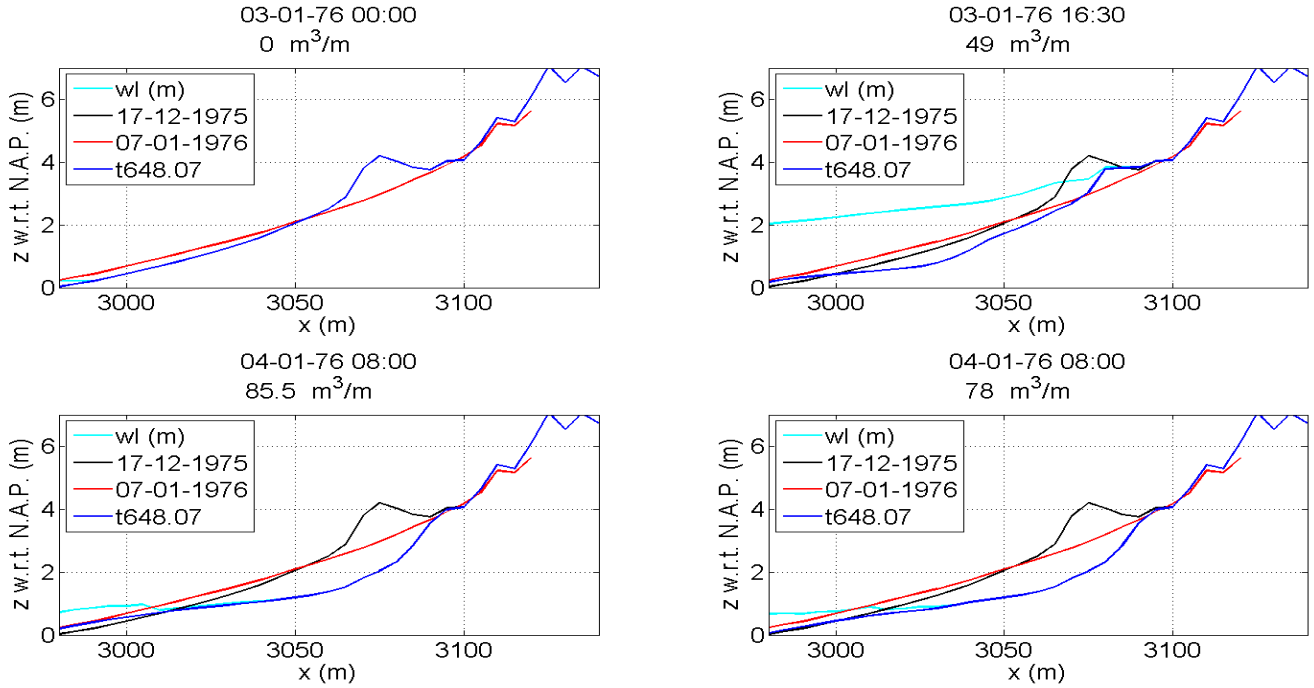

Fig. 6.16: Beach and dune evolution during the 1976 storm surge at the four periods of the study for the test case t648.07; in the beginning of the storm (top left panel), at the peak of the storm (top right panel), at the end of the storm period (bottom left panel) and 42 hours after the arrival of the storm (bottom right panel). Measured pre-storm profile at the 17-12-1975 (black profile), measured post storm profile at the 7-1-1976 (red profile) and computed profile for the test t648.07 (blue profile).

The highest erosion volume rate is observed at the second period, after the peak of the storm surge (top panel in Fig. 6.17) due to the receding water level. At the end of the storm period (bottom left panel in Fig. 6.16), the first dune appears entirely wiped out, in contrast with the second dune which was not reached due to the decreasing water level. The total erosion volume is calculated equal to 85.4m^3/m, lower than the computed volume change in Bergen (approximately 95m^3/m, see also the green profile in Fig. 6.11, top panel) and in Castricum (approximately 90m^3/m, Fig. 6.15 top panel). The maximum dune retreat is estimated equal to 20m. Significant amount of sediment is deposited at the nearshore trough and further offshore

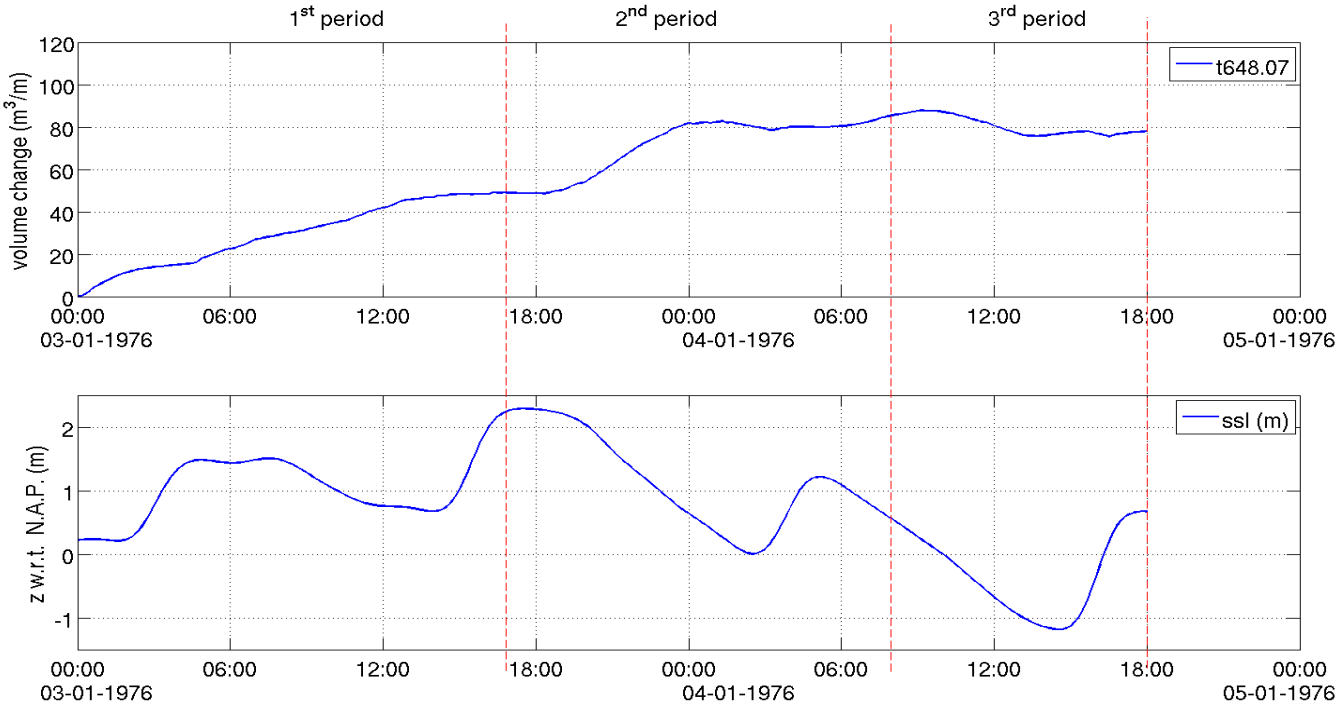

Fig. 6.17: Top panel; Erosion volume during the three periods of the storm for the test case t648.07. Bottom panel; Computed storm surge level in Julianadorp.

at the landward side of the deepest trough (around x= 2800m and x= 2650 m respectively, see Fig. C8 in App. C). Differences appear between the computed and the measured profile. The measured data attest that, the first dune row sustained significant erosion, but not of the order that the model estimates. Consequently, the computed dune profile appears significantly scoured.

Ten hours after the end of the storm, the volume change at the reference frame is lower, as the upper foreshore zone sustained more erosion and the sediment is transported seaward to the lower foreshore zone, elevating this area. No further changes appear at the profile above N.A.P. +1m.

6.5 Discussion

In this chapter the performance of the XBeach model is investigated on estimating both qualitatively and quantitatively the impact of the 1976 storm surge at three sites along the North Holland province. The sensitivity analysis of the model has been performed by varying the internal physical parameters and boundary hydrodynamic conditions. The computed profiles were examined at three periods during the storm evolution, with basic criterion if the physical reflection of the extreme events nature is satisfied. The second criterion was to examine the computed results with the available measured data at the end of the storm surge

and under the influence of the tide. Whenever no data were available, which was the case when the post storm dune profile was not accessible to be surveyed, then the trend was quantified.

Furthermore, the model performance is examined both at the end of the storm surge period (at 08:00 04-01-1976) and at the end of the simulation (at 18:00 04-01-1976) as the measurements were performed many days after the storm had passed. Table 6.3 presents the Brier Skill Score (hereafter BSS) for the test cases described in this chapter, in addition with the computed and measured horizontal surface retreat at the maximum storm surge level, and the maximum dune retreat. The BSS [Van Rijn et al. 2003] correlates the modelled post storm profile b_{comp} with the surveyed pre-storm profile b_{orig} and the measured post storm profile b_{meas} as:

$$BSS = 1 - \frac{\overline{(b_{comp} - b_{meas})^2}}{\overline{(b_{meas} - b_{orig})^2}} \qquad (6.5)$$

where b_{comp} : modelled post storm profile [-]
b_{meas} : surveyed post storm profile [-]
b_{orig} : pre-storm profile [-]

Table 6.2: Error limits for the BSS [Van Rijn et al. 2003].

	value	model performance
BSS	< 0	Bad
	0 - 0.3	Poor
	0.3 - 0.6	Reasonable/ fair
	0.6 - 0.8	Good
	0.8 - 1	Excellent

Table 6.3: Horizontal surface retreat at the maximum storm surge level, maximum dune retreat, profile volume change (m^3/m) and Brier Skill Score for the test cases t34.13 to t648.07. The elevation z is calculated with respect to N.A.P.

	parameter					horizontal surface retreat at max. ssl (m)		maximum dune retreat (m)		ΔV (m3/m)			BSS	
											model prediction			
test case	wave asymmetry	critical wet slope	lws	surge	wind	measurements	model prediction	measurements	model prediction	measurements	end of storm	10 hours after the storm	end of storm	10 hours after the storm
t34.13	0	0.3	0	comp.	-	8 (z=2.36m)	13	13 (z=3.27m)	3	52.0	74.6	79.0	-0.32	-0.33
t34.10	0.5	0.3	0	comp.	-	8 (z=2.36m)	11	13 (z=3.27m)	1	52.0	89.0	77.5	-0.77	-0.5
t34.15	0	0.15	0	comp.	-	8 (z=2.36m)	14	13 (z=3.27m)	7	52.0	80.0	82.1	-0.07	-0.05
t34.17	0	0.15	1	comp.	-	8 (z=2.36m)	14	13 (z=3.27m)	7	52.0	80.0	82.1	-0.07	-0.05
t34.19	0	0.15	1	measured	-	5 (z=3.00m)	9	12 (z=3.27m)	9	52.0	94.0	88.3	0.34	0.3
t34.20	0	0.15	1	comp.	20m/sec	8 (z=2.36m)	13	13 (z=3.27m)	6	52.0	78.4	80.0	0.09	0.11
t45.04	0	0.15	1	measured	-	9 (z=3.00m)	7	10 (z=3.15m)	6	83.3	90.0	107.0	0.84	0.72
t648.07	0	0.15	1	comp.	-	1 (z=2.36m)	23	20 (z=3.60m)	21	61.3	85.4	77.8	-1.01	-0.97

The model results concerning the Jarkus transect 3400 in Bergen are characterized by a very low skill (see Table 6.2 for the error limits of the BSS), which tends to increase when the changes are applied according to the best fit observations. The model reacts as expected at most of the applied changes. This is maintained arguably by the highest demonstrated skill of test case t45.04 and t34.19 where the measured storm surge level has been applied as the hydrodynamic water level boundary condition. Additionally, in some cases the skill appears marginally different when it is considered at the end of the storm or at ten hours later (see the last two columns in Table 6.3 respectively), due to the continuous profile changes that take place at the lower foreshore zone.

Among the test cases concerning the transect 3400 in Bergen, the lowest skill is observed when the parameter which determines the wave asymmetry (facua) is tuned at the value of 0.5. This is due to the higher onshore directed velocities and the consequent onshore migration of the sediment, which leads to lower degradation of the backshore zone. When the facua parameter is set to zero, then higher skill is achieved, but it is located at non-acceptable levels. Neither the horizontal surface retreat at the maximum storm surge level nor the maximum dune retreat are in good agreement with the measurements, as it has been also observed in Fig. 6.4.

Higher correlation than the previous cases appears when the lower critical wet slope is applied (test t34.15), thus when the sediment is more prone to avalanche. While the correlation between the computed and the measured data for the higher value of the wet slope is not significant higher, the difference is obvious during the simulation as the system appears not to be supplied by the avalanched sediment and thus leading to lower degradation of the dune profile. The avalanching algorithm implemented at the XBeach model proves its robustness, especially when the wave asymmetry is not considered; this combination results to higher offshore directed sediment transport which is observed during extreme storm events and better agreement with the measurements concerning the maximum dune retreat. While the BSS is located at the “no skill” level, the model presents a better performance than the previously considered cases. The test case t34.17 - the long waves’ sediment stirring is enabled – does not improve the model’s skill. By applying this module, no difference at the maximum dune retreat or at the horizontal retreat at the maximum storm surge level is observed.

At the test case t34.19 the measured storm surge level at the entrance of the port of IJmuiden is applied as the offshore water level boundary condition. The BSS considering this case is the highest among the test cases for the area near Bergen, reflecting also a better estimation of the maximum dune retreat; the model estimates 9m while the measurements showed 12m maximum dune retreat. This increased correlation, between the computed and the surveyed post storm profiles made evident the significant influence of the underestimated hydrodynamic conditions as computed from the operational model, despite the reasonable performance of the XBeach model.

The test case t34.20, where the induced wind setup is increased due to gales of 20m/sec, does not provide better model performance. Despite of the fact that the short waves eroded the upper part of the backshore berm, which was the area that the erosion profile was underestimated at the previous test cases, the performance of the model is justified as “poor”.

The test case t45.04 in Castricum gives the highest overall correlation among the test cases presented in this chapter. As it is also observed in Fig. 6.13 (blue profile at the bottom left panel), the model estimates with an excellent skill (BSS= 0.84) the post storm profile including the trend above the available measured data. The horizontal retreat at the storm surge level (N.A.P.+3m) was measured equal to 9m which is in good agreement with the model estimations (7m). Additionally, the model estimates the maximum dune retreat equal to 6m while the observations indicate 10m. Probably, this overall skill is related with the water level boundary condition, which at this case is the measured water level instead of the computed water level. Ten hours after the end of the storm, the model is characterized by good skill (BSS= 0.72) which reflects the continuous erosion of the lower beach profile, even if the numerical parameters were tuned to simulate extreme events.

The test case t648.07 in Julianadorp presents the lowest skill among the presented cases. At the bottom left panel in Fig 6.16, the upper backshore area of the computed post storm profile is significantly scoured and the model overestimates the horizontal retreat at the storm surge level; the measurements indicate 1m while the model estimations are 23m (Table 6.3). In contrast, better agreement is observed at the dune face, where the model estimates very well the maximum dune retreat. It should be mentioned that at this test case the waves are approaching normal to the coastline and that the effect of the groins is not accounted, which have forbidden a realistic simulation of the impact observed in this area.

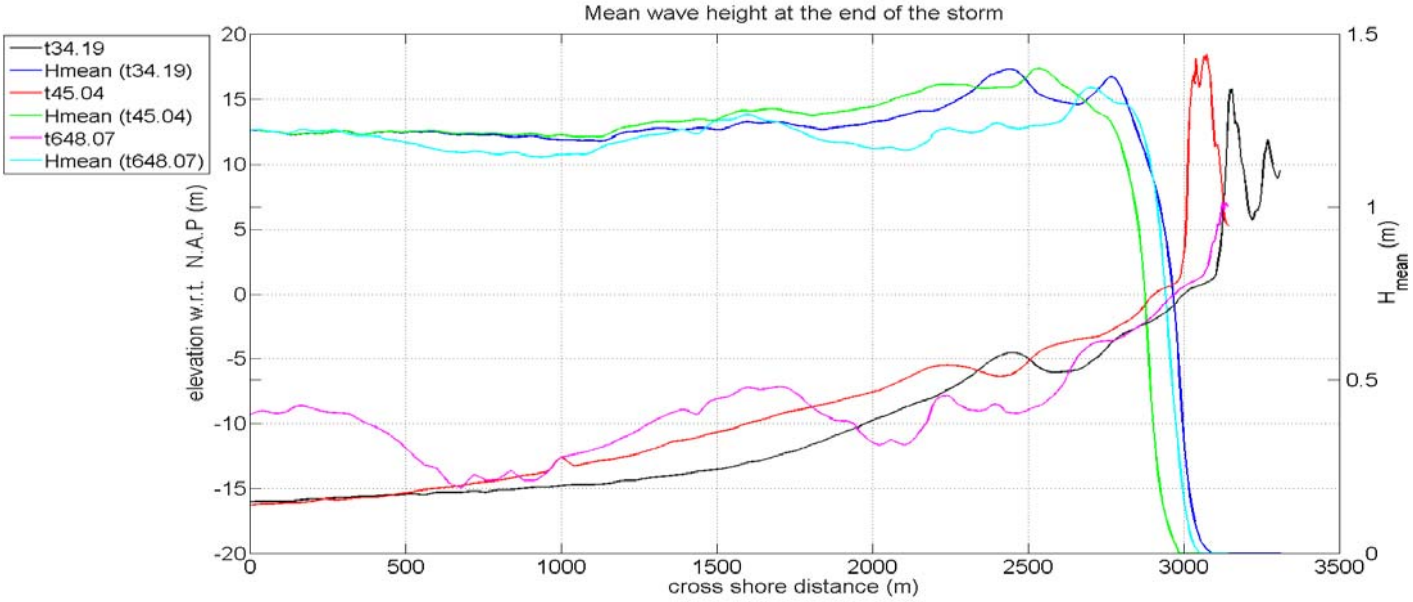

Figure 6.18: Computed H_{mean} at the end of the storm in Bergen (blue line), Castricum (red line) and Julianadorp (cyan line), for the test cases t34 19 in Bergen (black line), t45.04 in Castricum (red line) and t648.07 in Julianadorp (magenta line) respectively.

Furthermore, the longshore variability which was observed during the volumetric analysis in Chapter 3 is proved to be valid. The volume change in Castricum is lower than in Bergen. The bottom profile of the breaker zone in Castricum is elevated and dissipates the energy faster (green profile in Fig. 6.18). Contrarily, in Bergen the waves seem to break due to the geological features (around x= 2500m) located in the breaker zone and due to the steeper foreshore zone (x= 2760m), allowing for higher damage of the dunes. According to the measurements and the computed results, at this area the dune face was protected due to the presence of the backshore berm, which absorbed most of the impact (see also the bottom left panel in Fig. 6.10). Similar observations may be formulated for the studied site in Julianadorp; the relative rough offshore profile due to the troughs and bars and the steeper foreshore zone in combination with the narrow beach resulted to higher degradation of the backshore berm, while the dune face remained unaltered.

In general, it can be stated that the XBeach model is characterized by high order of sensitivity, as at most of the cases presented, the physical aspects of the extreme events were satisfied according to the changes of the numerical parameters. Concerning the morphological validation of the model, its performance is dependable not only on the boundary conditions as calculated by the operational model, but also at the morphological characteristics of each area. The coastal response of the 1976 storm surge was highly related with the presence of these geological features and varied along the coastline of the North Holland province.

7. CONCLUSIONS AND RECOMMENDATIONS

7.1 Conclusions

In this study two major storm surge events are studied, which hit the coastline of the Netherlands during the past century. The ultimate end is to examine the validity of the real-time storm forecast system in the Netherlands and its capability to estimate the morphodynamic response on prototype scale during extreme events. This system integrates into an operational mode the weather forecast models with hydrodynamic and morphodynamic models.

Concerning the storm event of 1953, the validity of the operational model system is examined only on its skill to represent the observed storm surge level, as no wave records were available (even though it can be stated that the wind-induced waves were relatively low during this storm event). Quantitative comparisons between the measured and the computed surge records obtained from five tidal stations along the Dutch coast show that the model estimates accurately the arrival time of the surge, while the surge level is underestimated up to 0.60m and the phase lag up to 45 minutes. Whether these underestimations may influence the storm-induced profile change, needs to be further elaborated with a morphodynamic model.

Since 1963 the coastline of the Netherlands is monitored twice a year, in line with the Jarkus programme. Additionally, the advanced weather forecast system and the flood protection system prevented the disaster of 1953, when the storm surge of 1976 hit the coastline of the Netherlands. Based on these records, the validity of the operational model system to estimate the impact of the 1976 storm surge is inspected along the North Holland province. The volumetric analysis of the pre and post storm coastal profile is performed by obtaining the most recent to the storm surge event measurements. This analysis pointed out the dissimilar impact even at neighboring sites. For the morphodynamic comparison of the XBeach model and in a broader sense of the operational model, three sites were selected; Bergen, Castricum and Julianadorp. Apart from the visual observations, the performance of the XBeach model is appraised qualitatively with the Brier Skill Score [Van Rijn et al. 2003] and quantitatively by calculating the actual volume change and the dune retreat.

For a proper assessment of the impact, first the sensitivity analysis of the XBeach model is performed in the area of Bergen. The model appears to respond according to the nature of the extreme storm events. When the waves' nonlinearity is accounted, then the onshore directed velocities bring more sediment onshore and the model's skill drops. Therefore, this parameter should be kept at low values. When the waves' nonlinearity is not accounted the model performs with higher skill, especially when combined with a low value of the parameter that determines the wet slope at the avalanching mechanism. This combination resulted to more severe erosion of the backshore zone; the area where the model performance was limited. The next test case concerns the sediment stirring due to the long waves, which at the XBeach model is deployed by averaging the Eulerian velocities. In the current study this

parameter did not alter the post storm profile and the model's performance did not improve. This case was the only one where the model's sensitivity was not satisfied. Furthermore, the additional imposed gales resulted to marginally better skill, as higher waves eroded the upper backshore berm. The small profile differences observed in this case may reflect an underestimation of the computed wave data.

The measurements concerning the 1976 storm surge showed that the computed storm surge level is underestimated up to 0.70m. When the profile in Bergen is examined under the measured storm surge level (obtained by the tidal station in IJmuiden), the model performs with fair skill. The higher water level increases the dune retreat and the area of the backshore berm approaches better the measured post storm profile.

The second investigated profile is located in Castricum. By imposing the measured storm surge level (obtained by the tidal station at the port of IJmuiden) instead of the surge level computed by the DCSM, higher correlation is obtained between the computed and the measured post storm profiles. At this case the XBeach model performs with an excellent skill and estimates with high accuracy the post storm dune retreat. At this test case the maximum rate of erosion is observed at the peak of the storm, which was not observed at the previous cases. The higher skill of the model demonstrates that the underestimation of the hydrodynamic conditions contributes significantly at the performance of the operational model chain.

The last considered case is about the Jarkus profile 648 in Julianadorp. In this area series of groins have been constructed which may have abated the impact of the 1976 storm surge. Without considering the waves' directional distribution and the influence of the groins, the model performance is bad. The model overestimates the volume change, as not only the first dune is eroded – a feature which was also recorded at the measurements - but the backshore zone appears scoured even more than the measurements indicate.

The variable impact along the coastal zone of the North Holland province is studied in Bergen and in Castricum. The numerical results proved a different pattern of the energy dissipation. In Castricum the lower offshore bed profile than the one in Bergen, and the location of the offshore bar induced the energy dissipation consequently affecting the beach and dune erosion profile. An onshore or offshore migration of these geological features accompanied by an elevated or submerged bottom profile may result to different post storm erosion profile.

According to this study, the overall performance of the XBeach model shows a dependency both on the hydrodynamic conditions and on the simpler or more complicated submarine or beach formations. As part of the operational model chain, the model's sensitivity presents favourable results and reflects the physical aspects of the extreme storm events.

7.2 Recommendations

The operational model should be tested in order to assess the reason that at the boundaries of the KST model the hydrodynamic conditions (especially the computation of the wind waves) are kept at the same low level. A possible reason is the numerical implementation of the wind drag coefficient. Additionally, the influence of the measured storm surge level seems to attest higher skill and better correlation with the measured coastal profiles of the cases t34.19 and t45.04; whether only the underestimation of the water level or the combination with a more recent to the storm offshore and nearshore bed profile may influence the results, needs to be further investigated.

A common observation of the presented numerical cases is that the backshore zone sustained severe scour and appeared submerged in relation with the measurements. This area was the most underestimated part of the post storm profile, and needs to be further examined.

One of the assumptions considering the 1D runs is that the waves directional spreading is neglected. Currently, the waves' directional distribution of the 1D cases is implemented at the XBeach model. It is recommended to study the effect of a broad and narrow distribution of the waves at the amount of dune erosion during extreme events.

According to Van Rijn et al. [2003] the presence of a transport gradient over the longshore direction (longshore currents or breaking waves) cannot be simulated simply by averaging over the longshore direction. Along the Dutch coast the presence of bars and rips may influence the propagation of the hydrodynamic conditions and the pattern of the coastal area during storm events.

The uniform pre-storm bathymetry describing the area in Bergen may not induce the formation of a varying nearshore post storm profile over the longshore direction. In contrast, the presence of groins in Julianadorp is expected to induce longshore transport gradients and probably the formation of a non-uniform pattern. Additionally, the 2D numerical simulations for the site in Julianadorp are recommended in order to examine the model's skill concerning the interaction with the 'hard' non-erodible structures. The varying grid resolution is recommended in order to reduce the computational time. In order to simulate the small scale morphological changes, it is recommended to preserve small grid resolution (less than 1m) at the lateral nearshore and backshore zone.

The hydrodynamic conditions of the studied storm events were widely different. The storm event of 1953 is described by the intense surge and the relatively low wind waves. In contrast, the 1976 storm is characterized by severe waves and lower surge level. Furthermore, the impact of the 1953 storm was more devastating in the Delta area, while the 1976 storm affected the northern part of the Netherlands. It is recommended to study the morphological impact of the 1953 storm surge at the southern part of the Netherlands, where extensive dike breaching and inundation was recorded.

REFERENCES

Aagaard, T. and Greenwood, B., 2008. Infragravity wave contribution to surf zone sediment transport – the role of advection. Marine Geology, 251: 1-14.

Andrews, D.G., and McIntyre, M.E., 1978. An exact theory of nonlinear waves on a Lagrangian-mean flow. J. Fluid Mech. 89 (4), 609–646.

Baart, F., Kaaij, T. van der, Ormondt, M. van, Dongeren, A. van, Koningsveld, M. van, Roelvink, J. A., 2009. Real-time forecasting of morphological storm impacts: a case study in the Netherlands. Journal of coastal research, SI 56, 1617-1621.

Barnard, P.L., O'Reilly, Bill, van Ormondt, Maarten, Elias, Edwin, Ruggiero, Peter, Erikson, L.H., Hapke, Cheryl, Collins, B.D., Guza, R.T., Adams, P.N., and Thomas, J.T., 2009, The framework of a coastal hazards model; a tool for predicting the impact of severe storms: U.S. Geological Survey Open-File Report 2009-1073, 21 p. [http://pubs.usgs.gov/of/2009/1073].

Booij, N., R.C. Ris and L.H. Holthuijsen, 1999. A third-generation wave model for coastal regions, Part I, Model description and validation, J.Geoph.Research, 104, C4, 7649-7666

Bruun, P., 1954. Coast erosion and the development of beach profiles. Beach Erosion Board Technical Memorandum No. 44, U.S. Army Engineer Waterways Experiment Station, Vicksburg, MS.

Bruun, P., 1962. Sea-Level Rise as a Cause of Shore Erosion. Journal of Waterways and Harbor Division, American Society of Civil Engineers, Vol 88, pp 117-130.

Caires, S., Groeneweg, J., Sterl, A., 2008, Past and futures changes in the North Sea extreme waves. 31st International Conference on Coastal Engineering, Hamburg, Germany.

Chiu, T. Y., 1977. Beach and dune response to Hurricane Eloise of September 1975. Coastal Sediments '77, ASCE, 1977, pp. 116-134.

Damsma, T., 2009. Dune growth on natural and nourished beaches: 'A new perspective'. MSc Thesis, Delft University of Technology, the Netherlands.

Dean, R. G. 1977. Equilibrium Beach Profiles: U.S. Atlantic and Gulf Coasts. Department of Civil Engineering, Ocean Engineering Report No. 12, University of Delaware, Newark, DE.

Dean, R. G. 1985. Physical Modelling of Littoral Processes. Physical Modelling in Coastal Engineering, R. A. Dalrymple, ed., A. A. Balkema, pp 119-139.

Dean, R. G., Kriebel D., L., Walton T., L., 2008. Cross-shore sediment transport processes. Coastal Engineering Manual, Part III , Chapter III-3-3 , Engineer Manual 1110-2-1100 , U.S. Army Corps of Engineers, Washington, DC

Deigaard, R., 1993. A note on the three dimensional shear stress distribution in a surf zone. Coast. Eng. 20, 157–171.

Deltares 2008. Effect van Tankers voor de kust. Deltares report H4596.27. Authors: Walstra, D.J.R.

Donker, A. W., 1993. Meteorologische aspekten van de stormvloed 1953. Meteorologica, 2, 4-8.

Edelman, T., 1968. Dune erosion during storm conditions. Proc. 11th Conf. Coastal Eng., London, pp. 719-722.

Edelman, T., 1972. Dune erosion during storm conditions. Proc. 13th Conf. Coastal Eng., Vancouver, pp. 1305 - 1312.

Etri, T., and Mayerle, R., 2006. Effect of storm events on the morphodynamics of a tidally-dominated coastal environment, 7th International conference on HydroScience and Engineering, Philadelphia, 10-13 Sept. 2006.

Foda, M. A., and C. C. Mei (1981), Nonlinear excitation of long-trapped wave by a group of short swells, J. Fluid Mech., 111, 319–345.

Galappatti, R., and Vreugdenhil, C.B., 1985. A depth integrated model for suspended transport. J. Hydraul. Res. 23 (4), 359–377.

Gerritsen, H., De Vries, J. W. & Philippart, M. E., 1995. The Dutch Continental Shelf Model. In AGU coastal and estuarine studies (ed. D. R. Lynch & A. M. Davies), vol. 47, pp. 425-467. Washington, DC: American Geophysical Union.

Gerritsen, H., 2005. What happened in 1953? The Big Flood in the Netherlands in perspective. Phil. Trans. R. Soc. A 363, 1271-1291, doi: 10.1098/rsta.2005.1568.

Hallermeier, R. J. 1978. Uses for a Calculated Limit Depth to Beach Erosion. Proceedings of the 16th International Conference on Coastal Engineering, American Society of Civil Engineers, Hamburg, pp 1493-1512.

Hallermeier, R. J. 1981. A Profile Zonation for Seasonal Sand Beaches from Wave Climate. Coastal Engineering, Vol 4, pp 253-277.

Harris, D.L., 1963. Characteristics of the Hurricane Storm Surge, Technical Paper No. 48, United States Weather Bureau, Washington, D.C., 139 p.

Hasselmann, K., 1962. On the non-linear energy transfer in a gravity-wave spectrum: I. General theory. J. Fluid Mech. 12, 481–500.

Hayes, M. O., 1967. Hurricanes as geological agents: case studies of hurricanes Carla, 1961, and Cindy, 1963. Rep. Invest. No. 61, Bur. Econ. Geol., Univ. Texas, Austin.

Hoefel, F., and Elgar, S., 2003. Wave-induced sediment transport and sandbar migration. Science, Vol. 299, no. 5614, pp. 1885-1887, doi: 10.1126/science.1081448

Holthuijsen, L. H., Waves in oceanic and coastal waters, Cambridge, Cambridge University Press, 2007, 387p.

Kraker, A.M.J. De, 2000, Storm surges, high tides and storms as extreme weather events, their impact on the coastal zone of the North Sea and the human response, 1350 tot 2000. In: B. Obrêbska-Starkel (ed.), Reconstructions of Climate and its modelling. Institute of Geography of the Jagiellonian University. Cracow 2000, 85-101.

Kriebel, D.L., and Dean, R., G., 1985. Numerical simulation of time-dependent beach and dune erosion. Coastal Engineering, Vol.9, pp. 221-245.

Lamb, H. H., Weather, climate and human affairs, pp. 11-187, London, Routledge, 1988, 364 p.

Lamb, H. H., Historic storms of the North Sea, British Isles and Northwest Europe, pp. 170-171, pp. 181-182, Cambridge, Cambridge University Press, 1991, 204p.

Lesser G.R., Roelvink J.A., van Kester J. A.T. M. and Stelling, G. S., 2004. Development and validation of a three-dimensional morphological model, Coastal Engineering **51**(8-9), pp. 883-915.

Longuet-Higgins, M. S., and R. W. Stewart (1962). Radiation stress and mass transport in gravity waves with application to ‘‘surf-beats,’’ J. Fluid Mech., 8, 565–583.

Longuet-Higgins, M. S., and R. W. Stewart (1964). Radiation stress in water waves: A physical discussion with applications, Deep Sea Res., 11, 529– 563.

McCall, R. T., 2008. The longshore dimension in dune overwash modelling. Development, verification and validation of XBeach model. MSc Thesis, Delft University of Technology, the Netherlands.
Phillips, O.M., 1977. The Dynamics of the Upper Ocean2nd ed. Cambridge Univ. Press, New York. 336 pp.

Phillips, O.M., 1977. The Dynamics of the Upper Ocean2nd ed. Cambridge Univ. Press, New York. 336 pp.

Pool, A. D., 2009. Modelling the 1775 storm surge deposits at the Heemskerk dunes. MSc Thesis, Delft University of Technology, the Netherlands.

Reniers, A. J. H. M., J.A. Roelvink and E.B. Thornton, 2004. Morphodynamic modelling of an embayed beach under wave group forcing. J. of Geophysical Res. , VOL. 109, C01030.

RIKZ and KNMI, 1991. Verslag over de stormvloed van 1953.

Roelvink, J. A., and Stive, M. J. F., 1989. Bar generating cross-shore flow mechanism on a beach. J. of Geophysical Res. 94 (C4), 4785-4800.

Roelvink, J.A., 1993. Dissipation in random wave groups incident on a beach. Coast. Eng. 19, 127–150.

Roelvink, J.A., (1993b). Surf beat and its effect on cross-shore profiles, Ph.D. thesis, Delft University of Technology, Delft, Netherlands.

Roelvink, J. A., and Broker, I. 1993. “Cross-Shore Profile Models,” Coastal Engineering, Vol 21, pp 163-191.

Roelvink, J.A., Reniers, A.J.H.M., Van Dongeren, A.R.,Van Thiel de Vries, J.S.M., Lescinski, J., McCall, R., (2009), XBeach model description and manual”, Unesco-IHE Institute for Water Education, Deltares, Delft University of Technology, Z4175.

Roelvink, J. A., Reniers, A.J.H.M., Van Dongeren, A.R., Van Thiel de Vries, J.S.M., McCall, R.T., Lescinski, J., 2009b. Modelling storm impacts on beaches, dunes and barrier islands. Coast. Eng. 56, 1133-1152.

Rogers, W.E., P.A. Hwang, and D.W. Wang. 2003. Investigation of wave growth and decay in the SWAN model: three regional-scale applications, J. Phys. Oceanogr., 33, 366-389.

Saville, T., 1957. Scale Effects in Two-Dimensional Beach Studies. Transactions of the Seventh General Meeting of the International Association of Hydraulic Research, Vol 1, pp A3.1 - A3.10.

Soulsby, R.L., 1997. Dynamics of Marine Sands. Thomas Telford, London.

Schaffer, H. A., and I. A. Svendsen (1988), Surf beat generation on a mild slope beach, in Proceedings of the 21st International Conference on Coastal Engineering, edited by B. Edge, pp. 1058–1072, Am. Soc. Of Civ. Eng., Reston, Va.

Schwartz, M., Encyclopedia of Coastal Science, pp. 162, Dordrecht, Springer, 2005, 796 p.

Smith, K. E.,1954. The weather and circulation of January 1953. Mon. Weather Rev. 18, 16–19.

Steetzel, H. J., 1993. Cross-shore transport during storm surges. PhD Thesis Technical University Delft. ISBN 90-9006345-5, CASPARIE publishers, Zwolle.
Stelling, G.S., and Duinmeijer, S.P.A., 2003. A staggered conservative scheme for every Froude number in rapidly varied shallow water flows. Int. J. Numer. Methods Fluids43, 1329–1354.

Svendsen, I.A., 1984. Wave heights and set-up in a surf-zone. Coast. Eng. 8, 303–329.

Swart, D. H. 1974. “Offshore Sediment Transport and Equilibrium Beach Profiles," Publ. No. 131, Delft Hydraulics Lab, Delft, The Netherlands.
Symonds, G., Huntley, D. A., and Bowen, A. J., 1982. Two-dimensional surf beat: long wave generation by a time varying breakpoint. J. Geophys. Res., 87, 492-498.

Tolman, H. L., 1997. User manual and system documentation of WAVEWATCH-III version 1.15. NOAA / NWS / NCEP / OMB Technical Note 151, 97 pp.

Tolman, H. L., 1999. User manual and system documentation of WAVEWATCH-III version 1.18. NOAA / NWS / NCEP / OMB Technical Note 166, 110 pp.

Tolman, H. L., 2009. User manual and system documentation of WAVEWATCH III version 3.14. NOAA / NWS / NCEP / MMAB Technical Note 276, 194 pp.+ Appendices.

Trenberth, K. E., Warmer Oceans, Stronger Hurricanes, Scientific American, July 2007, p44-51.

Tucker, M.J., 1950. Surf beats: sea waves of 1 to 5 minutes period, Proc. Roy. Soc. A, 202, 565-73.

TUD 2009. The effect of submerged tankers at coastal erosion, Internship report, Technical University of Delft and Deltares. Authors: Walstra, D.J.R, Van Dongeren, A., Voukouvalas, E.

Uppala, S.M., Kållberg, P.W., ... Simmons, A.J., Andrae, U., da Costa Bechtold, V., Fiorino, M., Gibson, J.K., Haseler, J., Hernandez, A., Kelly, G.A., Li, X., Onogi, K., Saarinen, S., Sokka, N., Allan, R.P., Andersson, E., Arpe, K., Balmaseda, M.A., Beljaars, A.C.M., van de Berg, L., Bidlot, J., Bormann, N., Caires, S., Chevallier, F., Dethof, A., Dragosavac, M., Fisher, M., Fuentes, M., Hagemann, S., Hólm, E., Hoskins, B.J., Isaksen, L., Janssen, P.A.E.M., Jenne, R., McNally, A.P., Mahfouf, J.-F., Morcrette, J.-J., Rayner, N.A., Saunders, R.W., Simon, P., Sterl, A., Trenberth, K.E., Untch, A., Vasiljevic, D., Viterbo, P., and Woollen, J., 2005. The ERA-40 re-analysis. Quart. J. R. Meteorol. Soc., 131, 2961-3012.

Van de Graaf, J., 1977. Dune erosion during a storm surge. Coastal Engineering, Vol.1, pp. 99-134.

Van de Graaf, J., 2006. Coastal morphology and coastal protection, Delft University of Technology, the Netherlands.

Van den Dool, H. M., Kistler, R. E., Saha, S., and den Tonkelaar, J.F., 2001. Reanalysis and Reforecast of the Jan 31-Feb 1 1953 North Sea Gale. www.knmi.nl/cms/mmbase/attachments/64635/1953_reanalysis_NCEP.pdf> (web page accessed 28 April 2009).

Van der Westhuysen, A. J. 2007. Advances in the spectral modelling of wind waves in the nearshore, Ph.D. Thesis, Technical report, Fac. of Civil Engineering, Delft University of Technology.

Van Dongeren, A.R., and Svendsen, I. A., 1997a. An absorbing–generating boundary condition for shallow water models. J. Waterw. Port Coast. Ocean Eng. 123 (6), 303–313.

Van Dongeren, A. R. 1997b. Quasi 3-D modeling of nearshore hydrodynamics, Rep. CACR-97-04, 243 pp., Cent. for Appl. Coastal Res., Univ. of Del., Newark.

Van Dongeren, A., Reniers, A., Battjes, J., Svendsen, I., 2003. Numerical modeling of infragravity wave response during DELILAH. J. Geophys. Res. 108 (C9), 3288. doi:10.1029/2002JC001332.

Van Dongeren, A., Battjes, J., Janssen, T., Van Noorloos, J., Steenhauer, K., Steenbergen, G. , and Reniers A., 2007. Shoaling and shoreline dissipation of low-frequency waves, J. Geophys. Res., 112, C02011, doi:10.1029/2006JC003701.

Van Dongeren, A., Plant, N., Cohen, A., Roelvink, J. A., Haller, M. C., Catalan, P., 2008. Beach wizard: Nearshore bathymetry estimation through assimilation of model computations and remote observations. Coastal Engineering, 55(12), pp. 1016–1027.

Van Rijn, L. C., Walstra, D. J., Grasmeijer, B.T., and Kleinhout, K., 2001. Hydrodynamics and morphodynamics in the surf zone of a dissipative beach. Coastal Dynamics, Lund, Sweden, p. 373-382.

Van Rijn, L.C., Walstra, D.J.R., Grasmeijer, B., Sutherland, J., Pan, S. and Sierra, J.P., 2003. The predictability of cross-shore bed evolution of sandy beaches at the time scale of storms and seasons using process-based Profile models. Coastal Engineering, Vol. 47, pp. 295-327.

Van Thiel de Vries, J.S.M., 2009. Dune erosion during storm surges. PhD Thesis, Delft University of Technology, the Netherlands

Vellinga, P., 1983. Predictive Computational Model for Beach and Dune Erosion During Storm Surges, Proceedings, American Society of Civil Engineers Specialty Conference on Coastal Structures' 83, pp 806-819.

Vellinga, P., 1986. Beach and dune erosion during storm surges. PhD Thesis, Delft University of Technology, the Netherlands.

Verlaan, M., A. Zijderveld, J.W. de Vries and J. Kroos, 2005. Operational storm surge forecasting in the Netherlands: developments in the last decade. Phil. Trans. R. Soc. A, 2005, 363, 1441-1453, doi:10.1098/rsta.2005.1578.

Walstra, D.J.R., Roelvink, J.A., Groeneweg, J., 2000. 3D calculation of wave-driven cross-shore currents. Proceedings 27th International Conference on Coastal Engineering, July 16-21, 2000, Sydney.

Wisner B., Blaikie P., Cannon T., and Davis I., At Risk - Natural hazards, people's vulnerability and disasters. Wiltshire: Routledge, 2004.

WL| Delft Hydraulics, 1978, Duinafslag ten gevolge van de stormvloed op 3 januari 1976. Toetsing van de voorlopige richtlijn. WL| Delft Hydraulics report R0587. Author: P. Vellinga.

Wolf, J., and Flather, R. A., 2005. Modelling waves and surges during the 1953 storm. Philosophical Transactions of the Royal Society A: Mathematical, Physical and Engineering Sciences, 363 (1831), 1359-1375.

Sites

[1] http://ww2010.atmos.uiuc.edu/(Gh)/wwhlpr/hurricane_preswind.rxml?hret=/guides/mtr/hurr/damg/surg.rxml
[2] http://www.aquarius.ifm-geomar.de/
[3] http://cordis.europa.eu/fp7/home_en.html
[4] http://en.wikipedia.org/wiki/North_Sea_flood_of_1953
[5] www.knmi.nl
[6] http://matroos.deltares.nl/
[7] www.micore.eu
[8] http://public.deltares.nl/display/OET/OpenEarth
[9] http://vlm089.citg.tudelft.nl/swan/index.htm
[10] www.waterbase.nl
[11] www.xbeach.org
[12] http://www.coastalwiki.org/coastalwiki/Argus_video_monitoring_system
[13] http://www.emc.ncep.noaa.gov/modelinfo/
[14] http://cil-www.oce.orst.edu/

APPENDIX A

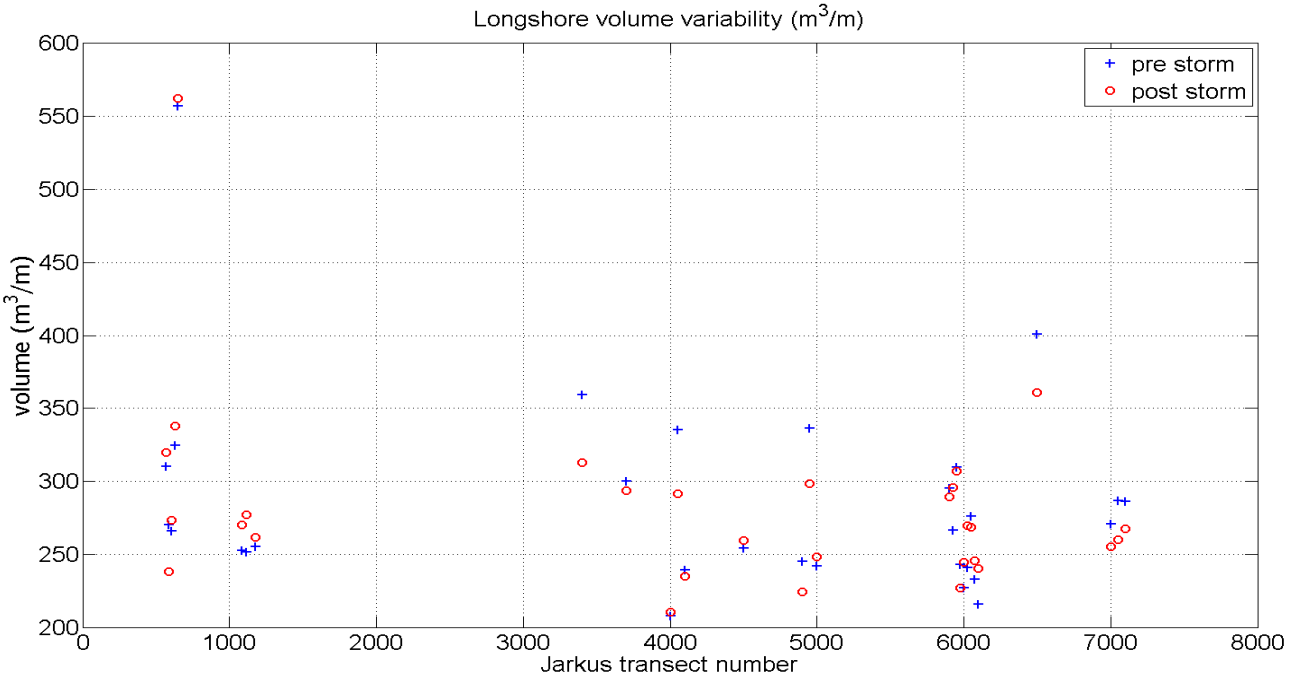

Figure A.1: Longshore volume variability along the North Holland province, prior (blue stars) and after the 1976 storm surge (red circles).

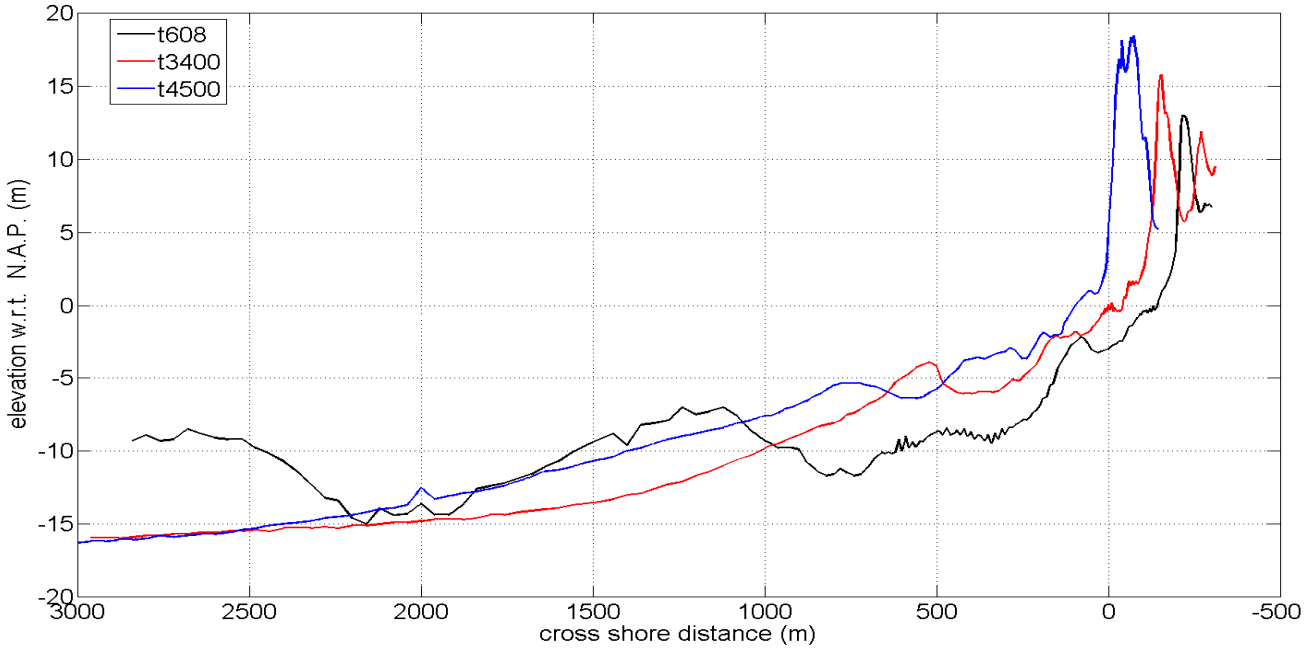

Figure A.2: Typical profiles in Julianadorp (black line), Bergen (red line) and Castricum (blue line) measured in 1976.

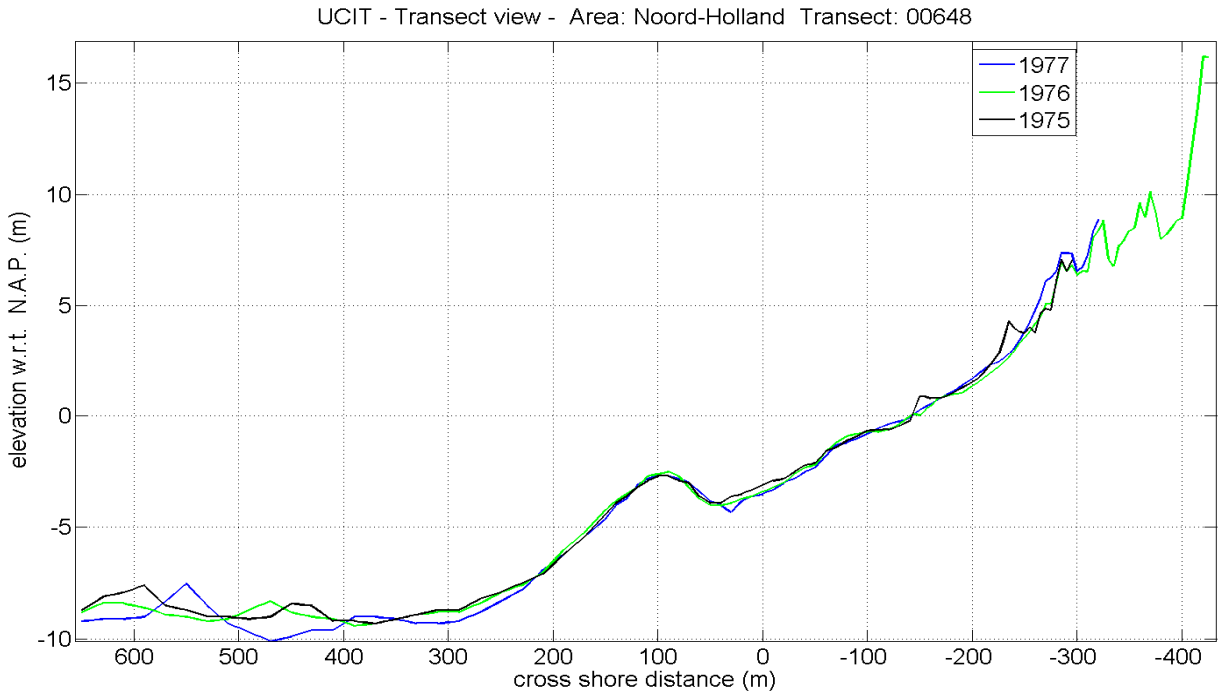

Figure A.3: Extended view of the Jarkus transect 648 as measured at the summer of 1975 (black line), 1976 (green line) and 1977 (blue line).

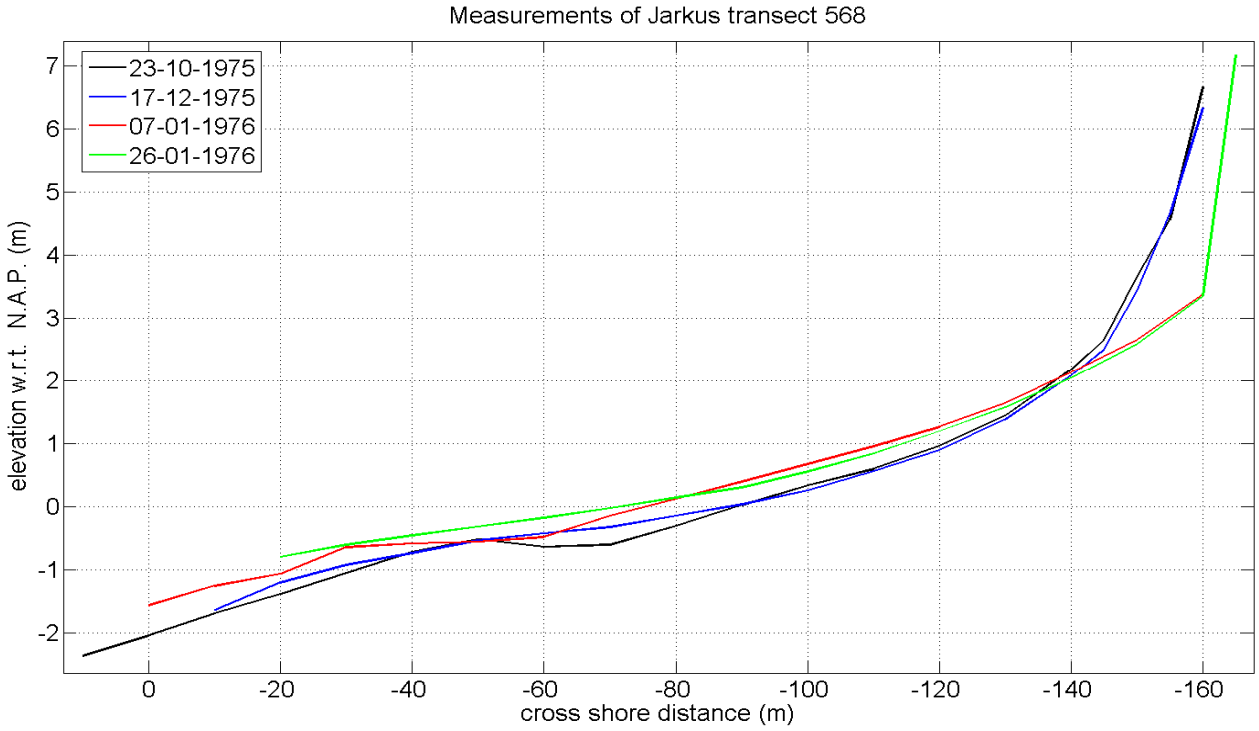

Figure A.4: Measurements of the Jarkus transect 568 in Julianadorp prior and after the 1976 storm surge.

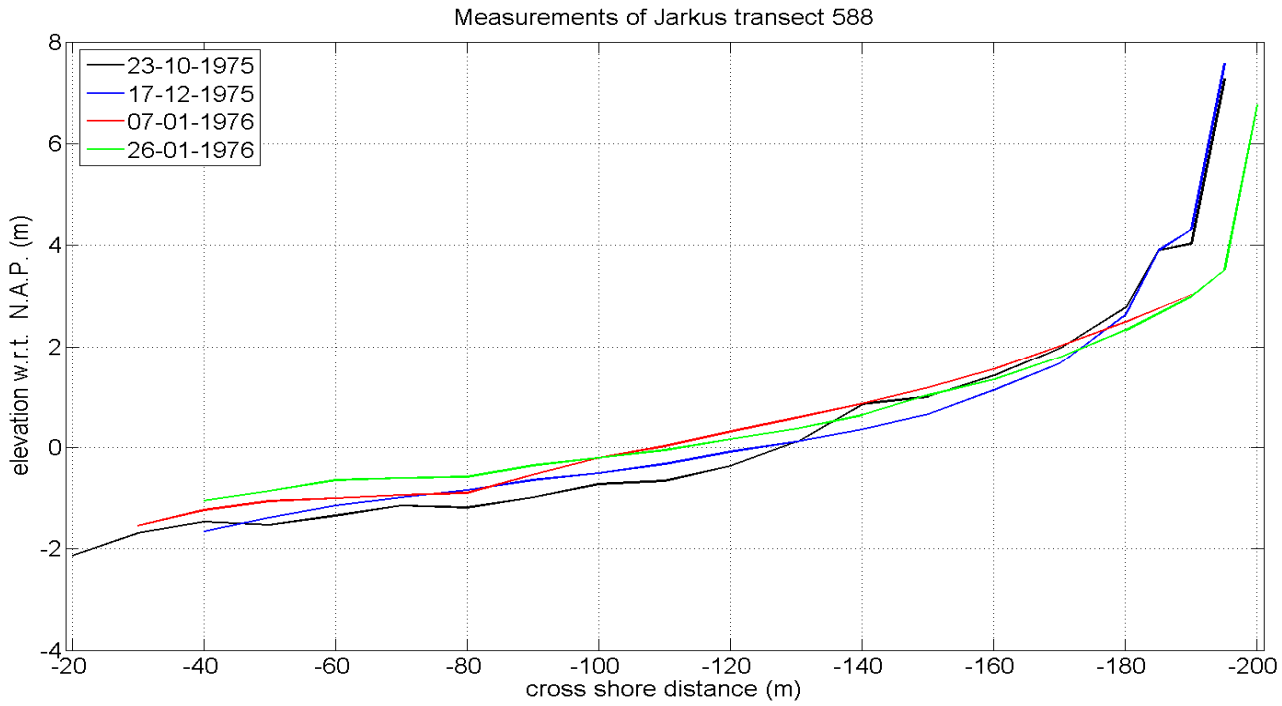

Figure A.5: Measurements of the Jarkus transect 588 in Julianadorp prior and after the 1976 storm surge.

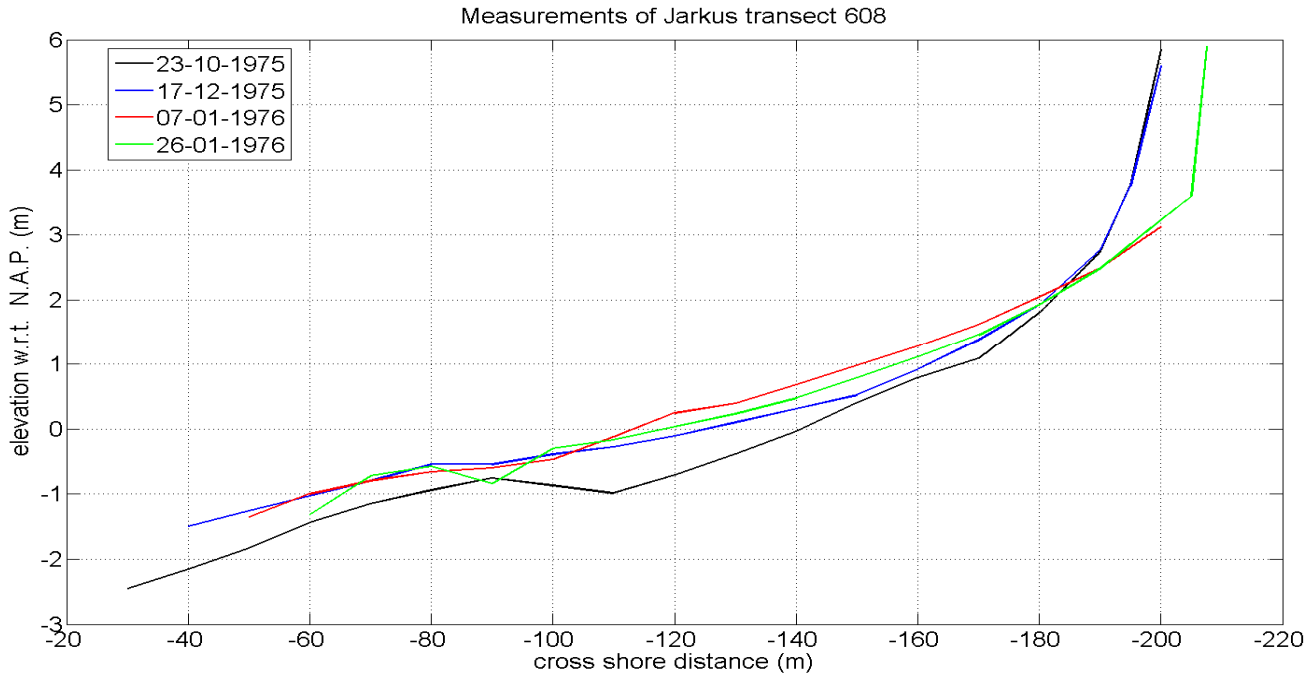

Figure A.6: Measurements of the Jarkus transect 608 in Julianadorp prior and after the 1976 storm surge.

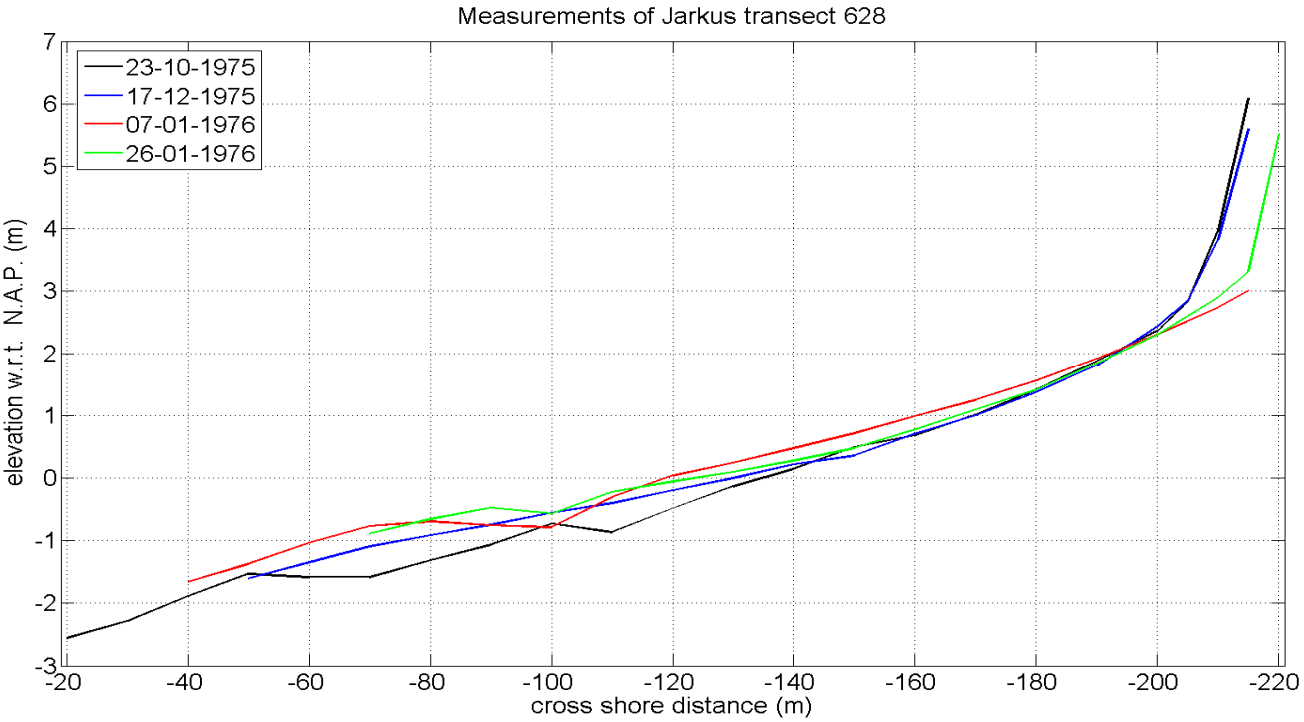

Figure A.7: Measurements of the Jarkus transect 628 in Julianadorp prior and after the 1976 storm surge.

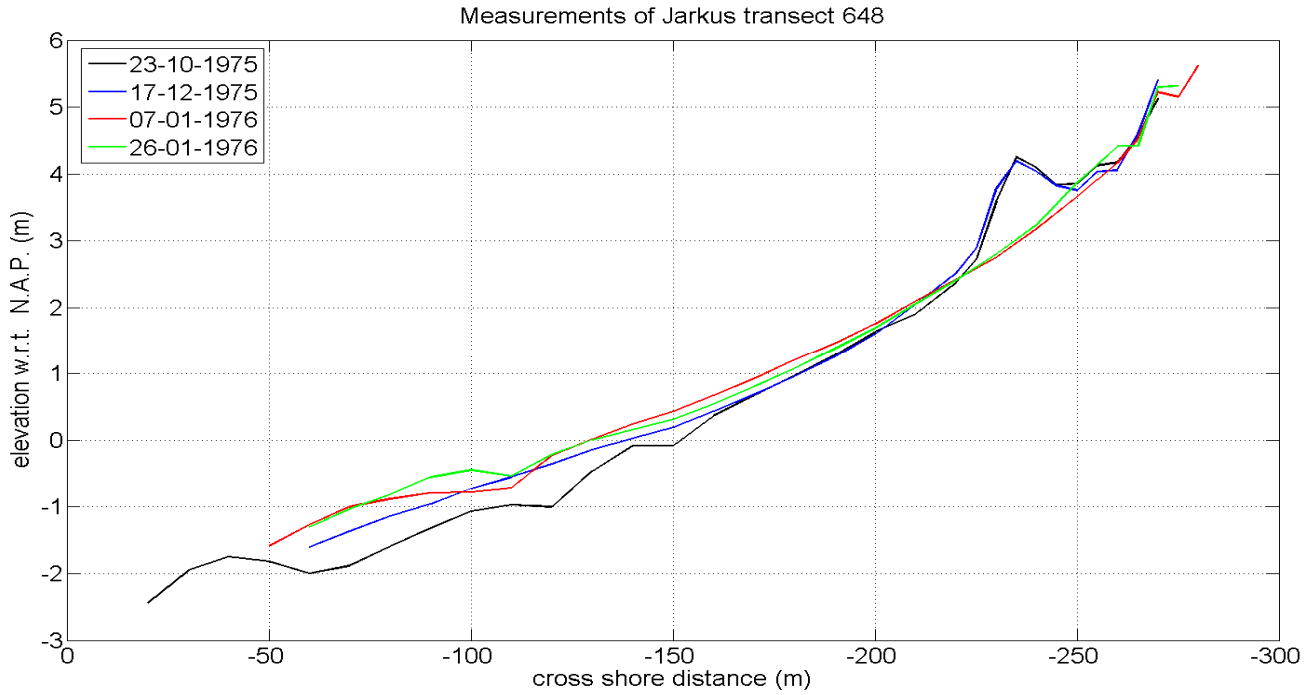

Figure A.8: Measurements of the Jarkus transect 648 in Julianadorp prior and after the 1976 storm surge.

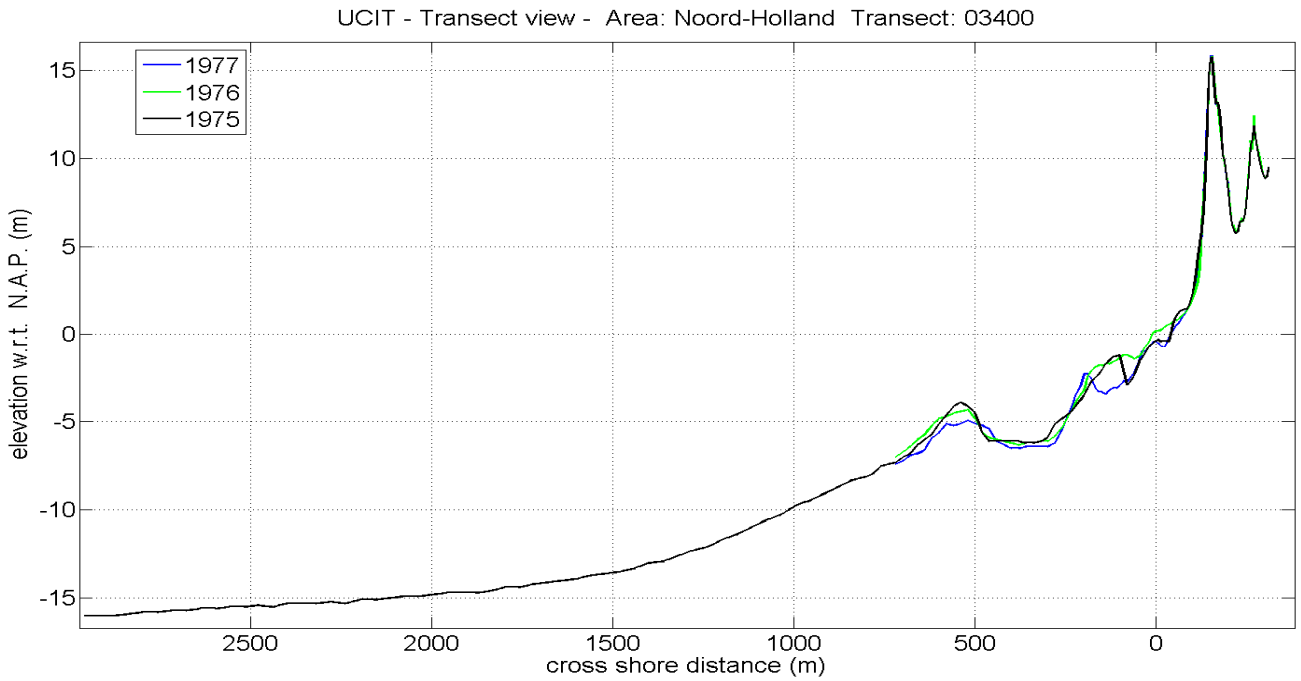

Figure A.9: Extended view of the Jarkus transect 3400 as measured at the summer of 1975 (black line), 1976 (green line) and 1977 (blue line).

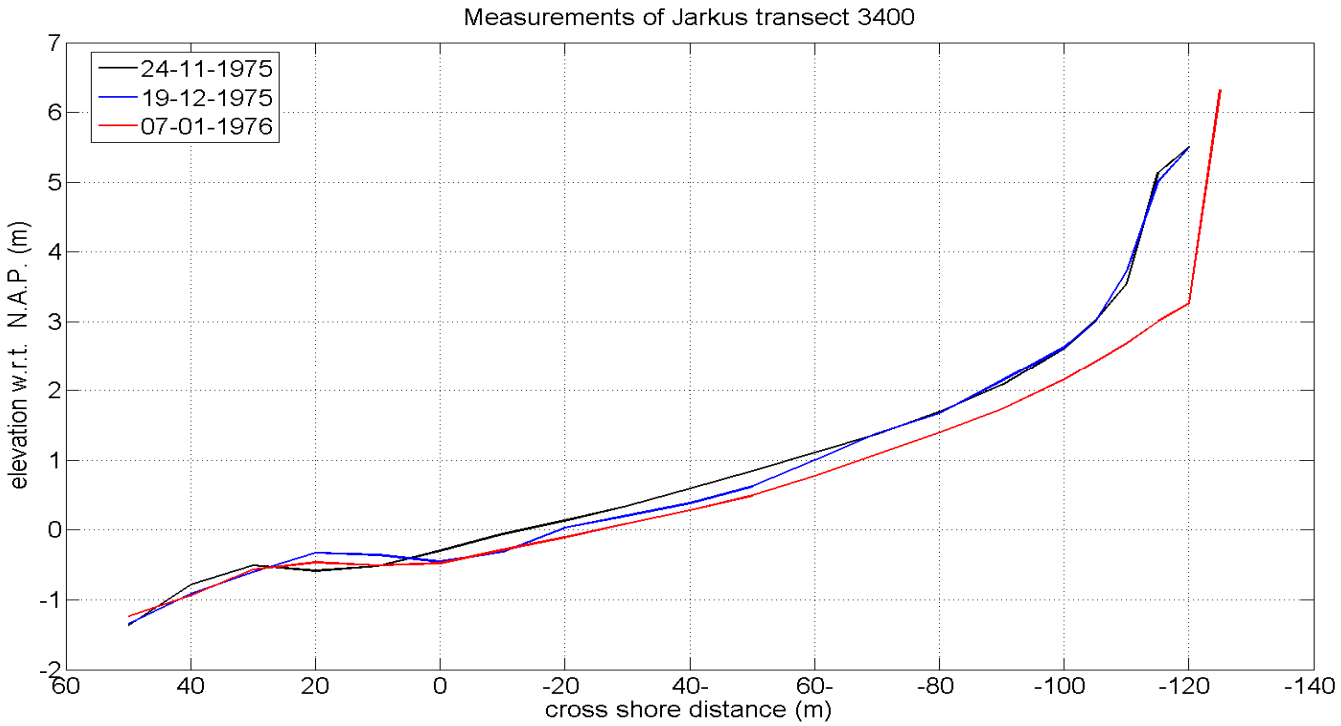

Figure A.10: Measurements of the Jarkus transect 3400 in Bergen prior and after the1976 storm surge.

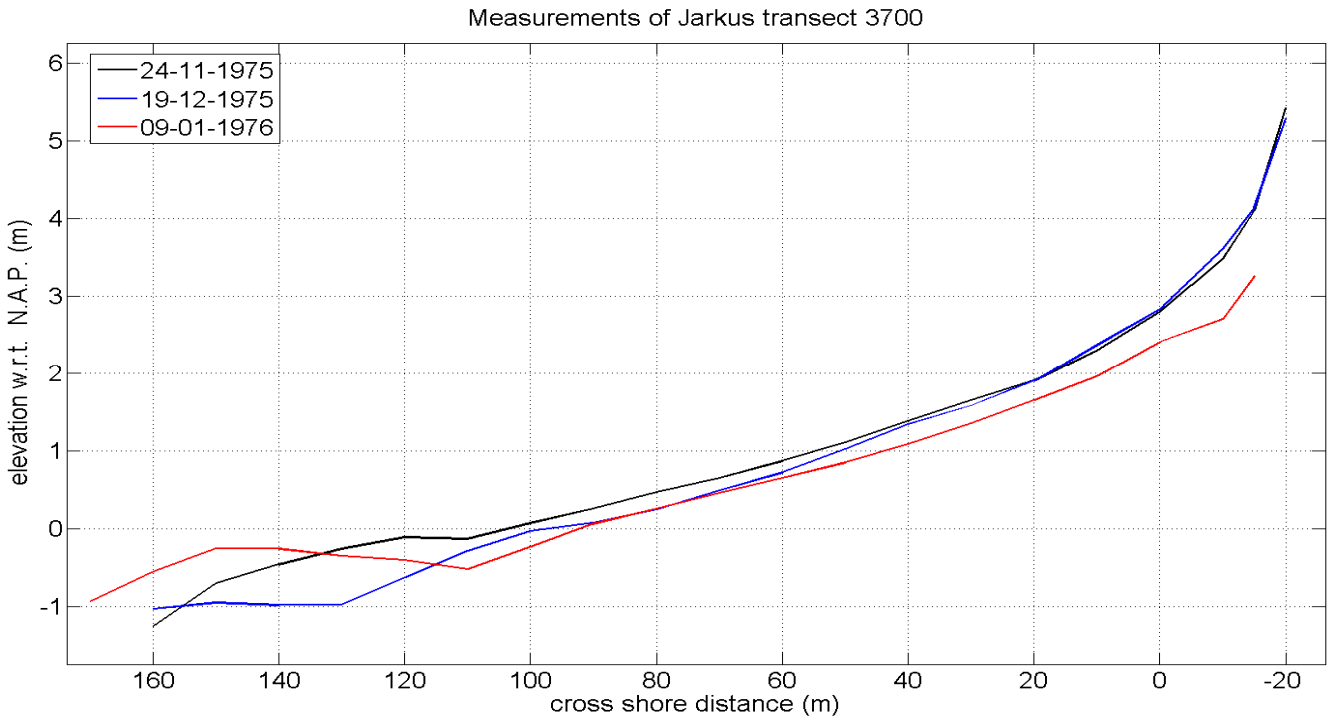

Figure A.11: Measurements of the Jarkus transect 3700 in Bergen prior and after the1976 storm surge.

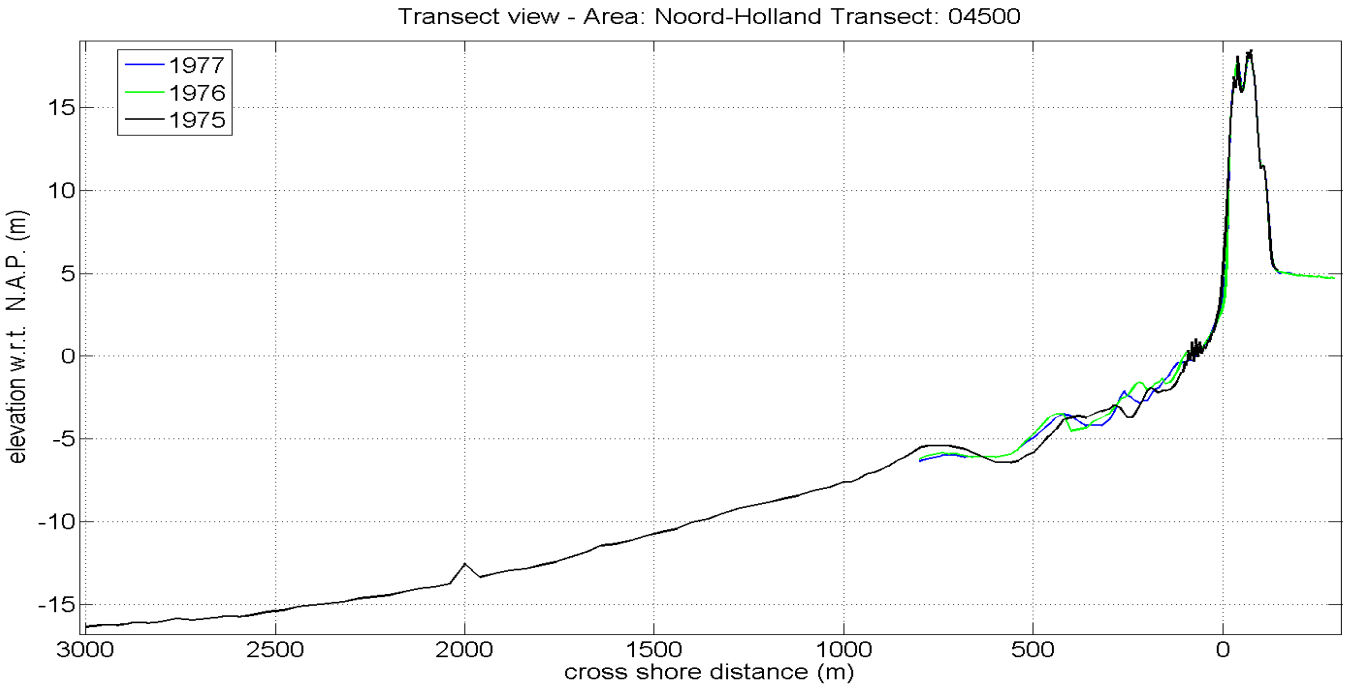

Figure A.12: Measurements in Castricum (transect 4500) at the summer of 1975 (black profile), 1976 (green profile) and 1977 (blue profile).

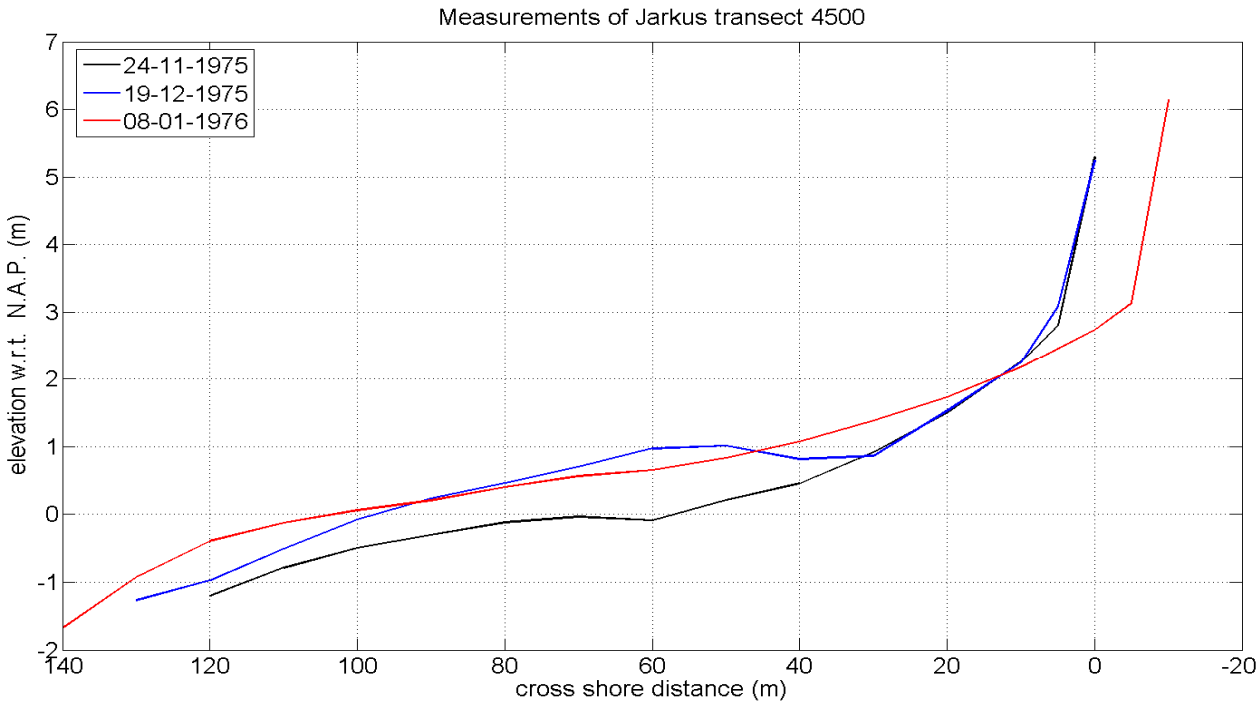

Figure A.13: Measurements of the Jarkus transect 4500 in Castricum prior and after the1976 storm surge.

APPENDIX B

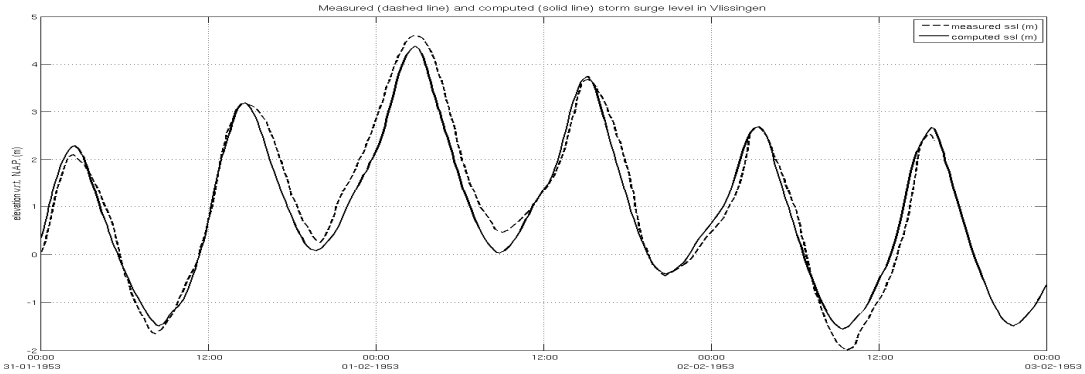

Figure B.1: Measured and computed storm surge level in Vlissingen during the 1953 storm surge.

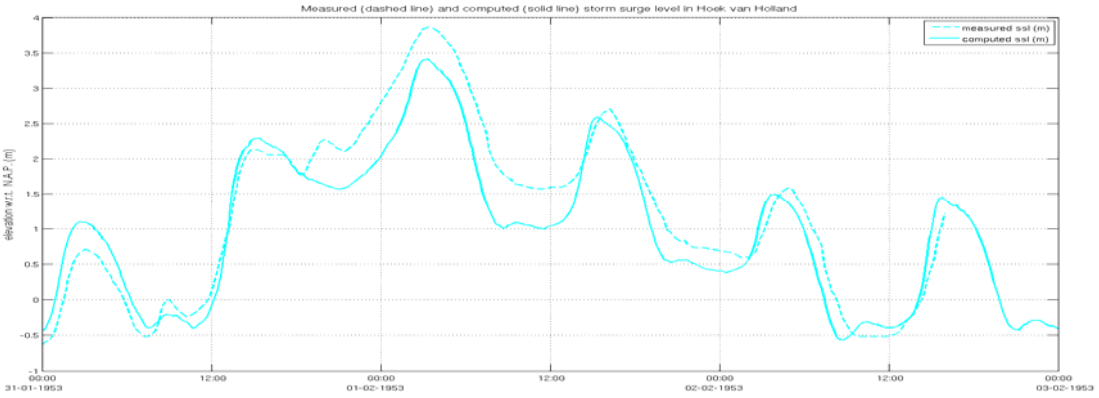

Figure B.2: Measured and computed storm surge level in Hoek van Holland during the 1953 storm surge.

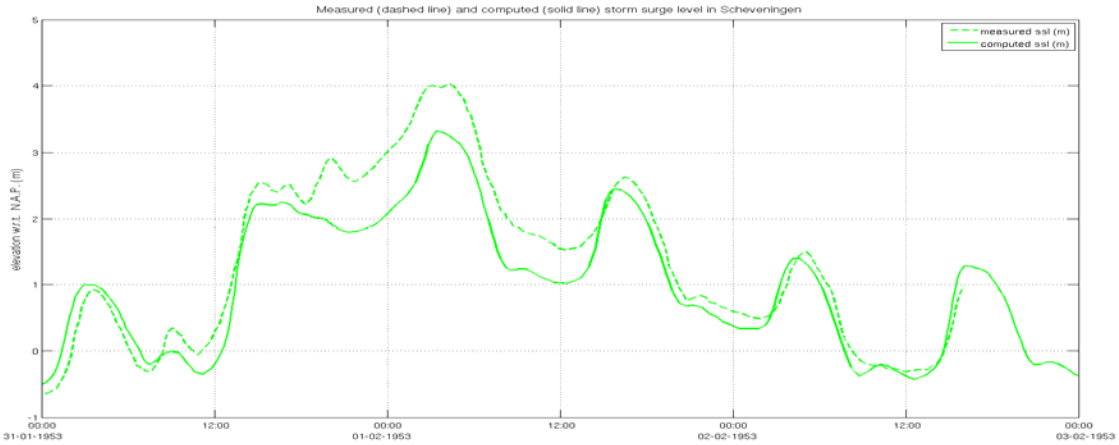

Figure B.3: Measured and computed storm surge level in Scheveningen during the 1953 storm surge.

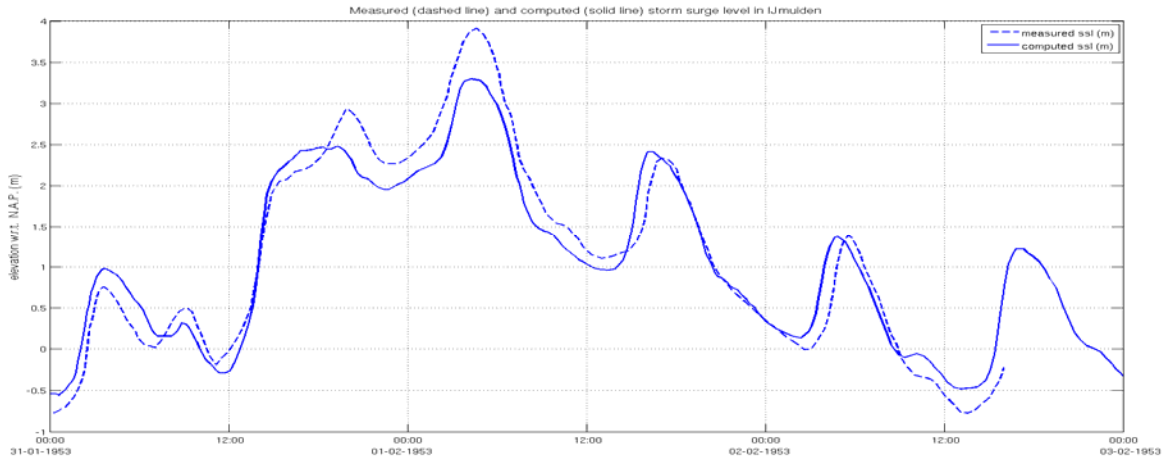

Figure B.4: Measured and computed storm surge level in IJmuiden during the 1953 storm surge.

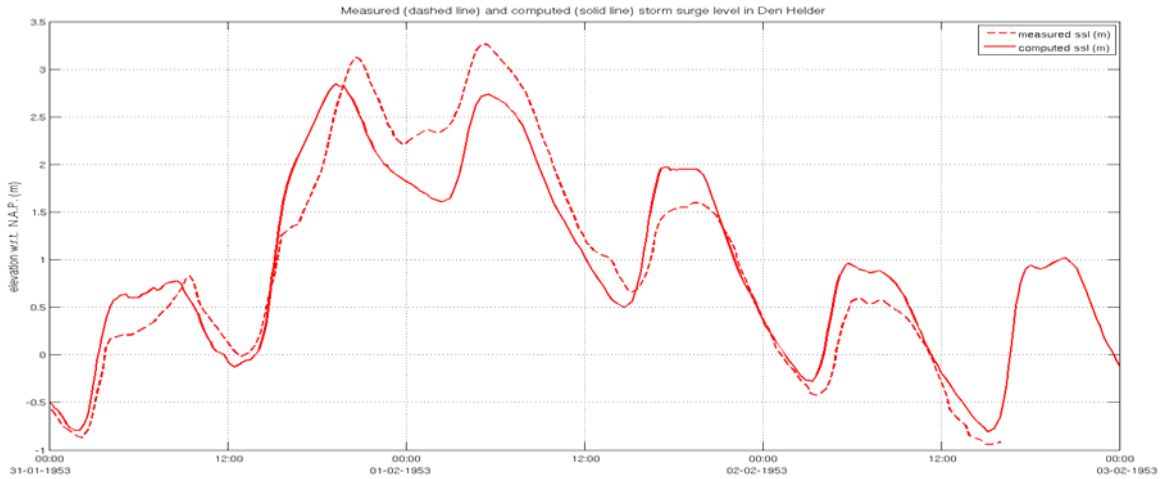

Figure B.5: Measured and computed storm surge level in Den Helder during the 1953 storm surge.

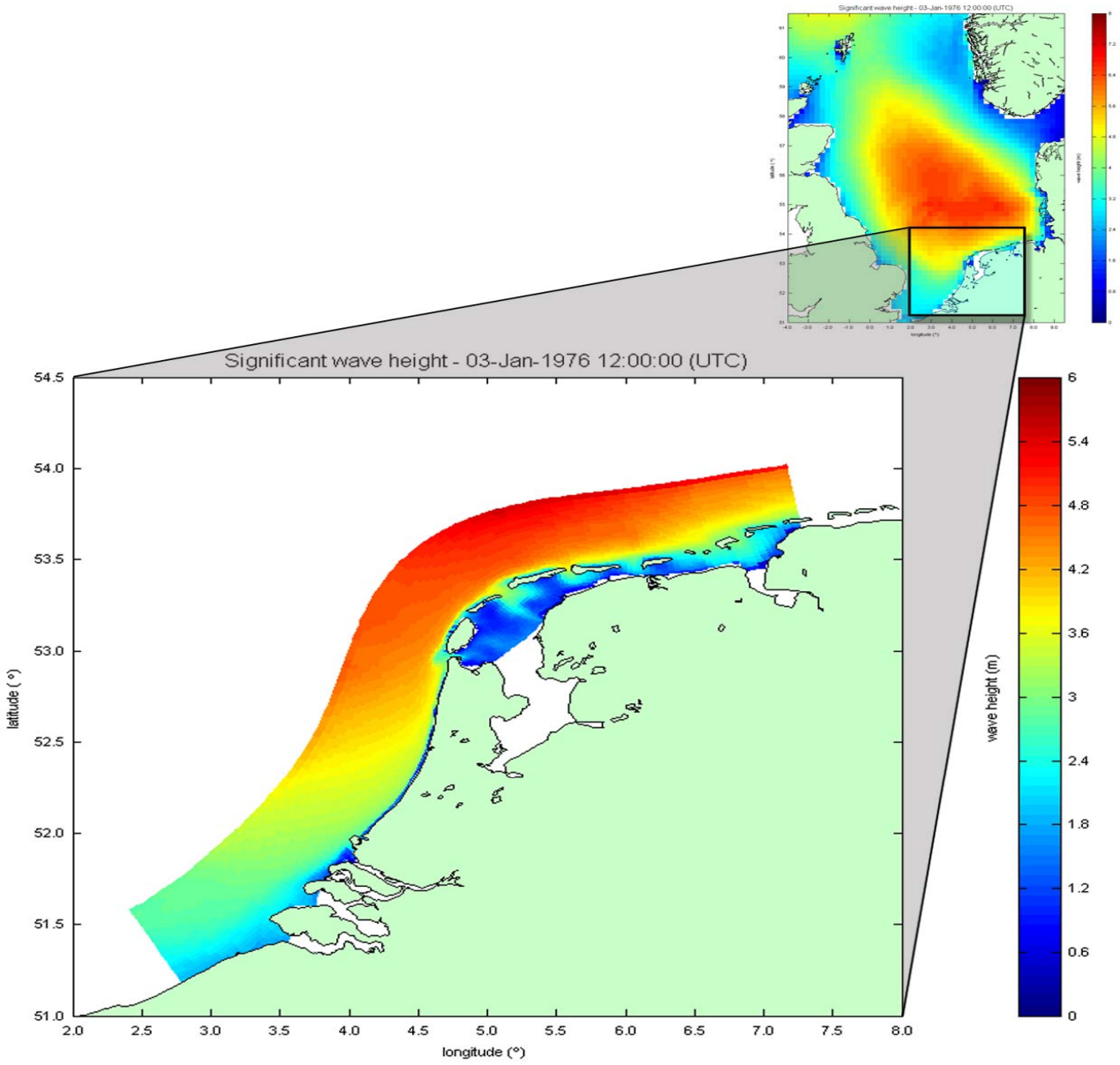

Figure B.6: Significant wave height (m) during the 1976 storm surge at 12:00 of the 3-1-1976 as computed from the CSM (top panel) and the KST models (bottom panel).

Table B.1: Wave conditions during the 1976 storm surge, for the period between the 1-1-1976 to 4-1-1976, as measured 10km NW of IJmuiden (52^{o} 32' 25" N, 4^{o} 25'37" E.). Redrawn after Table 6d, WL| Delft Hydraulics R587, 1978.

date	time	depth w.r.t. N.A.P. (m)	Hsig (cm)	Hmax (cm)	Tmean (sec)
01-01-1976	19:00	16:00	166	-	4.8
02-02-1976	01:00	16:00	300	525	5.6
02-02-1976	07:00	16:00	187	350	5.3
02-02-1976	13:00	16:00	113	178	4.7
02-02-1976	19:00	16:00	126	210	3.5
03-01-1976	01:00	16:00	408	635	6.7
03-01-1976	07:00	16:00	495	788	7.4
03-01-1976	13:00	16:00	606	806	9.0
03-01-1976	17:00	16:00	586	955	9.1
03-01-1976	19:00	16:00	618	840	8.9
04-01-1976	01:00	16:00	548	910	7.9
04-01-1976	07:00	16:00	343	546	6.9
04-01-1976	13:00	16:00	215	350	7.1
04-01-1976	19:00	16:00	122	204	4.3

APPENDIX C

Input parameters of the base case t34.13

General constants

rho = 1000 density [kg/m^3]
g = 9.811.0 gravitational acceleration [kgxm/sec^2]

Wave discretisation

thetamin = -180. lower directional limit [^{o}]
thetamax = 180. upper directional limit [^{o}]
dtheta = 360. directional resolution [^{o}]

Numerics input

CFL = 0.9 maximum Courant number [-]
eps = 0.001 threshold depth [m]
scheme = 2 numerical scheme for wave and roller energy [-]

Boundary condition options

order = 2 order of wave steering at seaward boundary [-]
front = 1 seaward boundary condition [-]
back = 2 bayside boundary condition [-]
right = 1 right lateral boundary condition [-]
left = 1 left lateral boundary condition [-]
zs0file = xbeach.tim file with the surge time series [-]
tidelen = 253 length of tidal record [-]
tideloc = 1 number of input tidal time series [-]
paulrevere = 0 option for sea/sea corner or sea/land corner specification [-]
instat = 5 option for wave boundary conditions [-]
bcfile = t.t file with the wave boundary data [-]

Wave calculation options

break = 1 option breaker model [-]
roller = 1 option roller model [-]
beta = 0.1 breaker slope coefficient in roller model [-]
gamma = 0.55 breaker parameter in Baldock or Roelvink formulation [-]
gammax = 2. maximum ration Hrms/hh [-]
alpha = 1. wave dissipation coefficient [-]
delta = 0.0 fraction of wave height to add to water depth [-]
n = 10 exponent breaking probability function (Roelvink 1993b)

Flow calculation options

nuh = 0.1 horizontal background viscosity [m^2/sec]
nuhfac = 1.0 viscosity coefficient for roller induced turbulent horizontal viscosity

hmin = 0.05 threshold water depth for concentration and return flow [m]
C = 65. Chezy coefficient [$m^{1/2}$ /sec]
umin = 0.0 threshold velocity for the upwind scheme [m/sec]
hswitch = 0.1 water depth at interface from wetslp to dryslp

Time input

tstart = 0 start time of simulation [sec]
tint = 600 time interval output global values [sec]
tintg = 600 time interval output global values [sec]
tintm = 600 time interval output mean global values [sec]
tstop = 151200 stop time of simulation [sec]

Sediment transport calculation options

D50 = 0.000225 D50 grain diameter of the first class of sediment [m]
D90 = 0.0003375 D90 grain diameter of the first class of sediment [m]
rhos = 2650 density of sediment [kg/m^3]
tsfac = 0.1 max value for fall velocity [-]
dico = 1.0 diffusion coefficient [m^2/sec]
facsl = 1.6 bed slope factor

Morphological calculation options

form = 1 equilibrium sediment concentration formulation [-]
morfac = 1 morphological factor [-]
morstart = 0 start time of morphological updates [sec]
por = 0.4 porosity [-]
dryslp = 1.0 critical avalanching slope above water [-]
wetslp = 0.30 critical avalanching slope under water [-]
facua = 0.0 calibration factor time averaged flow due to wave asymmetry [-]
lws = 0 long wave stirring [-]
dzmax = 0.2 maximum bed level change due to avalanching [m/sec/m]

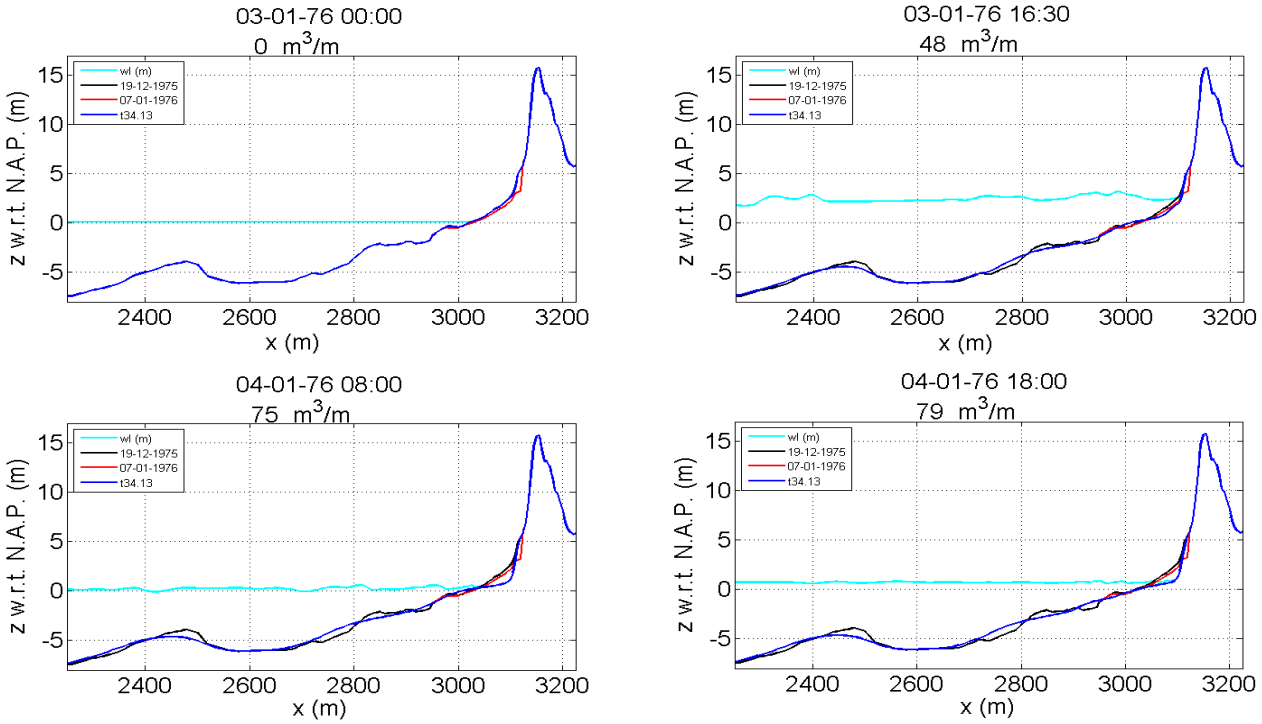

Figure C.1: Extended view of test case t34.13.

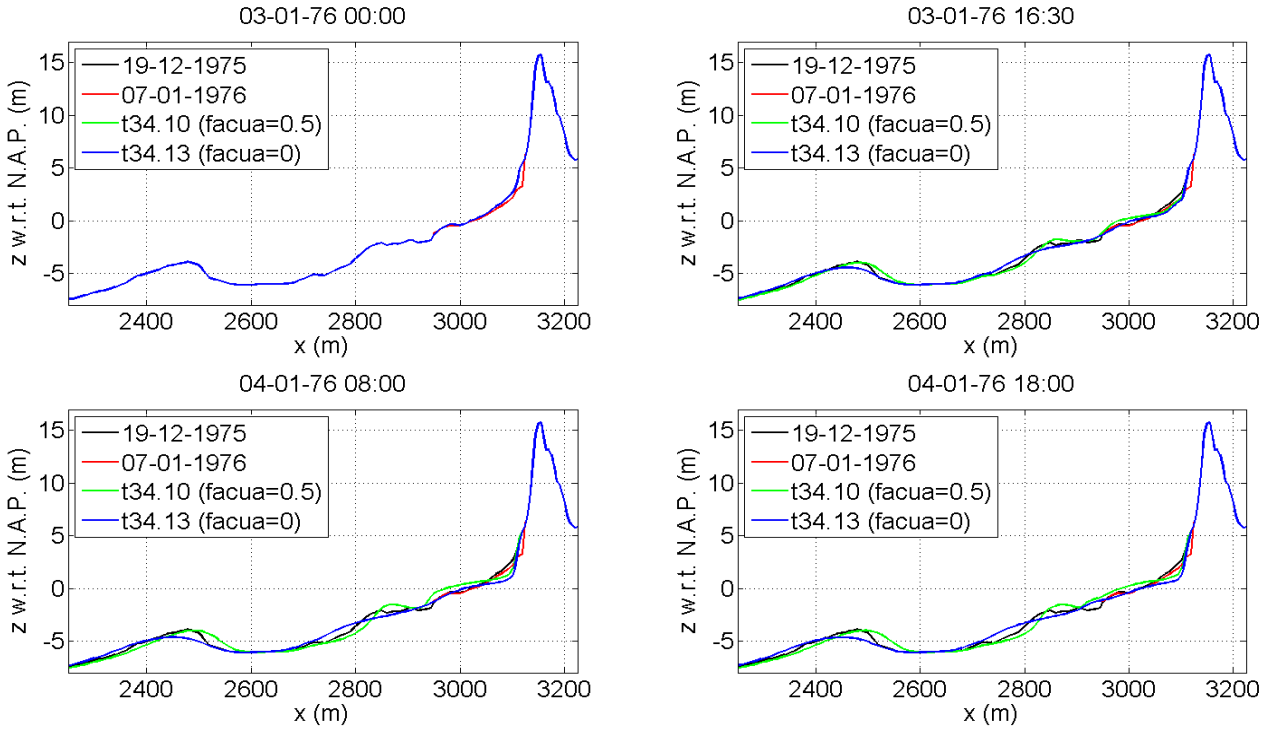

Figure C.2: Extended view of test cases t34.10 (green line) and t34.13 (blue line).

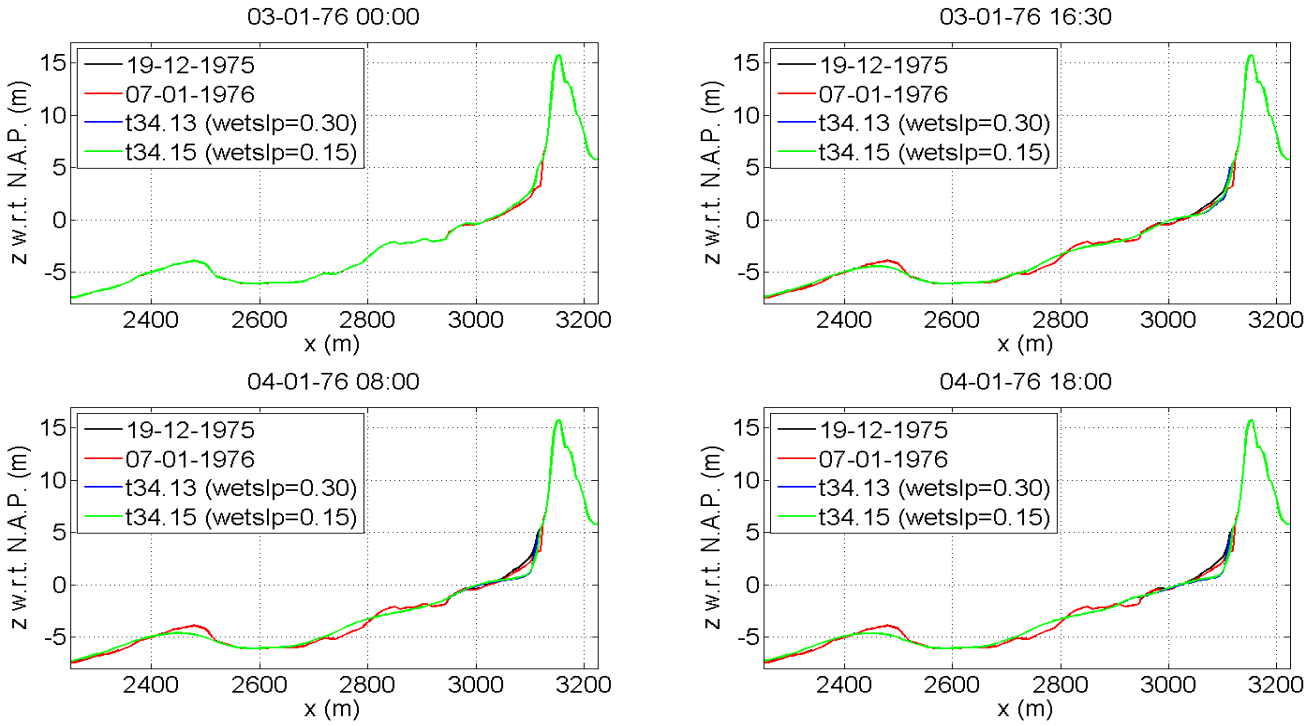

Figure C.3: Extended view of test cases t34.13 (blue line) and t34.15 (green line).

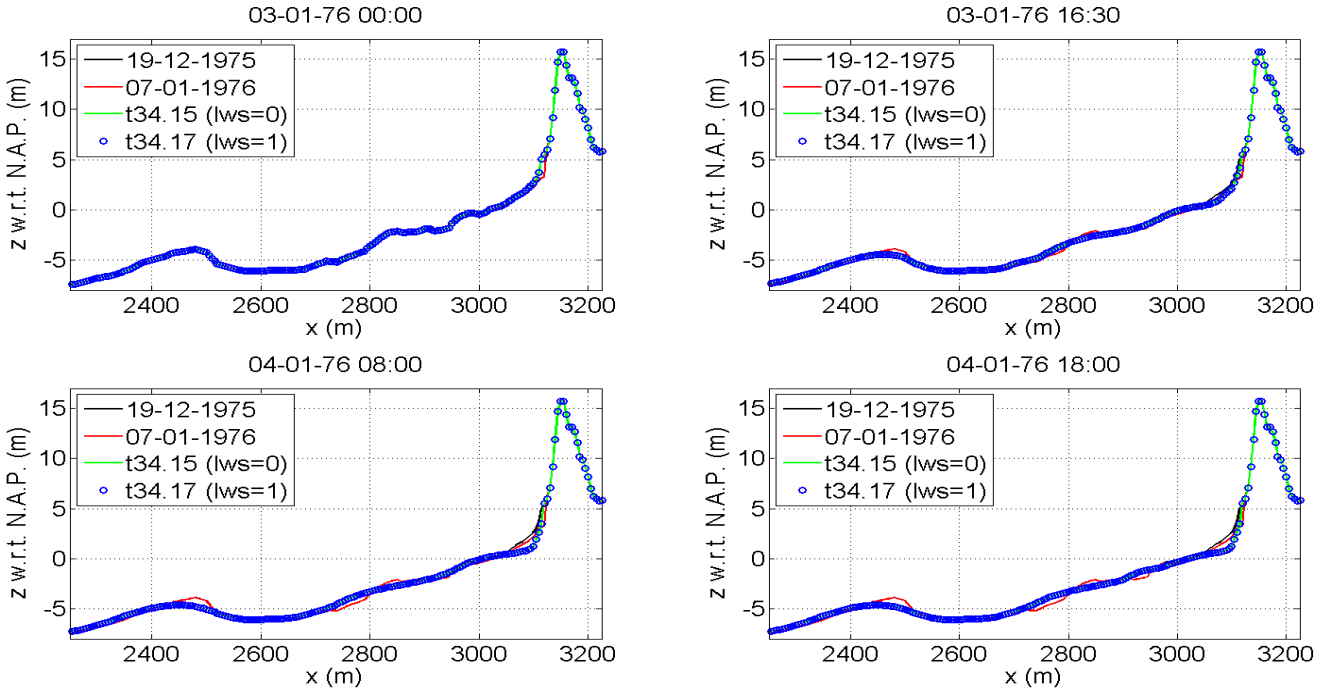

Figure C.4: Extended view of test cases t34.15 (green line) and t34.17 (blue line with circles).

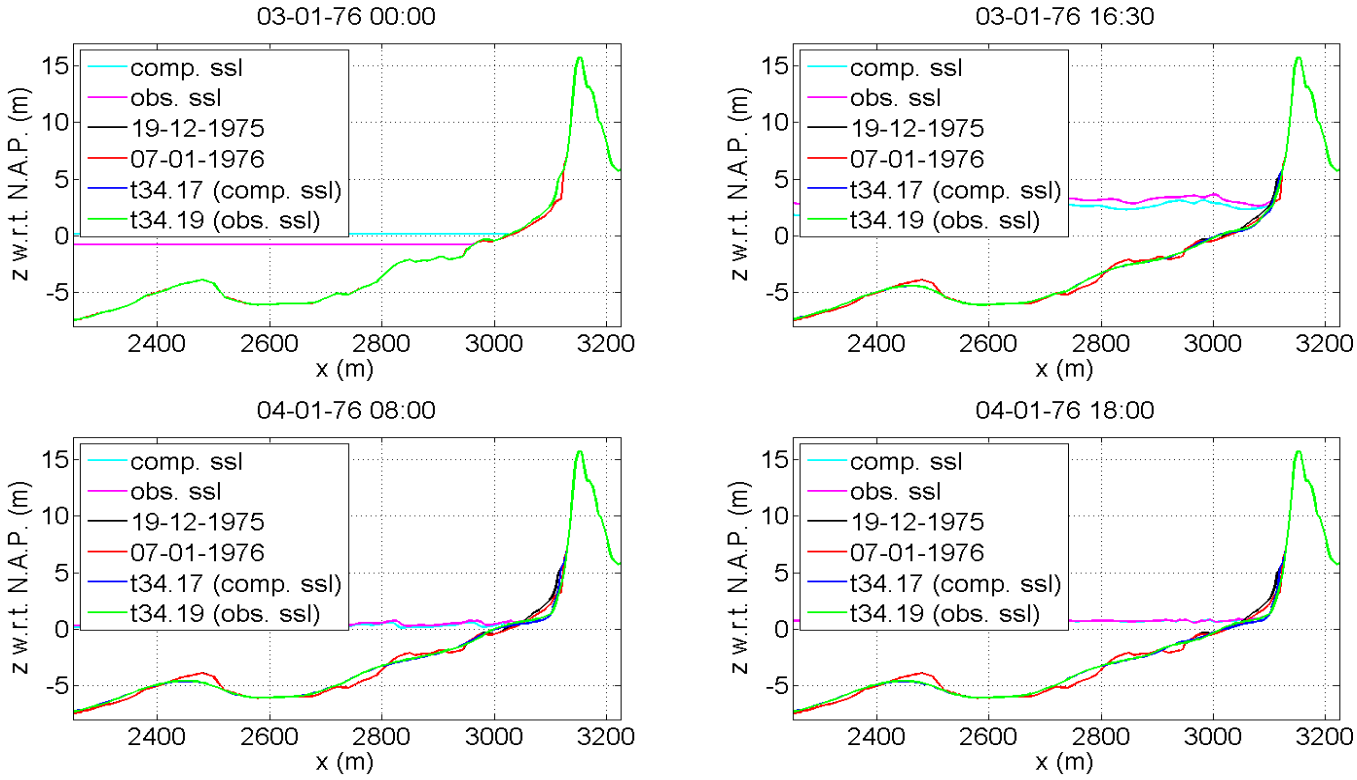

Figure C.5: Extended view of test cases t34.17 (blue line) and t34.19 (green line).

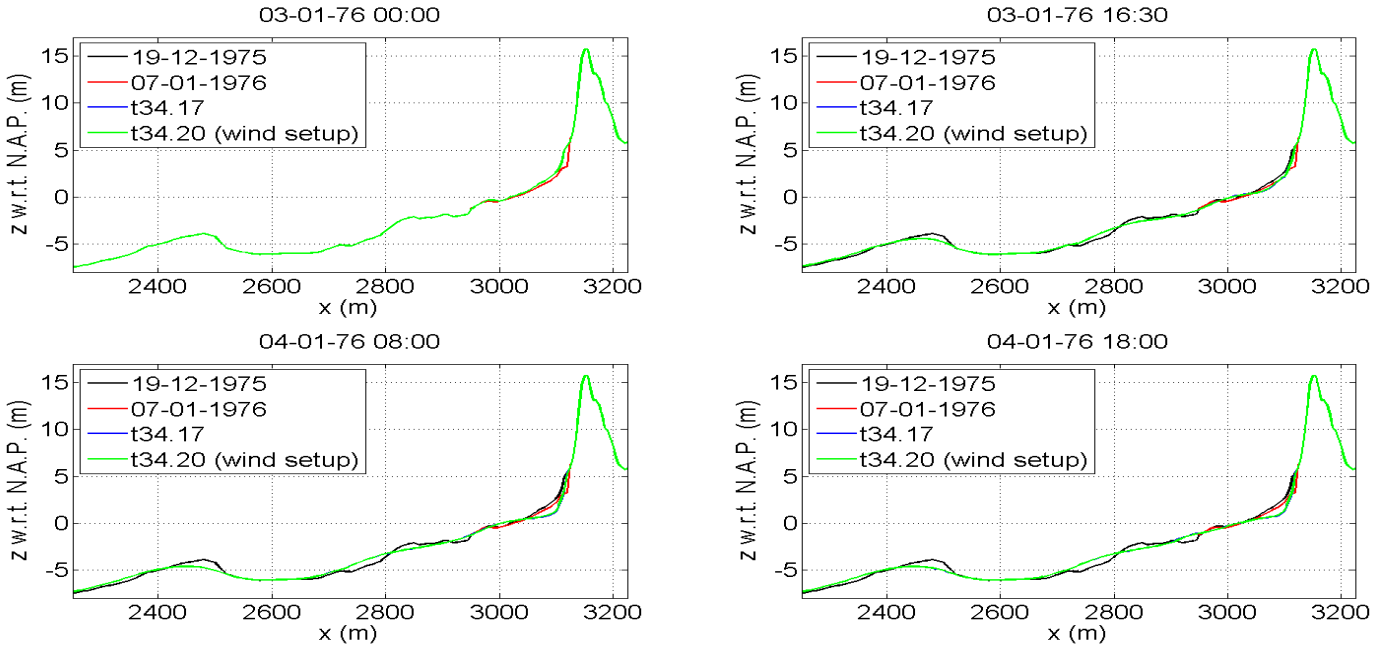

Figure C.6: Extended view of test cases t34.17 (blue line) and t34.20 (green line).

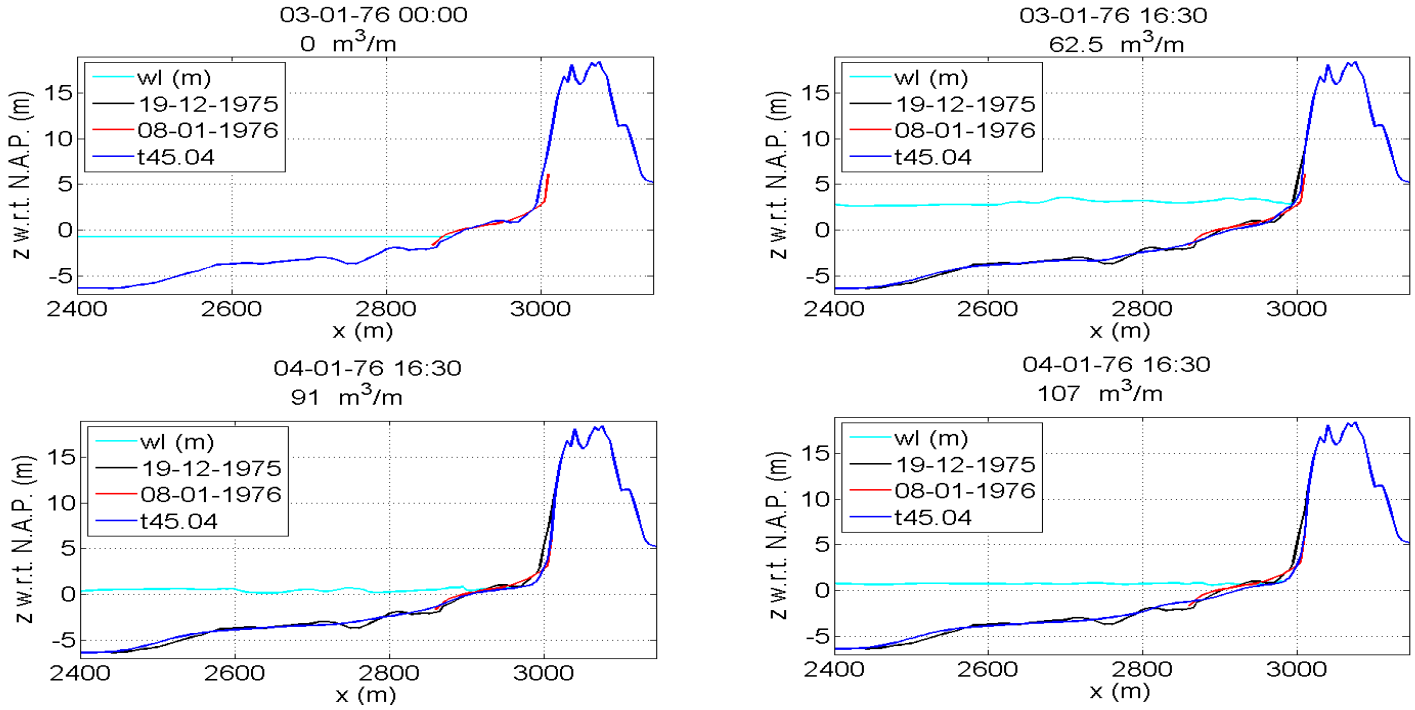

Figure C.7: Extended view of test case t45.04 (blue line).

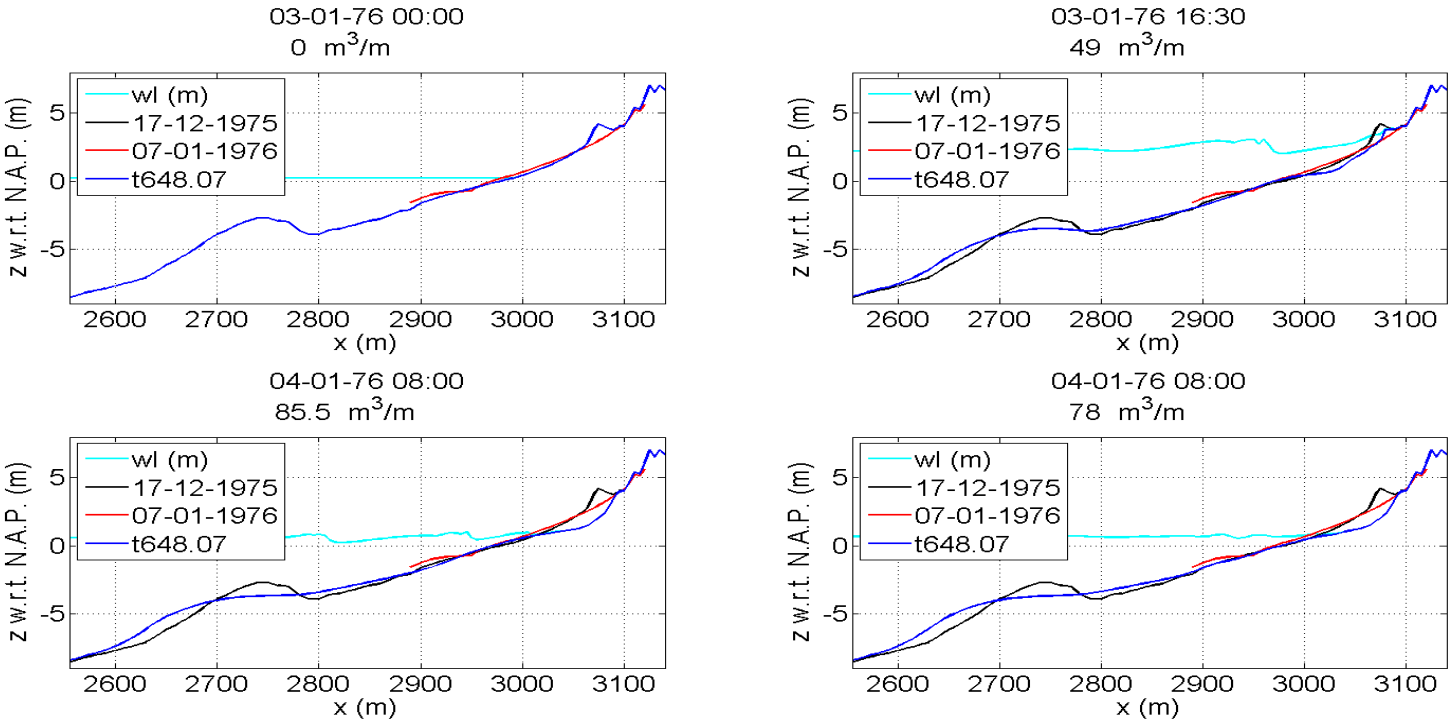

Figure C.8: Extended view of test case t648.07 (blue line).